

# NNLO Computational Techniques: the Cases $H \rightarrow \gamma\gamma$ and $H \rightarrow gg$ †‡

STEFANO ACTIS \*

*Institut für Theoretische Physik E, RWTH Aachen University,  
52056 Aachen, Germany*

GIAMPIERO PASSARINO †

*Dipartimento di Fisica Teorica, Università di Torino, Italy  
INFN, Sezione di Torino, Italy*

CHRISTIAN STURM ‡

*Physics Department, Brookhaven National Laboratory,  
Upton, NY 11973, USA*

SANDRO UCCIRATI §

*Institut für Theoretische Teilchenphysik, Universität Karlsruhe,  
76128 Karlsruhe, Germany*

A large set of techniques needed to compute decay rates at the two-loop level are derived and systematized. The main emphasis of the paper is on the two Standard Model decays  $H \rightarrow \gamma\gamma$  and  $H \rightarrow gg$ . The techniques, however, have a much wider range of application: they give practical examples of general rules for two-loop renormalization; they introduce simple recipes for handling internal unstable particles in two-loop processes; they illustrate simple procedures for the extraction of collinear logarithms from the amplitude. The latter is particularly relevant to show cancellations, e.g. cancellation of collinear divergencies. Furthermore, the paper deals with the proper treatment of non-enhanced two-loop QCD and electroweak contributions to different physical (pseudo-)observables, showing how they can be transformed in a way that allows for a stable numerical integration. Numerical results for the two-loop percentage corrections to  $H \rightarrow \gamma\gamma, gg$  are presented and discussed. When applied to the process  $pp \rightarrow gg + X \rightarrow H + X$ , the results show that the electroweak scaling factor for the cross section is between  $-4\%$  and  $+6\%$  in the range  $100 \text{ GeV} < M_H < 500 \text{ GeV}$ , without incongruent large effects around the physical electroweak thresholds, thereby showing that only a complete implementation of the computational scheme keeps two-loop corrections under control.

Keywords: Feynman diagrams, Two-loop calculations, Radiative corrections, Higgs physics

PACS classification: 11.15.Bt, 12.38.Bx, 13.85.Lg, 14.80.Bn, 14.80.Cp

---

†‡Work supported by MIUR under contract 2001023713\_006, by the European Community's Marie Curie Research Training Network *Tools and Precision Calculations for Physics Discoveries at Colliders* under contract MRTN-CT-2006-035505, by the U.S. Department of Energy under contract No. DE-AC02-98CH10886 and by the Deutsche Forschungsgemeinschaft through Sonderforschungsbereich/Transregio 9 *Computergestützte Theoretische Teilchenphysik*.

\*actis@physik.rwth-aachen.de

†giampiero@to.infn.it

‡sturm@bnl.gov

§uccirati@particle.uni-karlsruhe.de

# Contents

<b>1</b>	<b>Introduction</b>	<b>1</b>
<b>2</b>	<b>Notation and conventions</b>	<b>3</b>
<b>3</b>	<b>The amplitude for <math>H \rightarrow \gamma\gamma(gg)</math></b>	<b>4</b>
3.1	Higgs-boson mass and wave-function renormalization	6
3.2	Ward-Slavnov-Taylor identities	7
3.3	One-loop counterterms	9
3.3.1	Higgs tadpoles	10
3.3.2	Diagonalization of the neutral sector	11
3.3.3	$\overline{\text{MS}}$ counterterms	11
3.4	Finite renormalization	13
3.4.1	Wave-function renormalization	14
3.4.2	Finite renormalization for masses and couplings	15
3.4.3	The doubly contracted WST identity for $H \rightarrow \gamma\gamma$ at two loops	17
<b>4</b>	<b>Manipulating Feynman integrals after generation of Feynman diagrams</b>	<b>18</b>
4.1	Reduction of scalar products	18
4.2	Vacuum diagrams	20
4.3	Symmetrization of loop integrals	21
<b>5</b>	<b>Behavior of two-loop diagrams around a normal threshold</b>	<b>22</b>
5.1	Square-root singularities	24
5.2	Logarithmic singularities	26
5.3	Complex masses	28
<b>6</b>	<b>Extraction of collinear singularities</b>	<b>30</b>
6.1	Collinear behavior and tensor reduction	31
6.2	Vertices with one photon coupled to light fermions	34
6.2.1	The collinear-finite part of $V_{\text{sc}}^G$	38
6.2.2	The collinear-finite part of $V_{\text{sc}}^K$	41
6.2.3	The collinear-finite part of $V_{\text{sc}}^H$	42
6.3	Vertices with two photons coupled to light fermions	44
6.3.1	The Master Integral $V_{\text{dc}}^G$	44
6.3.2	The Master Integral $V_{\text{dc}}^H$	45
6.4	The special case of the $V^M$ family	49
<b>7</b>	<b>Evaluation of massive diagrams</b>	<b>51</b>
<b>8</b>	<b>Numerical results</b>	<b>55</b>
<b>9</b>	<b>Conclusions</b>	<b>58</b>
<b>A</b>	<b>Self-energies, vertices and tadpoles</b>	<b>61</b>
<b>B</b>	<b>Properties of projectors</b>	<b>62</b>
<b>C</b>	<b>Non-abelian soft and collinear diagrams in <math>H \rightarrow gg</math></b>	<b>64</b>
<b>D</b>	<b>Loop integrals with complex masses and momenta</b>	<b>66</b>

# 1 Introduction

In this paper we have collected and systematized a large set of techniques needed to compute decay rates and production cross sections at the two-loop level in a spontaneously broken theory characterized by a large number of scales. Although the main emphasis will be on the Standard Model (SM) Higgs-boson decays to two photons and two gluons and on the related production processes, our techniques have a broader range of application. Firstly, they represent practical applications of general rules for two-loop renormalization and introduce simple recipes for handling internal unstable particles. Secondly, they illustrate useful procedures for the analytical extraction of collinear logarithms: we explicitly prove that the complete  $H \rightarrow \gamma\gamma$  amplitude is free from collinear logarithms in spite of the fact that single Feynman diagrams show a collinear-divergent behavior. Finally, our techniques allow to represent the non-enhanced two-loop QCD and electroweak contributions to different physical (pseudo-)observables in a form suitable for a stable numerical integration.

The lastly mentioned feature represents the important and difficult part of our computation. Since we do not rely on any kind of approximation, we can safely cover all kinematical regions including different normal thresholds, like the  $WW$  one, which are peculiar of Higgs- and vector-boson decays. Therefore, we are able to place the electroweak component on the same footing as the QCD one: a non-trivial but essential task, since in several situations the size of the pure electroweak higher order corrections is comparable to the theoretical uncertainty related to the parton distribution functions.

Note that two-loop electroweak corrections to  $1 \rightarrow 2$  processes are currently investigated by several groups: the authors of Ref. [1] have derived the dominant contributions to the  $H \rightarrow b\bar{b}$  decay width, and two different collaborations have computed the fermionic [2] and bosonic [3,4] corrections to the effective electroweak mixing angle.

With the advent of the LHC era, it is clear that the production process  $gg \rightarrow H$  and the decay mode  $H \rightarrow \gamma\gamma$  are going to play a crucial role for a precise comparison of the experimental data with the SM predictions.

Gluon fusion is the main production channel of the SM Higgs boson at hadron colliders, and both virtual and real corrections have been thoroughly investigated since the beginning of the 90's. The QCD next-to-leading order (NLO) radiative corrections to the total Higgs-production cross section have been first computed below the  $t\bar{t}$  threshold in Ref. [5], and using an effective-Lagrangian approach, where the top quark is integrated out, in Ref. [6]. Formally, the second method defines the heavy-top limit, and it has represented the starting point for subsequent higher order improvements. A one-dimensional integral representation which proves well-set for numerical evaluation has been later derived in Refs. [7,8] for the entire Higgs-mass range; moreover, the virtual component has been evaluated analytically in a closed form by the authors of Ref. [9].

Recently, two different groups [10,11] have provided independent checks of the work of Ref. [9], generalizing the analytic result in a framework where the coupling of the Higgs to the external particles is mediated by a scalar field (see also Ref. [12]). Since QCD NLO corrections increase the cross section by more than 70%, there was a flurry of activity on higher order QCD effects. Partial results for the next-to-next-to-leading order (NNLO) corrections to the total cross section in the heavy-top limit have been obtained in Ref. [13] for the two-loop virtual corrections to the effective heavy-top  $Hgg$  vertex, and in Ref. [14] for the soft components; the complete NNLO result has been finally derived by three different groups in Ref. [15], and later supplemented by an all-order resummed calculation of multiple soft-gluon emission at next-to-next-to-leading logarithmic (NNLL) accuracy in Ref. [16] and including the fourth logarithmic (N<sup>3</sup>LL) order in Ref. [17] (see also Ref. [18]). In addition, the effect of a jet veto on the inclusive cross section has been studied at NNLO in Ref. [19], and an improvement with respect to the heavy-top limit has been recently obtained by the authors of Ref. [20]. Because of the cuts on the final states typical for hadron-collider phenomenology, fully differential perturbative results have a privileged role; the differential cross section for Higgs production has been derived through NNLO in QCD in Ref. [21], and later cross-checked through an independent subtraction formalism by the authors of Ref. [22]. Note that the techniques used in Ref. [21] have been recently extended in Ref. [23] to compute the QCD NNLO cross section for the  $H \rightarrow WW \rightarrow l\nu l\nu$  signal at the LHC. The Higgs-production mechanism in the gluon-fusion channel has clearly a close affinity with the Higgs decay to two gluons; the state of the art in QCD is presently represented by the two works

of Ref. [24], with the full NNLO result and the N<sup>3</sup>LO calculation in the heavy-top limit respectively.

While QCD corrections to Higgs production through gluon fusion at hadron colliders are well under control, electroweak effects are less understood. The NLO corrections to the total cross section were evaluated in Ref. [25,26] in the heavy-top limit, and turned out to be less than 1%. The contribution due to the light fermions has been calculated analytically in Ref. [27], and found to be more sizable; the remaining component of the amplitude involving the top quark has been computed by means of a Taylor expansion in the Higgs external momentum in Ref. [28]. It is worth stressing that the work of Refs. [27,28] has not been independently cross-checked by a different group; moreover, for obvious reasons, the validity of the result of Ref. [28] is restricted to the kinematical region below the  $WW$  threshold. Under the hypothesis of factorization with respect to the dominant QCD soft and collinear radiation, the impact of the electroweak corrections to Higgs-production in proton-proton collisions has been estimated in Ref. [29].

The decay of the SM Higgs boson into two photons has also a great phenomenological interest: on the one hand, it provides a precious information for the discovery at hadron colliders [30]; on the other hand, an upgrade option at the planned ILC will allow for a high-precision measurement of the partial width into two photons [31], leading to quantitative tests on the existence of new charged particles. QCD corrections to the decay width of an intermediate-mass Higgs boson have been computed at NLO in Ref. [32] and at NNLO in Ref. [33]; the NLO result has later been extended in Ref. [34] to the whole Higgs-mass range.

Electroweak NLO corrections have been computed in Ref. [35,26] in the large top-mass scenario (the so-called “dominant” corrections) and in Ref. [36] in the large Higgs-mass scenario. The complexity of this complicated (multi-scale) computation is reflected into the fact that seldom an *a priori* dominance lives up to its promise; for instance,  $\mathcal{O}(G_F M_t^2)$  corrections in the range 80 – 150 GeV do not dominate at all. Recently, the two-loop contributions induced by light fermions have been derived in Ref. [27], and electroweak corrections due to gauge bosons and the top quark have been given in term of an expansion in the Higgs external momentum in Ref. [37], a result subsequently extended in Ref. [38] to cover all kinematical regions including the notoriously difficult  $WW$  threshold and the NLO QCD corrections.

In this paper we show details about the evaluation carried on for the  $H \rightarrow \gamma\gamma$  decay in Ref. [38] and generalize the result to the  $gg \rightarrow H$  process to the entire Higgs-mass range. Since we are not bound to rely on any kind of expansion, neither in the bosonic sector nor in the top-bottom one, we can produce extremely accurate results for any value of the Higgs-boson mass, including the full dependence on the  $W$ -,  $Z$ - and Higgs-boson masses and on the top-quark mass. A consistent and gauge-invariant treatment of unstable particles allows to produce precise results around the  $WW$  threshold.

In our approach, Feynman diagrams, up to two loops and including QCD, are generated by means of an automated procedure which does not rely on any external package, and is implemented in the FORM [39] program *GraphShot* [40]. After projecting the amplitude for a given (pseudo-)observable onto form factors and taking traces over Dirac matrices, three basic simplifications are done recursively: at first, reducible scalar products are removed; next, tadpole integrals are reduced using integration-by-parts identities (IBPIs) [41]; finally, the symmetries of each diagram are exploited in order to reduce the number of integrals to be evaluated.

The second step in the calculation of any two-loop process concerns renormalization; here we heavily rely on the results of Refs. [42,43,44]. After assembling diagrams we perform the usual canonical tests to ensure that our result is correct, checking all possible unrenormalized Ward-Slavnov-Taylor (WST) identities. The next logical steps consist in removing all ultraviolet divergencies, with the due caution to the problem of overlapping divergencies, and checking the renormalized WST identities. Then, we express renormalized parameters in terms of physical observables belonging to some input-parameter set.

The third step consists in the analytical extraction of collinear logarithms of Feynman diagrams. It is worth noting that the amplitude for  $H \rightarrow \gamma\gamma$  is collinear free, and one could adopt the approach where all light fermions are considered massless; therefore, the collinear behavior of single components is controlled in dimensional regularization and collinear poles cancel in the total. We prefer another approach, where collinear singularities are controlled by the light-fermion masses; partial components of the complete result are divergent, but we check that all logarithms of collinear origin cancel in the complete answer.

Finally, the remaining collinear-free contributions are written in terms of smooth integral representations using the methods developed in Refs. [45,46,47,48,49], and then evaluated numerically.

The outline of the paper is as follows: in section 2 we summarize our notation and conventions. Details about the construction of the  $H \rightarrow \gamma\gamma(gg)$  amplitude, including renormalization and choice of the input-parameter set, are discussed in section 3. In section 4 we explain how we manipulate Feynman integrals in order to simplify the amplitude, removing scalar products, reducing tadpole integrals and symmetrizing Feynman diagrams. The behavior of two-loop diagrams around a normal threshold is thoroughly investigated in section 5. In section 6 we discuss the extraction of collinear singularities, and in section 7 we describe details about the evaluation of massive diagrams. Numerical results are shown and discussed in section 8. Finally, we summarize our conclusions in section 9. Additional material is contained in the appendices.

## 2 Notation and conventions

*Regularization.* We employ dimensional regularization [50], denoting the number of space-time dimensions by  $n = 4 - \epsilon$ , and we define short-hand notations for regularization-dependent factors,

$$\Delta_{UV} = \gamma + \ln \pi + \ln \frac{M^2}{\mu^2}, \quad \Delta_{UV}(x) = \Delta_{UV} - \ln \frac{M^2}{x}, \quad (1)$$

where  $\gamma = 0.5772156\dots$  is the Euler constant,  $\mu$  is the 't Hooft mass unit,  $M$  stands for the bare or renormalized  $W$ -boson mass (in the following we will not distinguish unless strictly needed) and  $x$  is a positive-definite kinematical variable. In our conventions the logarithm has a cut along the negative real axis and it is understood that for all masses  $M^2 \rightarrow M^2 - i0$ .

The structure of poles in dimensional regularization is better exploited in terms of universal factors. Any one-loop integral  $f^1$  can be formally decomposed as  $f^1(\{l\}) = \sum_{k=-1}^1 f^1(\{l\}; k) F_k^1(x)$ , where  $\{l\}$  stands for a set of arguments representing powers of inverse propagators, external kinematical variables and masses of internal particles and  $x$  denotes a scale which depends on the kind of integral:  $M$  for tadpoles and a squared external momentum for other configurations. The dependence on the dimensional regulator  $\epsilon$  and the regularization-dependent factors introduced in Eq.(1) is encapsulated in the universal one-loop ultraviolet (hereafter UV) factors

$$F_{-1}^1(x) = \frac{1}{\epsilon} - \frac{1}{2} \Delta_{UV}(x) + \frac{1}{8} \Delta_{UV}^2(x) \epsilon, \quad F_0^1(x) = 1 - \frac{1}{2} \Delta_{UV}(x) \epsilon, \quad F_1^1(x) = \epsilon. \quad (2)$$

It is worth noting that, because of overlapping divergencies due to UV-divergent one-loop sub-diagrams, we include  $\mathcal{O}(\epsilon)$  terms in all one-loop results.

A generic two-loop integral  $f^2$  can be written as  $f^2(\{l\}) = \sum_{k=-2}^0 f^2(\{l\}; k) F_k^2(x)$ , with two-loop UV factors given by

$$F_{-2}^2(x) = \frac{1}{\epsilon^2} - \frac{\Delta_{UV}(x)}{\epsilon} + \frac{1}{2} \Delta_{UV}^2(x), \quad F_{-1}^2(x) = \frac{1}{\epsilon} - \Delta_{UV}(x), \quad F_0^2(x) = 1. \quad (3)$$

Note that the product of two one-loop integrals can be written in terms of the same UV decomposition of a genuine two-loop integral.

Finally, let us define our soft/collinear factors; for the electroweak part of the calculation they are equal to the UV factors of Eq.(3). In appendix C we will extend their definition to cover non-abelian QCD configurations.

*Classification of two-loop integrals.* In this paper we frequently use the notion of scalar, vector and tensor two-loop Feynman integrals. An arbitrary two-loop scalar diagram can be cast as

$$G^{\alpha\beta\gamma} = \frac{\mu^{2\epsilon}}{\pi^4} \int d^n q_1 d^n q_2 \prod_{i=1}^{\alpha} (k_i^2 + m_i^2)^{-1} \prod_{j=\alpha+1}^{\alpha+\gamma} (k_j^2 + m_j^2)^{-1} \prod_{l=\alpha+\gamma+1}^{\alpha+\gamma+\beta} (k_l^2 + m_l^2)^{-1}, \quad (4)$$

where  $\alpha, \beta$  and  $\gamma$  give the number of internal lines containing the integration momenta  $q_1, q_2$  and  $q_1 - q_2$ , and we have introduced

$$\begin{aligned} k_i &= q_1 + \sum_{j=1}^N \eta_{ij}^1 p_j, & i &= 1, \dots, \alpha, \\ k_i &= q_1 - q_2 + \sum_{j=1}^N \eta_{ij}^{12} p_j, & i &= \alpha + 1, \dots, \alpha + \gamma, \\ k_i &= q_2 + \sum_{j=1}^N \eta_{ij}^2 p_j, & i &= \alpha + \gamma + 1, \dots, \alpha + \gamma + \beta. \end{aligned} \quad (5)$$

Here  $N$  is the number of vertices connected to external lines,  $\eta_{ij}^a = \pm 1, 0$  and  $\{p\}$  is the set of external momenta. The capital letter  $G$  identifies the number of external legs:  $T$  for tadpoles,  $S$  for self-energies and  $V$  for vertices.

The triplet of numbers  $\alpha\beta\gamma$  can be represented in an extremely compact way: first, we introduce  $\kappa = \gamma_{\max} [\alpha_{\max} (\beta - 1) + \alpha - 1] + \gamma$ , where for tadpoles  $\alpha_{\max} = 1$  and  $\gamma_{\max} = 1$ , for self-energies  $\alpha_{\max} = 2$  and  $\gamma_{\max} = 1$  and for vertices  $\alpha_{\max} = 2$  and  $\gamma_{\max} = 2$ ; next, we associate a letter of the alphabet to each value of  $\kappa$  and we derive a set of alpha-numerical correspondences,

$$\begin{aligned} G = T &\Rightarrow 111 \rightarrow A, & G = S &\Rightarrow 111 \rightarrow A, & 121 &\rightarrow C, & 131 &\rightarrow E, & 221 &\rightarrow D, \\ G = V &\Rightarrow 121 \rightarrow E, & 131 &\rightarrow I, & 141 &\rightarrow M, & 221 &\rightarrow G, & 231 &\rightarrow K, & 222 &\rightarrow H. \end{aligned} \quad (6)$$

All the different groups (sometimes called families or topologies) of Feynman diagrams with different numbers of external and internal legs have been classified for completeness in Figs. 25, 26, 27 and 28 of appendix A, where the graphical relation between the diagrams and the corresponding integrals can be found. Note that we follow the notation of Ref. [51] for one-loop integrals. At the two-loop level we identify one tadpole (vacuum) topology,  $T^A$ , four self-energy topologies,  $S^A, S^C, S^E, S^D$ , and six vertex topologies,  $V^E, V^I, V^M, V^G, V^K, V^H$ . Note that factorized two-loop topologies, associated with the product of two one-loop Feynman integrals, do not receive a particular name.

For a detailed analysis of scalar two-loop self-energies and vertices we refer the interested reader to Refs. [45,46,47,48]. The presence of non-trivial structures containing integration momenta in the numerators of two-loop integrals requires to introduce tensor structures and form factors, as described in sections 7 and 9 of Ref. [49] for higher rank self-energies and vertices.

Miscellanea. In order to keep our results as compact as possible, we introduce a short-hand notation for integrals over a simplex of Feynman parameters,

$$\int dS_n(\{x\})f(x_1, \dots, x_n) = \prod_{i=1}^n \int_0^{x_{i-1}} dx_i f(x_1, \dots, x_n), \quad \int dC_n(\{x\})f(x_1, \dots, x_n) = \int_0^1 \prod_{i=1}^n dx_i f(x_1, \dots, x_n), \quad (7)$$

where  $x_0 = 1$ . In addition, the so-called  $'+'$  and  $'++'$  distributions will be extensively used,

$$\begin{aligned} \int_0^1 dx \frac{f(x, \{z\})}{x-a} \Big|_+ &= \int_0^1 dx \frac{f(x, \{z\}) - f(a, \{z\})}{x-a}, \quad a = 0, 1, \\ \int_0^1 dx \frac{f(x, \{z\}) \ln^n x}{x} \Big|_+ &= \int_0^1 dx \frac{[f(x, \{z\}) - f(0, \{z\})] \ln^n x}{x}, \end{aligned} \quad (8)$$

$$\int_0^1 dx dy \frac{f(x, y, \{z\})}{xy} \Big|_{++} = \int_0^1 dx dy \frac{f(x, y, \{z\}) - f(x, 0, \{z\}) - f(0, y, \{z\}) + f(0, 0, \{z\})}{xy}. \quad (9)$$

### 3 The amplitude for $H \rightarrow \gamma\gamma(gg)$

We consider the decay of an arbitrary Higgs boson into two photons  $h(-P) + \gamma(p_1) + \gamma(p_2) \rightarrow 0$ , where  $P = p_1 + p_2$  (all momenta are incoming). The amplitude  $\mathcal{A}$  can be written as

$$\mathcal{A} = \mathcal{Z}_A^{-1} \mathcal{Z}_H^{-\frac{1}{2}} e_1^\mu e_2^\nu \mathcal{A}_{\mu\nu}(0, 0, -M_H^2), \quad (10)$$

where  $e_i^\mu = e^\mu(p_i, \lambda_i)$ , with  $i = 1, 2$  and  $\lambda_i = \pm$ , are the photon polarization vectors and  $\mathcal{Z}_A$  and  $\mathcal{Z}_H$  are the photon and Higgs-boson wave-function renormalization factors.  $\mathcal{A}_{\mu\nu}$  is the amputated Green's function for  $h \rightarrow \gamma\gamma$ , whose tensor structure reads

$$\mathcal{A}_{\mu\nu}(p_1^2, p_2^2, P^2) = \frac{G}{16\pi^2} \left[ F_D(p_1^2, p_2^2, P^2) \delta_{\mu\nu} + \sum_{i,j=1}^2 F_P^{(ij)}(p_1^2, p_2^2, P^2) p_{i\mu} p_{j\nu} + F_\epsilon(p_1^2, p_2^2, P^2) \epsilon_{\mu\nu\alpha\beta} p_1^\alpha p_2^\beta \right]. \quad (11)$$

If  $h = H$ , the Standard Model CP-even Higgs boson, then  $F_\epsilon = 0$  and  $G = g^3 s_\theta^2$ , where  $g$  is the bare  $SU(2)$ -coupling constant and  $s_\theta = \sin \theta$  ( $c_\theta = \cos \theta$ ) is the sine (cosine) of the bare weak-mixing angle. The form factors  $F_D$ ,  $F_P^{(ij)}$  and  $F_\epsilon$  are functions of the off-shell kinematical invariants  $p_1^2$ ,  $p_2^2$  and  $P^2$ ; they have to be extracted with suitable projection operators and can be subsequently evaluated for on-shell external momenta,  $p_1^2 = p_2^2 = 0$  and  $P^2 = -M_H^2$ , where  $M_H$  is the on-shell Higgs-boson mass. A general framework for projection operators is discussed in appendix B following the approach of Ref. [52].

Note that the amplitude for the decay of the SM Higgs boson into two gluons,  $H \rightarrow gg$ , is obtained from Eq.(10) and Eq.(11), replacing  $\mathcal{Z}_A$  with  $\mathcal{Z}_g$ , the gluon wave-function renormalization factor, and introducing the appropriate color indices for the gluon fields; in addition, the overall factor  $g^3 s_\theta^2$  of Eq.(11) is replaced by  $g g_s^2$ , where  $g_s$  is the  $SU(3)$ -coupling constant of strong interactions.

Because of the absence of a tree-level  $H\gamma\gamma(gg)$  coupling in the SM, the lowest-order amplitude is generated by one-loop fermionic and bosonic diagrams, as shown in Fig. 1; note that the virtual particles do not decouple also for masses larger than the Higgs one, since their coupling to the Higgs boson grows with their mass.

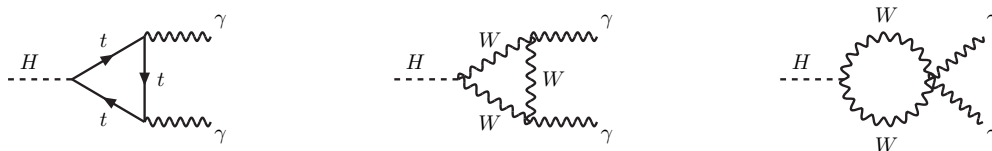


Figure 1: Examples of one-loop diagrams for the decay  $H \rightarrow \gamma\gamma$ . Other bosonic diagrams, not shown here, contain charged unphysical Higgs-Kibble scalar and Faddeev-Popov ghost fields. For  $H \rightarrow gg$ , only fermionic diagrams appear.

Having singled out the  $s_\theta$  dependence due to the couplings of the external photons, the one-loop form factors do not show any residual dependence on  $\theta$ , because one-loop diagrams containing  $Z$  bosons or neutral unphysical Higgs-Kibble scalar and Faddeev-Popov ghost fields do not show up. Therefore, form factors at one loop contain only the bare masses of the  $W$  boson,  $m_W$ , the Higgs boson,  $m_H$ , and the fermions,  $m_f$ . This simple observation will allow in the following for a straightforward implementation of two different renormalization schemes. On the one hand, the on-shell masses of the  $W$  boson,  $M_W$ , the Higgs boson,  $M_H$ , and the fermions,  $M_f$ , will be part of any renormalization scheme, and the associated derivatives of the one-loop form factors will have to be evaluated. On the other hand,  $g$  and  $s_\theta$ , collected as simple pre-factors in Eq.(11), will be connected to  $G_F$ , the Fermi-coupling constant, and  $\alpha$ , the fine-structure constant, or  $M_Z$ , the on-shell  $Z$ -boson mass. The choice of the two different input-parameter sets  $(G_F, \alpha)$  or  $(G_F, M_Z)$  will define our renormalization scheme. Finally, the  $SU(3)$ -coupling constant  $g_s$  will be related to the strong-coupling constant  $\alpha_s(\mu_R^2)$  evaluated at the appropriate renormalization scale  $\mu_R$ .

The form factor  $F_\epsilon$  is present at two loops in diagrams containing a fermion sub-loop, as shown in Fig. 2, but it does not arise at one loop due to the lacking of axial fermion couplings. Due to CP invariance the contribution of  $F_\epsilon$  vanishes in the total. Therefore, we can circumvent the notorious problems associated with the definition of the  $\gamma_5$  matrix in dimensional regularization [50] (see a detailed discussion in Ref. [53]) employing a completely anticommuting  $\gamma_5$ .

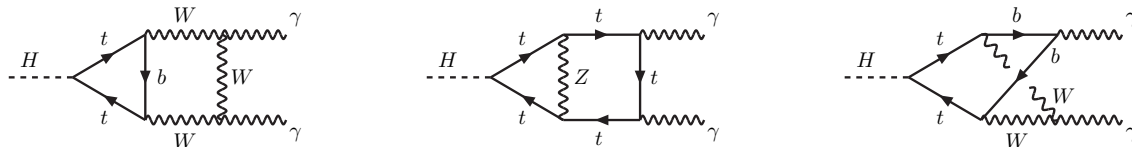


Figure 2: Representative two-loop diagrams giving a non-vanishing contribution to the form factor  $F_\epsilon$ , because of the presence of an axial coupling between a massive vector boson and a virtual fermion pair.

Finally, we observe that Bose symmetry sets four constraints on the other form factors for off-shell

external particles,

$$\begin{aligned} F_D(p_1^2, p_2^2, P^2) &= F_D(p_2^2, p_1^2, P^2), & F_P^{(11)}(p_1^2, p_2^2, P^2) &= F_P^{(22)}(p_2^2, p_1^2, P^2), \\ F_P^{(12)}(p_1^2, p_2^2, P^2) &= F_P^{(12)}(p_2^2, p_1^2, P^2), & F_P^{(21)}(p_1^2, p_2^2, P^2) &= F_P^{(21)}(p_2^2, p_1^2, P^2). \end{aligned} \quad (12)$$

Although  $F_P^{(11)}$ ,  $F_P^{(22)}$  and  $F_P^{(12)}$  are irrelevant for the calculation of the amplitude due to the condition  $e_i \cdot p_i = 0$  for on-shell photons (gluons), they play an essential role in computing the relevant Ward-Slavnov-Taylor identities (hereafter WSTIs) for  $H \rightarrow \gamma\gamma(gg)$ .

Before discussing WSTIs in more detail, let us define what we use for the Higgs-boson mass and wave-function renormalization factor.

### 3.1 Higgs-boson mass and wave-function renormalization

We evaluate the amplitude for  $P^2 = -M_H^2$ , where  $M_H$  is the on-shell Higgs-boson mass, defined as the location of the pole of the real part of the associated Dyson-resummed propagator  $\overline{\Delta}_H$ ,

$$\text{Re} [\overline{\Delta}_H(p^2)]^{-1} |_{p^2=-M_H^2} = 0 \quad \Rightarrow \quad M_H^2 = m_H^2 - \text{Re} \Sigma_H(-M_H^2). \quad (13)$$

Here  $m_H$  is the bare mass and  $\Sigma_H$  is the sum of all one-particle irreducible (1PI) diagrams for the Higgs self-energy. For definiteness,  $M_H$  would be the experimental mass extracted from a fit of the hypothetical Higgs-resonance line shape obtained by means of a Breit-Wigner function with a running width,

$$\overline{\Delta}_H(p^2) \propto \frac{1}{p^2 + M_H^2 + i p^2 \Gamma_H / M_H}. \quad (14)$$

It is well-known that the on-shell definition of mass for an unstable particle is gauge-parameter dependent beyond one loop, and it should be replaced by the complex pole,  $s_H$  in our case, including real and imaginary parts of  $\overline{\Delta}_H$ ,

$$[\overline{\Delta}_H(p^2)]^{-1} |_{p^2=-s_H} = 0 \quad \Rightarrow \quad s_H = m_H^2 - \Sigma_H(-s_H). \quad (15)$$

As it is often stated [54], the complex pole is a property of the  $\mathcal{S}$  matrix, and therefore gauge-parameter independent at all orders in perturbation theory; the proof of this property relies on the Nielsen identities and can be found in Ref. [55]. Therefore, fixed-order computations beyond one loop or resummation-improved one-loop predictions require to perform mass renormalization dropping the concept of on-shell masses and employing complex poles; for a thorough discussion at one and two loops we refer to Ref. [44].

Concerning  $H \rightarrow \gamma\gamma$  at two loops, the absence of a tree-level amplitude implies that Higgs-mass renormalization has to be performed at one loop: this suggests that an on-shell definition of the Higgs-boson mass, being gauge-parameter independent at one loop, proves adequate for our purposes. Nevertheless, we will show in the following that a naive implementation of on-shell mass renormalization for the Higgs boson breaks the standard two-loop WSTI for  $H \rightarrow \gamma\gamma$  above the  $WW$ -production threshold (light-fermion masses are neglected). On the one hand, the bare identity develops an imaginary part above the  $WW$  threshold; on the other hand, the Higgs self-energy appearing in Eq.(13),  $\Sigma_H$ , develops an imaginary part at one loop for  $M_H > 2M_W$ , but on-shell mass renormalization selects its real part only. This introduces a mismatch between real and imaginary parts at the level of the renormalized WSTI. Therefore, the usual statement that renormalization schemes with complex poles or on-shell masses are equivalent at one loop should be taken with some caution; for  $H \rightarrow \gamma\gamma$  at two loops, the two schemes are equivalent only below the  $WW$ -production threshold.

A second delicate point concerns the use of a Higgs-boson wave-function renormalization (hereafter WFR) factor introduced *à la* Lehmann-Symanzik-Zimmermann (LSZ) [56]. The LSZ formalism, in fact, is unambiguously defined for stable particles, but it requires some care when external unstable particles appear.

Let us consider first the case of the photon in QED. Here, the LSZ WFR factor is fixed by the condition that the transverse part of the photon Dyson-resummed propagator,  $\overline{\Delta}_A^T$ , dressed by its WFR factor  $\mathcal{Z}_A$ , has unity residue at the pole in the  $p^2$  plane,

$$\mathcal{Z}_A = \frac{\partial}{\partial p^2} [\overline{\Delta}_A^T(p^2)]^{-1} |_{p^2=0} \quad \Rightarrow \quad \mathcal{Z}_A = 1 - \Sigma_{A,p}(0), \quad \Sigma_{A,p}(p^2) = \frac{\partial \Sigma_A(p^2)}{\partial p^2}, \quad (16)$$

where  $\Sigma_A$  is the sum of all 1PI diagrams for the transverse part of the photon self-energy (we will show in the following that the presence of a photon/ $Z$ -boson mixing in the SM does not change the structure of Eq.(16)). Note that it has been shown long ago [57,58] that the LSZ definition of WFR factors leads to gauge-parameter independent  $\mathcal{S}$ -matrix elements and respects unitarity.

For a stable particle, the pole of the Dyson-resummed propagator is real; being the Higgs boson an unstable particle, the pole of its Dyson-resummed propagator in the  $p^2$  plane is complex, and the Higgs WFR factor is not unambiguously defined. We define it requiring that the real part of the Higgs-boson Dyson-resummed propagator, dressed by its WFR factor  $\mathcal{Z}_H$ , has unity residue at the on-shell Higgs-boson mass,

$$\mathcal{Z}_H = \text{Re} \frac{\partial}{\partial p^2} [\overline{\Delta}_H(p^2)]^{-1} \Big|_{p^2=-M_H^2} \Rightarrow \mathcal{Z}_H = 1 - \text{Re} \Sigma_{H,p}(-M_H^2), \quad \Sigma_{H,p}(p^2) = \frac{\partial \Sigma_H(p^2)}{\partial p^2}. \quad (17)$$

Other definitions, involving the real part of the derivative of the propagator at the complex pole [59], or the complete derivative, including imaginary parts [60], do not look appropriate for our computation, which deals with the ideal situation of an asymptotic state containing the Higgs boson, whose momentum is required to be real.

Note, however, that the definition of a real WFR factor at the on-shell mass is a possible source of inconsistencies. The authors of Ref. [61], for example, have shown that unitarity-breaking terms can show up in the final form for the amplitude. From a formal perspective, indeed, transition amplitudes have to be defined in terms of asymptotic states containing stable particles only. To this respect, the necessary modifications to the theory have been described in Ref. [62], where unitarity and causality of the resulting  $\mathcal{S}$  matrix are proven.

In the following, we will use a compromise. At first, we will show that, concerning  $H \rightarrow \gamma\gamma(gg)$  at two loops, a naive use of Eq.(17) leads to unphysical singularities at thresholds. Then, we will modify our renormalization scheme introducing complex poles.

### 3.2 Ward-Slavnov-Taylor identities

Ward-Slavnov-Taylor identities (WSTIs) [63] for  $H \rightarrow \gamma\gamma(gg)$  are essential for organizing our computation. They allow to perform severe checks on the algebraic structure of the amplitude, and set strong constraints on the number of independent form factors. Although in the following we will focus on the  $H \rightarrow \gamma\gamma$  process, it is evident that analogous considerations can be applied to  $H \rightarrow gg$ .

Let us consider the simplest case, the so-called doubly contracted WSTI with an on-shell Higgs boson and both off-shell photons. After replacing in Eq.(10) the photon polarization vectors with their associated four-momenta, we get

$$\begin{aligned} \mathcal{WI}_{dc}(p_1^2, p_2^2) &= \mathcal{Z}_H^{-1/2} p_1^\mu p_2^\nu \mathcal{A}_{\mu\nu}(p_1^2, p_2^2, -M_H^2) \\ &= -\frac{g^3 s_\theta^2}{32\pi^2} \mathcal{Z}_H^{-1/2} \left\{ (M_H^2 + p_1^2 + p_2^2) \left[ F_D(p_1^2, p_2^2, -M_H^2) + \sum_{i=1}^2 p_i^2 F_P^{(ii)}(p_1^2, p_2^2, -M_H^2) \right] \right. \\ &\quad \left. - \frac{1}{2} (M_H^2 + p_1^2 + p_2^2) F_P^{(21)}(p_1^2, p_2^2, -M_H^2) \right] - 2p_1^2 p_2^2 F_P^{(12)}(p_1^2, p_2^2, -M_H^2) \left. \right\} = 0. \quad (18) \end{aligned}$$

Here the Higgs boson is assumed on its mass shell,  $P^2 = -M_H^2$ , and provided with its WFR factor  $\mathcal{Z}_H^{-1/2}$ , whereas the form factors are evaluated for off-shell photons and photon WFR factors are consistently not included. After showing that all form factors are regular for on-shell photons, one can set  $p_1^2 = p_2^2 = 0$  and get the well-known constraint

$$\mathcal{WI}_{dc}(0, 0) = -\frac{g^3 s_\theta^2}{32\pi^2} \mathcal{Z}_H^{-1/2} M_H^2 \left[ F_D(0, 0, -M_H^2) - \frac{M_H^2}{2} F_P^{(21)}(0, 0, -M_H^2) \right] = 0, \quad (19)$$

which shows that the  $H \rightarrow \gamma\gamma$  amplitude can be described through a single form factor. Before attempting any evaluation of the amplitude, we extract both  $F_D$  and  $F_P^{(21)}$  employing projection operators for off-shell

photon momenta. Next, we check that form factors are regular for on-shell photons, and we compute the WSTI, verifying that Eq.(19) holds at the algebraic level. This provides a strong test on several procedures used throughout the calculation of the amplitude, like the reduction of tensor integrals to scalar ones. Note, however, that the WSTI, being satisfied at the algebraic level, does not provide any information on the analytic structure of the loop integrals themselves. Here, a severe test on the result will be supplemented by the extraction of all collinear logarithms: they have to cancel in the full amplitude, and indeed we will show that they cancel.

Two additional relations among the form factors can be readily obtained by considering simply contracted WSTIs, where one off-shell photon leg is contracted with its four-momentum, and the other one is saturated with the polarization vector, put on the mass shell and provided with its WFR factor,

$$\begin{aligned} \mathcal{W}\mathcal{I}_{sc,1}(p_1^2) &= \mathcal{Z}_A^{-1/2} \mathcal{Z}_H^{-1/2} p_1^\mu e_2^\nu \mathcal{A}_{\mu\nu}(p_1^2, 0, -M_H^2) \\ &= \frac{g^3 s_\theta^2}{16 \pi^2} (p_1 \cdot e_2) \mathcal{Z}_A^{-1/2} \mathcal{Z}_H^{-1/2} \left[ F_D(p_1^2, 0, -M_H^2) + p_1^2 F_P^{(11)}(p_1^2, 0, -M_H^2) \right. \\ &\quad \left. - \frac{1}{2}(M_H^2 + p_1^2) F_P^{(21)}(p_1^2, 0, -M_H^2) \right] = 0, \end{aligned} \quad (20)$$

$$\begin{aligned} \mathcal{W}\mathcal{I}_{sc,2}(p_2^2) &= \mathcal{Z}_A^{-1/2} \mathcal{Z}_H^{-1/2} e_1^\mu p_2^\nu \mathcal{A}_{\mu\nu}(0, p_2^2, -M_H^2) \\ &= \frac{g^3 s_\theta^2}{16 \pi^2} (p_2 \cdot e_1) \mathcal{Z}_A^{-1/2} \mathcal{Z}_H^{-1/2} \left[ F_D(0, p_2^2, -M_H^2) + p_2^2 F_P^{(22)}(0, p_2^2, -M_H^2) \right. \\ &\quad \left. - \frac{1}{2}(M_H^2 + p_2^2) F_P^{(21)}(0, p_2^2, -M_H^2) \right] = 0. \end{aligned} \quad (21)$$

In Fig. 3 we show diagrammatically Eq.(18), Eq.(20) and Eq.(21). In addition, we introduce the notions of: 1) physical source: the external on-shell leg is multiplied by the appropriate WFR factor, and, for the case of photons, supplemented by the polarization vector; 2) contracted source: the external off-shell photon leg is contracted with its four-momentum.

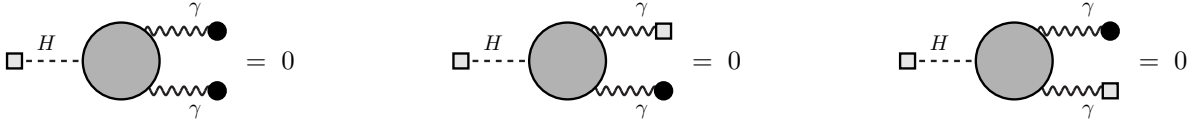


Figure 3: Diagrammatic representation of Eq.(18) (doubly contracted WST identity), Eq.(20) and Eq.(21) (simply contracted WST identities). Physical sources are denoted by a gray box, contracted ones, for photons, by a black circle. In the latter case the on-shell relation  $p_i^2 = 0$  is relaxed.

The computation of a doubly or simply contracted WSTI for an on-shell Higgs boson beyond the leading order approximation requires to pay special attention to the interplay between the bare and on-shell Higgs-boson masses. Let us consider the doubly contracted WSTI of Eq.(19) at two loops. The full set of diagrams can be organized in three classes: 1) two-loop diagrams where the Higgs-boson WFR factor is set to unity,  $\mathcal{Z}_H = 1$ , and the bare Higgs-boson mass is identified with its on-shell experimental value,  $m_H = M_H$ ; 2) one-loop diagrams supplemented with  $\mathcal{Z}_H$  evaluated at one loop by means of Eq.(17), where we employ again the tree-level relation  $m_H = M_H$ ; 3) one-loop diagrams where  $\mathcal{Z}_H = 1$ , and we replace the tree-level identity between the bare and the on-shell Higgs-boson masses with the solution of the Higgs-boson mass renormalization equation of Eq.(13), with the Higgs-boson self-energy  $\Sigma_H$  evaluated at one loop.

In Fig. 4 we show a representative diagram for each class; let us consider in detail their expansions in terms of the bare  $SU(2)$ -coupling constant  $g$ . The first diagram is  $\mathcal{O}(g^5)$ ; the second one is  $\mathcal{O}(g^3)$ , and gives an  $\mathcal{O}(g^5)$  contribution once provided with the WFR factor  $\mathcal{Z}_H$  at one loop. The most subtle point is related to the third diagram, which is  $\mathcal{O}(g^3)$  and is multiplied by a tree-level WFR factor,  $\mathcal{Z}_H = 1$ . However, it entails a vertex where one Higgs boson and two unphysical charged Higgs-Kibble scalar fields are coupled proportionally to  $m_H^2$ . Since we put the Higgs boson on its mass shell, the bare mass  $m_H$  has to be removed, introducing everywhere the on-shell value  $M_H$ . Therefore, first we use Eq.(13) and evaluate  $\Sigma_H$  at order

$\mathcal{O}(g^2)$ ; next, we replace the solution in the third diagram and obtain an  $\mathcal{O}(g^5)$  contribution, which proves essential in fulfilling the WSTI.

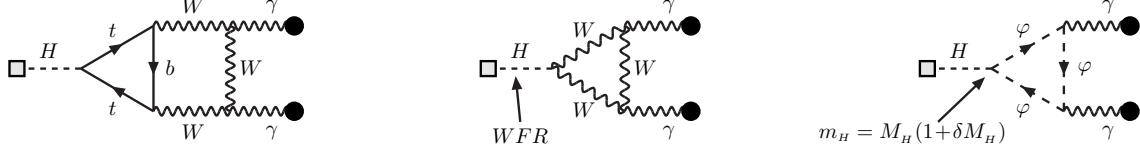


Figure 4: Representative diagrams for the doubly contracted WSTI of Eq.(18) at next-to-leading order. As in Fig. 3, black circles correspond to off-shell photons contracted with their four-momenta, and a gray box stands for a physical Higgs-boson source. Inclusion of the Higgs-boson WFR factor  $\mathcal{Z}_H$  in the second diagram and Higgs-boson mass renormalization in the third one are both performed at one loop.

Finally, we stress that both doubly and simply contracted WSTIs assume that the Higgs boson is emitted by a physical source. However, as shown by 't Hooft and Veltman in their seminal paper [58], a broader class of WSTIs can be obtained when we inspect, at the diagrammatic level, the effect of an infinitesimal shift of the gauge-fixing functions,  $\mathcal{C}^a \rightarrow \mathcal{C}^a + \epsilon \mathcal{R}$ , with  $\epsilon \rightarrow 0$ . Here  $a$  denotes one of the gauge fields and  $\mathcal{R}$  stands for an off-shell source emitting one or more off-shell particles. As shown in Ref. [58], off-shell WSTIs connect physical or contracted sources to special sources obtained by: 1) subjecting  $\mathcal{R}$  to an infinitesimal local gauge transformation; 2) replacing the parameters of the transformation with the related Faddeev-Popov ghost fields. Let us consider a simple example one can derive for  $H \rightarrow \gamma\gamma$ . After choosing the gauge-fixing function for the photon field  $A_\mu$  in 't Hooft-Feynman gauge,  $\mathcal{C}^A = -\partial^\mu A_\mu$ , we introduce two off-shell sources emitting one photon or one Higgs boson,  $\mathcal{R}_A = J_A^\mu A_\mu$  and  $\mathcal{R}_H = J_H H$ . Next, we perform a local  $SU(2) \times U(1)$  gauge transformation, and replace the infinitesimal gauge parameters of the transformation by the appropriate Faddeev-Popov ghost fields. We derive two special sources,

$$\begin{aligned} \mathcal{R}_A &\rightarrow J_A^\mu \left[ A_\mu + i g s_\theta (X^- W_\mu^+ - X^+ W_\mu^-) - \partial_\mu Y^A \right], \\ \mathcal{R}_H &\rightarrow J_H \left[ H + \frac{g}{2 c_\theta} Y^Z \varphi^0 + \frac{g}{2} (X^- \varphi^+ + X^+ \varphi^-) \right], \end{aligned} \quad (22)$$

where  $Y^A$ ,  $Y^Z$ ,  $X^+$  and  $X^-$  are the Faddeev-Popov ghost fields and  $\varphi^0$ ,  $\varphi^+$  and  $\varphi^-$  are the unphysical Higgs-Kibble scalar fields. Off-shell WSTIs for  $H \rightarrow \gamma\gamma$  are then readily obtained connecting at least one special source with physical or contracted sources. In Fig. 5 we show two examples: in the first case, the Higgs boson and one photon are emitted by physical sources, and the second off-shell photon is connected to a special source; in the second case, both off-shell photons are contracted with their four-momenta, and the off-shell Higgs boson is emitted by a special source. In this case, WFR factor and mass renormalization for the Higgs boson have not to be included.

### 3.3 One-loop counterterms

In this section we shortly summarize three aspects of the renormalization procedure which are needed before performing finite renormalization: tadpole renormalization, diagonalization of the neutral sector and ultraviolet counterterms. A detailed analysis can be found in Refs. [42,43].

We fix the gauge for the electroweak sector of the SM Lagrangian introducing six gauge parameters  $\xi_i$  ( $i = A, Z, AZ, \varphi^0, W, \varphi$ ),

$$\begin{aligned} \mathcal{L}_{gf}^{\text{EW}} &= -\mathcal{C}^+ \mathcal{C}^- - \frac{1}{2} \left[ (\mathcal{C}^A)^2 + (\mathcal{C}^Z)^2 \right], \\ \mathcal{C}^A &= -\frac{1}{\xi_A} \partial_\mu A_\mu - \xi_{AZ} \partial_\mu Z_\mu, \quad \mathcal{C}^Z = -\frac{1}{\xi_Z} \partial_\mu Z_\mu + \xi_{\varphi^0} \frac{m_W}{c_\theta} \varphi^0, \quad \mathcal{C}^\pm = -\frac{1}{\xi_W} \partial_\mu W_\mu^\pm + \xi_\varphi m_W \varphi^\pm. \end{aligned} \quad (23)$$

Here  $A_\mu$ ,  $Z_\mu$  and  $W_\mu^\pm$  are the fields for the photon and the  $Z$  and the  $W$  bosons and  $\varphi^0$  and  $\varphi^\pm$  are the fields for the neutral and charged unphysical Higgs-Kibble scalars. For the QCD sector, we employ the following

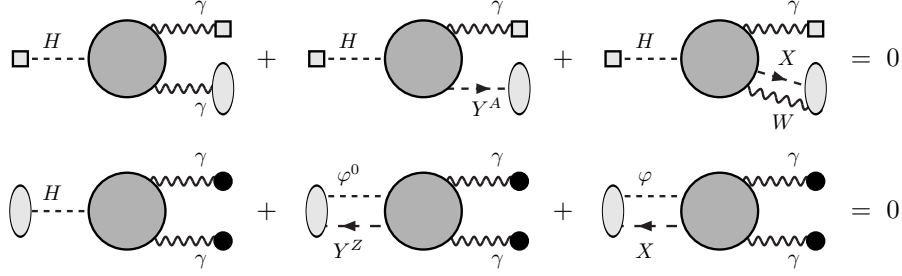


Figure 5: Off-shell WSTIs involving special sources, denoted by gray ovals. The special source for the photon field can emit a Faddeev-Popov (FP) ghost field (dot-line) and two  $W$ -boson/charged FP field (wavy/dot-lines) couples. The special source for the Higgs boson can emit three neutral and charged Higgs-Kibble/FP field couples. See Eq.(22) for the explicit expressions of the special sources. As usual, contracted sources are denoted by black circles and physical ones by gray boxes.

choice,

$$\mathcal{L}_{gf}^{\text{QCD}} = -\frac{1}{2} \sum_a \mathcal{C}^{G,a} \mathcal{C}^{G,a}, \quad \mathcal{C}^{G,a} = -\frac{1}{\xi_{G,a}} \partial_\mu G_\mu^a, \quad (24)$$

which for  $\xi_G = 1$  reduces to the usual 't Hooft-Feynman gauge.

### 3.3.1 Higgs tadpoles

Tadpoles in spontaneously broken theories have been discussed by many authors (see Refs. [64,65]). The tadpole-renormalization prescription used in this paper will be the  $\beta_t$  scheme, thoroughly discussed in section 2.3 of Ref. [42].

Following notation and conventions of Ref. [65], the minimal Higgs sector of the SM is provided by the Lagrangian

$$\mathcal{L}_S = -(D_\mu K)^\dagger (D_\mu K) - \mu^2 K^\dagger K - (\lambda/2)(K^\dagger K)^2, \quad (25)$$

where the covariant derivative is given by

$$D_\mu K = \left( \partial_\mu - \frac{i}{2} g B_\mu^a \tau^a - \frac{i}{2} g' B_\mu^0 \right) K, \quad K^\dagger = \frac{1}{\sqrt{2}} (\zeta - i\varphi_0, -\varphi_2 - i\varphi_1), \quad (26)$$

where  $g'/g = -s_\theta/c_\theta$ ,  $\tau^a$  are the standard Pauli matrices,  $B_\mu^a$  is a triplet of vector gauge bosons and  $B_\mu^0$  a singlet. For the theory to be stable we must require  $\lambda > 0$ . In addition, we choose  $\mu^2 < 0$  in order to have spontaneous symmetry breaking. The scalar field belongs to the minimal realization of the SM, where  $\zeta$  and the Higgs-Kibble fields  $\varphi_0$ ,  $\varphi_1$  and  $\varphi_2$  are real. In particular, we choose  $\zeta + i\varphi_0$  to be the component of  $K$  to develop the non-zero vacuum expectation value, and we set  $\langle \varphi_0 \rangle_0 = 0$  and  $\langle \zeta \rangle_0 \neq 0$ . We then introduce the (physical) Higgs field as  $H = \zeta - v$ . The parameter  $v$  is not a new parameter of the model and its value must be fixed by the requirement that  $\langle H \rangle_0 = 0$  (i.e.  $\langle K \rangle_0 = (1/\sqrt{2})(v, 0)$ ), so that the vacuum does not absorb or create Higgs particles.

It is then convenient to define the bare parameters  $m_W$  (the  $W$  boson mass),  $m_H$  (the mass of the physical Higgs particle) and  $\beta_t$  (the tadpole constant) according to the following “ $\beta_t$  scheme”,

$$\begin{cases} m_W(1 + \beta_t) = gv/2 \\ m_H^2 = \lambda(2m_W/g)^2 \\ 0 = \mu^2 + \frac{\lambda}{2}(2m_W/g)^2 \end{cases} \implies \begin{cases} v = 2m_W(1 + \beta_t)/g \\ \lambda = (gm_H/2m_W)^2 \\ \mu^2 = -\frac{1}{2}m_H^2 \end{cases}. \quad (27)$$

Next, we define  $\beta_t = \beta_{t_0} + \beta_{t_1}g^2 + \beta_{t_2}g^4 + \dots$  and we fix the parameter  $\beta_t$  such that the vacuum-expectation value of the Higgs field remains zero order by order in perturbation theory. At the lowest order we can simply set  $\beta_t = 0$ , i.e.  $\beta_{t_0} = 0$ . At one loop we take into account all tadpole diagrams and we get

$$\beta_{t_1} = \frac{m_W^2}{16\pi^2 m_H^2} \left\{ 3 \sum_{i=1}^3 \left[ \frac{m_{d,i}^4}{m_W^4} a_0(m_{d,i}) + \frac{m_{u,i}^4}{m_W^4} a_0(m_{u,i}) \right] + \sum_{i=1}^3 \frac{m_{l,i}^4}{m_W^4} a_0(m_{l,i}) - \frac{1}{4c_\theta^2} \left( \frac{n-1}{c_\theta^2} + \frac{m_H^2}{2m_W^2} \right) a_0(m_Z) - \frac{1}{2} \left( n-1 + \frac{m_H^2}{2m_W^2} \right) a_0(m_W) - \frac{3}{8} \frac{m_H^4}{m_W^4} a_0(m_H) \right\}, \quad (28)$$

where  $m_Z = m_W/c_\theta$  is the bare mass of the  $Z$  boson. The tadpole integral  $a_0$  reads

$$a_0(m) = \sum_{k=-1}^1 a_0(m; k) F_k^1(m_W^2), \quad (29)$$

with universal one-loop UV factors given by Eq.(2) and coefficients

$$a_0(m; -1) = -2, \quad a_0(m; 0) = -1 + \ln \frac{m^2}{m_W^2}, \quad a_0(m; 1) = \frac{1}{2} \left[ -1 - \frac{1}{2} \zeta(2) + \left( 1 - \frac{1}{2} \ln \frac{m^2}{m_W^2} \right) \ln \frac{m^2}{m_W^2} \right], \quad (30)$$

where  $\zeta(x)$  is the Riemann's zeta function. The full list of  $\beta_t$ -dependent Feynman rules needed for our computation is given in appendix B of Ref. [42].

### 3.3.2 Diagonalization of the neutral sector

The  $Z$ - $\gamma$  transition in the SM does not vanish at zero squared momentum transfer. Although this fact does not pose any serious problem, not even for the renormalization of the electric charge, it is preferable to use an alternative strategy. We will follow the treatment of Ref. [66]; consider the new  $SU(2)$ -coupling constant  $\bar{g}$ , the new mixing angle  $\bar{\theta}$  and the new  $W$  mass  $\bar{m}_W$  in the  $\beta_t$  scheme,

$$g = \bar{g}(1 + \Gamma), \quad g' = -\frac{\sin \bar{\theta}}{\cos \bar{\theta}} \bar{g}, \quad v = \frac{2\bar{m}_W}{\bar{g}}(1 + \beta_t), \quad \lambda = \left( \frac{\bar{g} m_H}{2\bar{m}_W} \right)^2, \quad \mu^2 = -\frac{1}{2} m_H^2, \quad (31)$$

where  $\Gamma = \Gamma_1 \bar{g}^2 + \Gamma_2 \bar{g}^4 + \dots$  is a new parameter yet to be specified. This change of parameters entails new  $A_\mu$  and  $Z_\mu$  fields related to  $B_\mu^3$  and  $B_\mu^0$  by

$$\begin{pmatrix} Z_\mu \\ A_\mu \end{pmatrix} = \begin{pmatrix} \cos \bar{\theta} & -\sin \bar{\theta} \\ \sin \bar{\theta} & \cos \bar{\theta} \end{pmatrix} \begin{pmatrix} B_\mu^3 \\ B_\mu^0 \end{pmatrix}. \quad (32)$$

In our approach  $\Gamma$  is fixed, order by order, requiring that the  $Z$ - $\gamma$  transition is zero at  $p^2 = 0$  in 't Hooft-Feynman gauge. The explicit result for  $\Gamma_1$  is

$$\Gamma_1 = \frac{n-2}{16\pi^2} a_0(m_W), \quad (33)$$

with  $a_0(m)$  given in Eq.(30). The full list of  $\Gamma$ -dependent Feynman rules needed for our computation is given in appendix C of Ref. [42]. In addition, for  $H \rightarrow \gamma\gamma$  we need also a three-leg vertex with one Higgs boson and two photons given by  $-g^5 s_\theta^2 m_W \Gamma_1^2 \delta_{\mu\nu}$ .

### 3.3.3 $\overline{MS}$ counterterms

We relate bare quantities to renormalized ones introducing multiplicative renormalization constants  $Z_i$  and (if not otherwise stated) we expand them through the renormalized  $SU(2)$ -coupling constant  $g_R$ ,

$$Z_i = 1 + \sum_{n=1}^{\infty} \left( \frac{g_R^2}{16\pi^2} \right)^n \delta Z_i^{(n)}, \quad (34)$$

where  $\delta Z_i^{(n)}$  are counterterms and the subscript  $i$  refers to masses, couplings, gauge parameters and fields.

In particular, for all bare masses we write  $m = Z_m^{1/2} m_R$  and for  $g, g_S$  and  $c_\theta$  ( $s_\theta$ ) we define  $p = Z_p p_R$ , where  $p = g, g_S, c_\theta, s_\theta$ . For a given bare field  $\phi$  we find convenient to write  $\phi = Z_\phi^{1/2} \phi_R$ , where  $\phi_R$  is a renormalized field, and we expand  $Z_\phi$  through Eq.(34). The bare photon field  $A^\mu$  represents an exception, and here we use

$$A^\mu = Z_{AA}^{1/2} A_R^\mu + Z_{AZ}^{1/2} Z_R^\mu, \quad Z_{AZ}^{1/2} = \sum_{n=1}^{\infty} \left( \frac{g_R^2}{16\pi^2} \right)^n \delta Z_{AZ}^{(n)}, \quad (35)$$

where  $A_R^\mu$  and  $Z_R^\mu$  are the renormalized fields for the photon and the  $Z$  boson. Note that  $Z_{AA}$  is expanded through Eq.(34). In addition, bare fermion fields  $\psi$  (we omit flavor labels) are written by means of bare left-handed and right-handed chiral fields  $\psi^L$  and  $\psi^R$ . The latter are traded for renormalized fields  $\psi_R^L$  and  $\psi_R^R$  expanding the renormalization constants through Eq.(34),

$$\psi^{L,R} = \frac{1}{2} (1 \pm \gamma^5) \psi, \quad \psi^{L,R} = Z_{\psi_{L,R}}^{1/2} \psi_R^{L,R}. \quad (36)$$

Faddeev-Popov ghost fields are not renormalized. For the bare gauge parameters introduced in Eq.(23) we use  $\xi = Z_\xi \xi_R$ , where  $\xi$  is one of the bare gauge parameters and  $\xi_R$  is the associated renormalized quantity.  $Z_\xi$  is expanded by means of Eq.(34) except for the case  $\xi = \xi_{AZ}$ , where we use

$$Z_{\xi_{AZ}} = \sum_{n=1}^{\infty} \left( \frac{g_R^2}{16\pi^2} \right)^n \delta Z_{\xi_{AZ}}^{(n)}. \quad (37)$$

After the expansions, we use the freedom in choosing the values for the renormalized gauge parameters and set  $\xi = 1$ . Next, we define a minimal  $\overline{MS}$  subtraction scheme,

$$\delta Z_i^{(1)} = \left( -\frac{2}{\epsilon} + \Delta_{UV} \right) \Delta Z_i^{(1)}, \quad (38)$$

and fix the counterterms in order to remove the poles at  $\epsilon = 0$  for any one-loop Green's function. The full list of one-loop counterterms in the  $\overline{MS}$  scheme can be found in section 5 of Ref. [43]. For completeness, we list here all the needed results, using short-hand notations for sums over fermions ( $l \rightarrow$  charged leptons,  $u, d \rightarrow$  quarks),

$$X_l^j = \sum_{i=1}^3 x_{l,i}^j, \quad X_u^j = \sum_{i=1}^3 x_{u,i}^j, \quad X_d^j = \sum_{i=1}^3 x_{d,i}^j, \quad (39)$$

and we introduce scaled masses,  $x_i = m_{i,R}^2/m_{W,R}^2$ . In the following we drop everywhere the subscript  $R$ , since all quantities are renormalized ones.

#### Gauge parameters.

$$\begin{aligned} \Delta Z_{\xi_A}^{(1)} &= \frac{1}{2} \Delta Z_{AA}^{(1)}, & \Delta Z_{\xi_{AZ}}^{(1)} &= -\Delta Z_{AZ}^{(1)}, \\ \Delta Z_{\xi_Z}^{(1)} &= \frac{1}{2} \Delta Z_Z^{(1)}, & \Delta Z_{\xi_{\varphi^0}}^{(1)} &= -\frac{1}{2} \left( \Delta Z_{\varphi^0}^{(1)} + \Delta Z_{m_W}^{(1)} \right) + \Delta Z_{c_\theta}^{(1)}, \\ \Delta Z_{\xi_W}^{(1)} &= \frac{1}{2} \Delta Z_W^{(1)}, & \Delta Z_{\xi_\varphi}^{(1)} &= -\frac{1}{2} \left( \Delta Z_\varphi^{(1)} + \Delta Z_{m_W}^{(1)} \right). \end{aligned} \quad (40)$$

#### Gauge-boson and Higgs-Kibble fields.

$$\begin{aligned} \Delta Z_{AA}^{(1)} &= \frac{23}{3} s_\theta^2, & \Delta Z_{AZ}^{(1)} &= -\frac{s_\theta}{3} \left( \frac{41}{2} \frac{1}{c_\theta} - 23 c_\theta \right), \\ \Delta Z_Z^{(1)} &= \frac{1}{3} \left( \frac{41}{2} \frac{1}{c_\theta^2} - 41 + 23 c_\theta^2 \right), & \Delta Z_{\varphi^0}^{(1)} &= -1 - \frac{1}{2} \left[ \frac{1}{c_\theta^2} - X_l - 3 \left( X_d + X_u \right) \right], \end{aligned}$$

$$\Delta Z_w^{(1)} = \frac{5}{6}, \quad \Delta Z_\varphi^{(1)} = \Delta Z_{\varphi^0}^{(1)}. \quad (41)$$

Masses and couplings.

$$\begin{aligned} \Delta Z_{m_W}^{(1)} &= -\frac{3}{4} \frac{1}{c_\theta^2} - \frac{7}{3} + \frac{1}{x_H} \left[ \frac{3}{2} \frac{1}{c_\theta^4} + 3 - 2 X_l^2 - 6 (X_d^2 + X_u^2) \right] + \frac{1}{2} \left[ \frac{3}{2} x_H + X_l + 3 (X_d + X_u) \right], \\ \Delta Z_{c_\theta}^{(1)} &= \frac{1}{2} \left( \frac{41}{6} \frac{1}{c_\theta^2} - \frac{29}{2} + \frac{23}{3} c_\theta^2 \right), \quad \Delta Z_{s_\theta}^{(1)} = -\frac{c_\theta^2}{s_\theta^2} \Delta Z_{c_\theta}^{(1)}, \quad \Delta Z_g^{(1)} = -\Delta Z_{s_\theta}^{(1)} - \frac{1}{2} \Delta Z_{A_A}^{(1)}. \end{aligned} \quad (42)$$

Higgs-boson field and mass.

$$\Delta Z_H^{(1)} = -1 - \frac{1}{2} \left[ \frac{1}{c_\theta^2} - X_l - 3 (X_d + X_u) \right], \quad \Delta Z_{M_H}^{(1)} = \frac{3}{2} \left[ \frac{1}{2} \frac{1}{c_\theta^2} + 1 - \frac{1}{2} x_H - \frac{1}{3} X_l - (X_d + X_u) \right]. \quad (43)$$

Fermion fields and masses.

$$\begin{aligned} \Delta Z_{\nu_R}^{(1)} &= 0, \quad \Delta Z_{l_R}^{(1)} = \frac{1}{c_\theta^2} - 1 + \frac{x_l}{2}, \quad \Delta Z_{u_R}^{(1)} = \frac{4}{9c_\theta^2} - \frac{4}{9} + \frac{x_u}{2} + \frac{4}{3} \frac{g_s^2}{g^2}, \quad \Delta Z_{d_R}^{(1)} = \frac{1}{9c_\theta^2} - \frac{1}{9} + \frac{x_d}{2} + \frac{4}{3} \frac{g_s^2}{g^2}, \\ \Delta Z_{\nu_L}^{(1)} &= \Delta Z_{l_L}^{(1)} = \frac{1}{4} \left( \frac{1}{c_\theta^2} + 2 + x_l \right), \quad \Delta Z_{u_L}^{(1)} = \Delta Z_{d_L}^{(1)} = \frac{1}{4} \left( \frac{1}{9c_\theta^2} + \frac{26}{9} + x_u + x_d + \frac{16}{3} \frac{g_s^2}{g^2} \right), \end{aligned} \quad (44)$$

$$\begin{aligned} \Delta Z_{m_l}^{(1)} &= 3 \frac{s_\theta^2}{c_\theta^2} + \frac{1}{x_H} \left[ \frac{3}{2} \frac{1}{c_\theta^4} + 3 - 2 X_l^2 - 6 (X_u^2 + X_d^2) \right] + \frac{3}{4} (x_H - x_l), \\ \Delta Z_{m_u}^{(1)} &= \frac{2}{3} \frac{s_\theta^2}{c_\theta^2} + \frac{1}{x_H} \left[ \frac{3}{2} \frac{1}{c_\theta^4} + 3 - 2 X_l^2 - 6 (X_u^2 + X_d^2) \right] + \frac{3}{4} (x_H - x_u + x_d) + 8 \frac{g_s^2}{g^2}, \\ \Delta Z_{m_d}^{(1)} &= -\frac{1}{3} \frac{s_\theta^2}{c_\theta^2} + \frac{1}{x_H} \left[ \frac{3}{2} \frac{1}{c_\theta^4} + 3 - 2 X_l^2 - 6 (X_u^2 + X_d^2) \right] + \frac{3}{4} (x_H + x_u - x_d) + 8 \frac{g_s^2}{g^2}. \end{aligned} \quad (45)$$

QCD Counterterms.

$$\Delta Z_{\xi_G}^{(1)} = \frac{1}{2} \Delta Z_G^{(1)}, \quad \Delta Z_G^{(1)} = -\frac{g_s^2}{g^2}, \quad \Delta Z_{g_s}^{(1)} = \frac{7}{2} \frac{g_s^2}{g^2}. \quad (46)$$

### 3.4 Finite renormalization

We devote this section to discuss: 1) wave-function renormalization (WFR): the one-loop photon (gluon) and Higgs-boson WFR factors,  $\mathcal{Z}_A$  ( $\mathcal{Z}_G$ ) and  $\mathcal{Z}_H$ , defined in Eq.(16) and Eq.(17), are inserted in the amplitude of Eq.(10); 2) finite renormalization: all renormalized parameters showing up in the UV-finite amplitude are related to two different experimental input-parameter sets (IPs) through the one-loop solutions of the SM renormalization equations. In addition, we show through a detailed analysis of finite renormalization that on-shell mass renormalization clashes with the simplest WST identity at hand, the doubly contracted relation for on-shell photons of Eq.(19).

In order to deal with compact expressions, we use the relations  $e_i \cdot p_i = 0$  for on-shell photons and set  $F_P = F_P^{(21)}$ ; the amplitude for  $H \rightarrow \gamma\gamma$  reads

$$\mathcal{A} = \frac{g^3 s_\theta^2}{16 \pi^2} \mathcal{Z}_A^{-1} \mathcal{Z}_H^{-1/2} \mathcal{M}, \quad \mathcal{M} = (e_1 \cdot e_2) F_D(0, 0, -M_H^2) + (e_1 \cdot p_2) (e_2 \cdot p_1) F_P(0, 0, -M_H^2). \quad (47)$$

The expression for the  $H \rightarrow gg$  amplitude is obtained introducing color indices and replacing  $g^2 s_\theta^2$  with  $g_s^2$  and  $\mathcal{Z}_A$  with  $\mathcal{Z}_G$ .

Furthermore, after expanding the form factors  $F_D$  and  $F_P$  and the function  $\mathcal{M}$  at two loops, we split pure  $\mathcal{O}(g^2)$  electroweak corrections and  $\mathcal{O}(g_s^2)$  QCD components, where  $g_s$  is the renormalized SU(3)-coupling constant of the QCD Lagrangian,

$$F = F^{(1)} + \frac{g^2}{16 \pi^2} F^{(2,EW)} + \frac{g_s^2}{16 \pi^2} F^{(2,QCD)}, \quad F = F_D, F_P, \mathcal{M}. \quad (48)$$

### 3.4.1 Wave-function renormalization

In the context of the  $\overline{\text{MS}}$ -renormalization prescription used in this paper, field-renormalization constants are not chosen in order to compensate virtual corrections induced by WFR factors *à la* LSZ. Therefore, at variance with the on-mass-shell prescription, external legs have to be properly dressed through the formalism introduced in Eq.(16) and Eq.(17).

Before expanding the WFR factors, we briefly recall our notation. Let  $\Sigma_i^{\mu\nu}$  be the sum of all 1PI diagrams for a vector-boson self-energy ( $i = A, Z, W$ ) or the transition between the photon and the  $Z$  boson ( $i = AZ$ ). We isolate tensor structures and introduce perturbative expansions according to

$$\Sigma_i^{\mu\nu}(p^2) = \Sigma_i(p^2) t^{\mu\nu} + P_i(p^2) l^{\mu\nu}, \quad \Sigma_i(p^2) = \sum_{n=1}^{\infty} \frac{g^{2n}}{(16\pi^2)^n} \Sigma_i^{(n)}(p^2), \quad (49)$$

where  $t^{\mu\nu} = \delta^{\mu\nu} - l^{\mu\nu}$  and  $l^{\mu\nu} = p^\mu p^\nu / p^2$ . The same expansion in  $g$  will be used for the Higgs boson or a fermion self-energy, both denoted by  $\Sigma_i$  ( $i = H, f$ ).

The LSZ WFR factor for a photon,  $\mathcal{Z}_A$ , is fixed through Eq.(16). The transverse part of the photon Dyson-resummed propagator  $\overline{\Delta}_A^{\mu\nu}$  can be expressed using Eq. (105) of Ref. [42]; it involves the transverse parts of the photon and  $Z$ -boson self-energies and the photon/ $Z$ -boson transition,

$$\overline{\Delta}_A^{\mu\nu}(p^2) = t^{\mu\nu} \overline{\Delta}_A^T(p^2) + l^{\mu\nu} \overline{\Delta}_A^L(p^2), \quad \left[ \overline{\Delta}_A^T(p^2) \right]^{-1} = p^2 - \Sigma_A(p^2) - \frac{[\Sigma_{AZ}(p^2)]^2}{p^2 + m_Z^2 - \Sigma_Z(p^2)}, \quad (50)$$

where  $m_Z$  is the renormalized  $Z$ -boson mass. For a one-loop accuracy, self-energies and transitions are computed at order  $\mathcal{O}(g^2)$ , and factors involving the weak-mixing angle  $\theta$  are singled out in the same spirit of the LQ-basis formalism, thoroughly discussed in section 6 of Ref. [42],

$$\Sigma_A^{(1)}(p^2) = p^2 s_\theta^2 \Pi_A^{(1)}(p^2), \quad \Sigma_{AZ}^{(1)}(p^2) = p^2 \frac{s_\theta}{c_\theta} \Pi_{AZ}^{(1)}(p^2), \quad \Sigma_Z^{(1)}(p^2) = \frac{1}{c_\theta^2} \Pi_Z^{(1)}(p^2). \quad (51)$$

The one-loop photon vacuum-polarization function  $\Pi_A^{(1)}$  and the residual function  $\Pi_Z^{(1)}$  are regular at  $p^2 = 0$ . In addition, because of the diagonalization procedure summarized in section 3.3.2, also  $\Pi_{AZ}^{(1)}$  is regular at  $p^2 = 0$ . Therefore, the canonical LSZ condition of Eq.(16) for the photon WFR factor allows to express  $\mathcal{Z}_A$  also in the full SM by means of  $\Pi_A^{(1)}$  evaluated at zero-momentum transfer, as in QED,

$$\mathcal{Z}_A = 1 - \frac{g^2 s_\theta^2}{16\pi^2} \Pi_A^{(1)}(0). \quad (52)$$

Note that an analogous relation holds at the two-loop level, see section 5 of Ref. [44] and Ref. [67], where the same result was obtained through a background-field method analysis.

The WFR factor for the Higgs boson,  $\mathcal{Z}_H$ , is fixed in Eq.(17); respect to the photon case, here mixings are not present because of CP conservation. After expanding the Higgs-boson self-energy at one loop and introducing the real part of its derivative,  $\Sigma_{H,p}^{(1)}$ , we get

$$\mathcal{Z}_H = 1 - \frac{g^2}{16\pi^2} \text{Re}\Sigma_{H,p}^{(1)}(-M_H^2), \quad \Sigma_{H,p}^{(1)}(p^2) = \frac{\partial \Sigma_H^{(1)}(p^2)}{\partial p^2}. \quad (53)$$

Including the WFR factors of Eq.(52) and Eq.(53) in the amplitude of Eq.(47), and expanding  $\mathcal{M}$  through Eq.(48), we get finally

$$\mathcal{A} = \frac{g^3 s_\theta^2}{16\pi^2} \left\{ \mathcal{M}^{(1)} + \frac{g^2}{16\pi^2} \left[ \mathcal{M}^{(2,\text{EW})} + \mathcal{M}^{(1)} \left( \frac{1}{2} \text{Re}\Sigma_{H,p}^{(1)}(-M_H^2) + s_\theta^2 \Pi_A^{(1)}(0) \right) \right] + \frac{g_s^2}{16\pi^2} \mathcal{M}^{(2,\text{QCD})} \right\}. \quad (54)$$

Of course, an on-mass-shell prescription for the counterterms would shift  $\Sigma_{H,p}^{(1)}$  and  $\Pi_A^{(1)}$  in the one-loop expressions for the counterterms themselves; the associated contribution, in our notation, would be hidden in  $\mathcal{M}^{(2,\text{EW})}$ .

### 3.4.2 Finite renormalization for masses and couplings

The second step in building the amplitude consists in performing finite renormalization; the residual dependence of the UV-finite amplitude on the renormalized parameters is removed through the solutions of the SM renormalization equations, truncated at the appropriate order. For a NLO accuracy, we need tree-level solutions for all  $\mathcal{O}(g^5)$  and  $\mathcal{O}(g^3 g_s^2)$  terms of Eq.(54) and one-loop ones for the  $\mathcal{O}(g^3)$  component. As a result, the final expression of the amplitude will contain only the selected experimental IPS and will be ready for numerical evaluation.

Note that the dependence of the amplitude on the renormalized parameters appears at two different levels: 1) explicitly, by means of the pre-factors containing the coupling constants  $g$ ,  $s_\theta$  and  $g_s$ ; 2) implicitly, through the functions  $\mathcal{M}^{(1)}$ ,  $\mathcal{M}^{(2,\text{EW})}$ ,  $\mathcal{M}^{(2,\text{QCD})}$ ,  $\Sigma_{H,p}^{(1)}$  and  $\Pi_A^{(1)}$ , which a priori depend on the renormalized  $W$ -boson, Higgs-boson and fermion masses  $m_W$ ,  $m_H$  and  $m_f$ , and the weak-mixing angle  $\theta$  (or, equivalently, on the renormalized  $Z$ -boson mass  $m_Z = m_W/c_\theta$ ). Here the Cabibbo-Kobayashi-Maskawa matrix is identified with the unit matrix.

Finite renormalization for  $\mathcal{M}^{(2,\text{EW})}$ ,  $\mathcal{M}^{(2,\text{QCD})}$ ,  $\Sigma_{H,p}^{(1)}$  and  $\Pi_A^{(1)}$  is trivially achieved by identifying the renormalized parameters showing up in their explicit expressions with the tree-level solutions of the renormalization equations, which will depend on the chosen IPS.

The case of  $\mathcal{M}^{(1)}$ , instead, is more subtle. Let us introduce an appropriate suffix,  $\mathcal{M}_r^{(1)}$ , to indicate that the renormalized parameters  $\{p_{i,r}\}$  appear in  $\mathcal{M}^{(1)}$ . Solving at one-loop the renormalization equations amounts to replacing  $\{p_{i,r}\} \rightarrow \{p_{i,e} + \delta p_i\}$ , where  $\{p_{i,e}\}$  are taken from experiment and belong to the chosen IPS, whereas  $\{\delta p_i\}$  summarize the one-loop corrections. Finite renormalization is obtained by

$$\mathcal{M}_r^{(1)} \rightarrow \mathcal{M}_e^{(1)} + \sum_j \mathcal{M}_{p_{j,e}}^{(1)} \delta p_j, \quad \mathcal{M}_{p_{j,e}}^{(1)} = \left. \frac{\partial \mathcal{M}_r^{(1)}}{\partial p_{j,r}} \right|_{\{p_{i,r}=p_{i,e}\}}. \quad (55)$$

For  $H \rightarrow \gamma\gamma$ , the dependence of  $\mathcal{M}^{(1)}$  on  $g$  and  $\theta$  is encapsulated in the overall pre-factors of the amplitude of Eq.(54), and the renormalized mass of the  $Z$  boson  $m_Z$  does not show up at one loop. Therefore, it is convenient to choose the on-shell masses of the  $W$  boson,  $M_W$ , the Higgs boson,  $M_H$ , and the fermions,  $M_f$ , to be part of any IPS, and to evaluate derivatives respect to the associated renormalized masses  $m_W$ ,  $m_H$  and  $m_f$ .

We employ on-shell mass renormalization, as already discussed for the Higgs boson in Eq.(13). We use the one-loop solution of the renormalization equations for the Higgs-,  $W$ -boson and fermion masses,

$$m_B^2 = M_B^2 + \frac{g^2}{16\pi^2} \text{Re}\Sigma_B^{(1)}(-M_B^2), \quad B = H, W, \quad m_f = M_f + \frac{g^2}{16\pi^2} \text{Re}\Sigma_f^{(1)}(-M_f^2), \quad (56)$$

and write the amplitude of Eq.(54) as

$$\mathcal{A} = \frac{g^3 s_\theta^2}{16\pi^2} \left\{ \mathcal{M}^{(1)} + \frac{g^2}{16\pi^2} \overline{\mathcal{M}}^{(2,\text{EW})} + \frac{g^2 s_\theta^2}{16\pi^2} \mathcal{M}^{(1)} \Pi_A^{(1)}(0) + \frac{g_s^2}{16\pi^2} \mathcal{M}^{(2,\text{QCD})} \right\}, \quad (57)$$

where we have factorized the residual dependence on the renormalized coupling constants  $g$ ,  $\theta$  and  $g_s$ , defining

$$\overline{\mathcal{M}}^{(2,\text{EW})} = \mathcal{M}^{(2,\text{EW})} + \frac{1}{2} \mathcal{M}^{(1)} \text{Re}\Sigma_{H,p}^{(1)}(-M_H^2) + \sum_{i=W,H} \mathcal{M}_{M_i^2}^{(1)} \text{Re}\Sigma_i^{(1)}(-M_i^2) + 2 \sum_f M_f \mathcal{M}_{M_f^2}^{(1)} \text{Re}\Sigma_f^{(1)}(-M_f^2). \quad (58)$$

The last term in Eq.(58) contains a dependence on  $g_s$  coming from QCD corrections to finite top-quark mass renormalization. At this stage, we can safely identify all renormalized parameters showing up in the explicit expressions for  $\mathcal{M}^{(1)}$ ,  $\overline{\mathcal{M}}^{(2,\text{EW})}$ ,  $\mathcal{M}^{(2,\text{QCD})}$  and  $\Pi_A^{(1)}$  with the tree-level solutions of the chosen renormalization equations.

For electroweak corrections to  $H \rightarrow gg$  a similar decomposition holds,

$$\mathcal{A} = \frac{g g_s^2}{16\pi^2} \left\{ \mathcal{M}^{(1)} + \frac{g^2}{16\pi^2} \overline{\mathcal{M}}^{(2,\text{EW})} \right\}, \quad (59)$$

provided with color indices. Note that, concerning  $H \rightarrow gg$ , the derivative with respect to the Higgs-boson mass in Eq.(58) vanishes, since there is no dependence on  $m_H$  at LO.

We complete finite renormalization by relating the renormalized coupling constants  $g$ ,  $\theta$  and  $g_S$ , collected as simple pre-factors, to three additional experimental input data. For  $g_S$ , we write  $g_S^2 = 4\pi\alpha_S(\mu_R^2)$ , where  $\alpha_S$  is the strong-coupling constant and  $\mu_R$  the appropriate renormalization scale. For  $g$  and  $\theta$ , instead, we can select two data among  $G_F$ , the Fermi-coupling constant,  $\alpha$ , the fine-structure constant, and  $M_Z$ , the on-shell  $Z$ -boson mass.

Finite renormalization for  $H \rightarrow \gamma\gamma$ : IPS 1. The first IPS is  $\{G_F, \alpha\}$ . We start writing  $g^2 s_\theta^2 = e^2$ , where  $e$  is the renormalized electromagnetic-coupling constant, and use the relation for one-loop electric-charge renormalization,

$$e^2 = \frac{4\pi\alpha}{1 + \frac{\alpha}{4\pi}\Pi_A^{(1)}(0)}, \quad (60)$$

where  $\Pi_A^{(1)}$ , the one-loop photon vacuum-polarization function, is defined in Eq.(51). After using charge renormalization in the amplitude of Eq.(57), we observe that all terms containing  $\Pi_A^{(1)}$  cancel out and we obtain

$$\mathcal{A} = \frac{g\alpha}{4\pi} \left\{ \mathcal{M}^{(1)} + \frac{g^2}{16\pi^2} \overline{\mathcal{M}}^{(2,\text{EW})} + \frac{\alpha_S(\mu_R^2)}{4\pi} \mathcal{M}^{(2,\text{QCD})} \right\}. \quad (61)$$

For  $g$ , we employ the relation following from muon decay [68],

$$g = 2M_W \left( \sqrt{2}G_F \right)^{1/2} \left\{ 1 + \frac{G_F}{4\sqrt{2}\pi^2} \left[ \text{Re}\Sigma_W^{(1)}(-M_W^2) - \Sigma_W^{(1)}(0) - M_W^2 \delta_G \right] \right\}, \quad (62)$$

where, following Ref. [69], we split universal hard corrections to the muon lifetime, encapsulated in the  $W$ -boson self-energy  $\Sigma_W^{(1)}$ , and process-dependent components, summarized by the quantity  $\delta_G$ , whose explicit expression reads

$$\delta_G = 6 + \frac{7 - 4s_\theta^2}{2s_\theta^2} \ln(c_\theta^2). \quad (63)$$

Note that  $s_\theta$  and  $c_\theta$  are consistently fixed at the lowest order in perturbation theory by

$$c_\theta^2 = 1 - s_\theta^2, \quad s_\theta^2 = \frac{e^2}{g^2} = \frac{\pi\alpha}{\sqrt{2}G_F M_W^2}, \quad (64)$$

and we are avoiding any reference to the on-shell  $Z$ -boson mass  $M_Z$ . The amplitude will finally read

$$\mathcal{A} = \frac{\alpha M_W}{2\pi} \left( \sqrt{2}G_F \right)^{1/2} \left\{ \mathcal{M}^{(1)} + \frac{G_F M_W^2}{2\sqrt{2}\pi^2} \left( \mathcal{M}^{(2,\text{EW})} + \mathcal{M}_{\text{IP}S1}^{(2,\text{EW})} \right) + \frac{\alpha_S(\mu_R^2)}{4\pi} \mathcal{M}^{(2,\text{QCD})} \right\}, \quad (65)$$

where the total contribution from finite renormalization reads

$$\begin{aligned} \mathcal{M}_{\text{IP}S1}^{(2,\text{EW})} &= \frac{1}{2} \mathcal{M}^{(1)} \left[ \frac{\text{Re}\Sigma_W^{(1)}(-M_W^2) - \Sigma_W^{(1)}(0)}{M_W^2} - \delta_G + \text{Re}\Sigma_{H,p}^{(1)}(-M_H^2) \right] \\ &+ \sum_{i=W,H} \mathcal{M}_{M_i^2}^{(1)} \text{Re}\Sigma_i^{(1)}(-M_i^2) + 2 \sum_f M_f \mathcal{M}_{M_f^2}^{(1)} \text{Re}\Sigma_f^{(1)}(-M_f^2). \end{aligned} \quad (66)$$

Finite renormalization for  $H \rightarrow \gamma\gamma$ : IPS 2. The second IPS is  $\{G_F, M_Z\}$ . We start replacing Eq.(62) in Eq.(57), removing  $g$ . We get

$$\begin{aligned} \mathcal{A} &= s_\theta^2 \frac{M_W^3}{2\pi^2} \left( \sqrt{2}G_F \right)^{3/2} \left\{ \mathcal{M}^{(1)} + \frac{G_F M_W^2}{2\sqrt{2}\pi^2} \left[ \overline{\mathcal{M}}^{(2,\text{EW})} + \frac{3}{2} \mathcal{M}^{(1)} \left( \frac{\text{Re}\Sigma_W^{(1)}(-M_W^2) - \Sigma_W^{(1)}(0)}{M_W^2} - \delta_G \right) \right] \right. \\ &\quad \left. + s_\theta^2 \frac{G_F M_W^2}{2\sqrt{2}\pi^2} \mathcal{M}^{(1)} \Pi_A^{(1)}(0) + \frac{\alpha_S(\mu_R^2)}{4\pi} \mathcal{M}^{(2,\text{QCD})} \right\}. \end{aligned} \quad (67)$$

Next, we write  $s_\theta^2 = 1 - c_\theta^2$  and use the relation between renormalized masses  $c_\theta = m_w/m_z$ . After using vector-boson on-shell mass renormalization it follows that

$$s_\theta^2 = \left(1 - \frac{M_w^2}{M_z^2}\right) \left\{1 - \frac{G_F M_w^4}{2\sqrt{2}\pi^2(M_z^2 - M_w^2)} \left[ \frac{\text{Re}\Sigma_{ww}(-M_w^2)}{M_w^2} - \frac{\text{Re}\Sigma_{zz}(-M_z^2)}{M_z^2} \right] \right\}. \quad (68)$$

After employing Eq.(68) in Eq.(67), the amplitude will then be expressed through  $G_F$ ,  $M_w$  and  $M_z$ ;  $\delta_G$  is given in Eq.(63),  $s_\theta$  and  $c_\theta$  are fixed at the lowest order in perturbation theory by  $s_\theta^2 = 1 - c_\theta^2$  and  $c_\theta^2 = M_w^2/M_z^2$ , and any reference to the fine-structure constant  $\alpha$  is avoided.

Finite renormalization for  $H \rightarrow gg$ . Concerning finite renormalization for  $H \rightarrow gg$ , we start from

$$\mathcal{A} = \frac{g\alpha_s(\mu_R^2)}{4\pi} \left\{ \mathcal{M}^{(1)} + \frac{g^2}{16\pi^2} \overline{\mathcal{M}}^{(2,\text{EW})} \right\}, \quad (69)$$

and we use the result of Eq.(62) for muon decay to express  $g$  through  $G_F$ .

### 3.4.3 The doubly contracted WST identity for $H \rightarrow \gamma\gamma$ at two loops

Having introduced WFR factors and finite renormalization, we can now have a closer look at the doubly contracted WST identity with two on-shell photons of Eq.(19). As previously stressed, the computation of the identity requires Higgs-boson mass renormalization as a key ingredient, because bosonic couplings proportional to the  $\overline{\text{MS}}$ -renormalized Higgs-boson mass,  $m_H$ , appear at the one-loop level. Since the Higgs boson is emitted from a physical source, the associated momentum is on the mass shell,  $P^2 = -M_H^2$ , and  $m_H$  has to be consistently traded everywhere with  $M_H$ , including radiative corrections.

We write  $\mathcal{WI}_{dc}$  of Eq.(19) through the same decomposition already used for the amplitude in Eq.(47),

$$\mathcal{WI}_{dc}(0,0) = \frac{g^3 s_\theta^2}{16\pi^2} \mathcal{Z}_H^{-1/2} \mathcal{X}, \quad \mathcal{X} = -\frac{M_H^2}{2} \left[ F_D(0,0,-M_H^2) - \frac{M_H^2}{2} F_P(0,0,-M_H^2) \right], \quad (70)$$

where  $F_P = F_P^{(21)}$ . Next, we expand at one loop the Higgs-boson WFR factor  $\mathcal{Z}_H$  employing Eq.(53), and the function  $\mathcal{X}$  through Eq.(48), for  $F = \mathcal{X}$ ,

$$\mathcal{WI}_{dc}(0,0) = \frac{g^3 s_\theta^2}{16\pi^2} \left\{ \mathcal{X}^{(1)} + \frac{g^2}{16\pi^2} \left[ \mathcal{X}^{(2,\text{EW})} + \frac{1}{2} \mathcal{X}^{(1)} \text{Re}\Sigma_{H,p}^{(1)}(-M_H^2) \right] + \frac{g_s^2}{16\pi^2} \mathcal{X}^{(2,\text{QCD})} \right\}. \quad (71)$$

Since the identity holds for an on-shell Higgs boson, we perform finite renormalization employing Eq.(55) and obtain

$$\mathcal{WI}_{dc}(0,0) = \frac{g^3 s_\theta^2}{16\pi^2} \left\{ \mathcal{X}^{(1)} + \frac{g^2}{16\pi^2} \left[ \mathcal{X}^{(2,\text{EW})} + \frac{\mathcal{X}^{(1)}}{2} \text{Re}\Sigma_{H,p}^{(1)}(-M_H^2) + \mathcal{X}_{M_H^2}^{(1)} \text{Re}\Sigma_H^{(1)}(-M_H^2) \right] + \frac{g_s^2}{16\pi^2} \mathcal{X}^{(2,\text{QCD})} \right\}. \quad (72)$$

Note that we do not need to employ other renormalization equations, since the identity has to be proven both for renormalized and experimental masses and couplings. We compute the identity at one loop and we prove that  $\mathcal{X}^{(1)} = 0$ . The final form for the identity at two loops reads

$$\mathcal{WI}_{dc}(0,0) = \frac{g^3 s_\theta^2}{16\pi^2} \left\{ \frac{g^2}{16\pi^2} \left[ \mathcal{X}^{(2,\text{EW})} + \mathcal{X}_{M_H^2}^{(1)} \text{Re}\Sigma_H^{(1)}(-M_H^2) \right] + \frac{g_s^2}{16\pi^2} \mathcal{X}^{(2,\text{QCD})} \right\}. \quad (73)$$

Finally, it is harmless to replace renormalized parameters with the tree-level solutions of the renormalization equations,

$$\mathcal{WI}_{dc}(0,0) = \frac{\alpha M_w}{2\pi} \left( \sqrt{2} G_F \right)^{1/2} \left\{ \frac{G_F M_w^2}{2\sqrt{2}\pi^2} \left[ \mathcal{X}^{(2,\text{EW})} + \mathcal{X}_{M_H^2}^{(1)} \text{Re}\Sigma_H^{(1)}(-M_H^2) \right] + \frac{\alpha_s(\mu_R^2)}{4\pi} \mathcal{X}^{(2,\text{QCD})} \right\}. \quad (74)$$

We prove that  $\mathcal{WI}_{dc} \neq 0$ , explicitly we obtain

$$\mathcal{WI}_{dc}(0,0) = \left( \sqrt{2} G_F \right)^{3/2} M_w^4 \frac{\alpha}{16\pi^3} C_0(-M_H^2, 0, 0; M_w, M_w, M_w) \text{Im}\Sigma_H^{(1)}(-M_H^2), \quad (75)$$

where  $C_0$  is the scalar three-point function. The analysis of this paradox – violation of WSTI – will be postponed till section 5.3.

## 4 Manipulating Feynman integrals after generation of Feynman diagrams

In this section we summarize the techniques used after the generation of Feynman diagrams, performed with the FORM [39] program *GraphShot* [40], the projection of the amplitude onto the form factors of Eq.(11) with the projectors discussed in appendix B and the standard operations concerning the Dirac algebra. Before attempting the semi-analytical or numerical evaluation of (pseudo-)observables, we perform three kinds of simplifications and symbolic manipulations: firstly, we remove reducible scalar products; secondly, we employ integration-by-parts (IBP) identities [41] (see also Ref. [50]) for simplifying tadpole diagrams; finally, we achieve an optimal level of symmetrization for loop integrals.

### 4.1 Reduction of scalar products

Given a generic loop integral, it is possible to assign a one-to-one correspondence between a specific reducible scalar product containing at least one integration momentum and a particular propagator. This simple observation allows to recursively write loop-momentum dependent scalar products in terms of propagators, and employ a basic cancellation mechanism, when non-trivial numerator structures appear, through the algebraic master relation

$$\frac{2q \cdot p}{(q^2 + m_1^2)[(q+p)^2 + m_2^2]} = \frac{1}{q^2 + m_1^2} - \frac{1}{(q+p)^2 + m_2^2} - \frac{p^2 - m_1^2 + m_2^2}{(q^2 + m_1^2)[(q+p)^2 + m_2^2]}. \quad (76)$$

Note that the cancellation of a scalar product is associated with the disappearance of lines in the corresponding diagram; as a result, each diagram generates a set of child diagrams with a smaller number of propagators.

The number of independent scalar products involving loop momenta can exceed the number of propagators in a given diagram; therefore, some irreducible scalar products cannot be removed from the numerator functions. This is the well-known obstacle in achieving a full reduction for two-loop diagrams; for the special case of two-point functions, it can be by-passed through a judicious sub-loop reduction, as shown by the authors of Ref. [70]. Obviously, for a fixed number of loops and external legs, diagrams with a large number of internal lines, and thus more propagators, exhibit less irreducible scalar products than diagrams with a small number of internal lines. Note also that the choice of the scalar products which are considered as reducible and irreducible is to a large extent arbitrary.

For two-loop three-point functions we have two independent external momenta and two integration momenta; therefore, we have to deal with  $7 - I$  irreducible scalar products, where  $I$ , with  $4 \leq I \leq 6$ , is the number of internal lines, and a full reducibility using Eq.(76) is clearly not at hand.

As an example, let us consider the  $V^H$ -family diagram shown on the left-hand side of Eq.(77), where the Higgs boson couples to photons through a couple of  $W$  bosons and a top-bottom loop. After acting on the diagram with the projector  $P_D^{\mu\nu}$  as described in appendix B and saturating all free Lorentz indices, we remove all possible reducible scalar products and obtain:

$$\otimes P_D^{\mu\nu} = \tilde{C}_H \left[ M_W^2 - M_t^2 + 2p_1 \cdot q_1 \left( 1 - \frac{p_1 \cdot q_1}{p_1 \cdot p_2} \right) \right] \xrightarrow{-P} \left( \text{diagram with } M_W, M_t, M_b \text{ and } p_1, p_2 \right) + \left( \text{reduced diagrams} \right). \quad (77)$$

Here the non-planar diagram on the right-hand side corresponds to the  $V^H$  configuration defined in Fig. 27 (the dot-line denotes a light fermion), where the tensor structures have been stripped and explicitly collected as an overall factor in square brackets; the symbol  $\tilde{C}_H$  is proportional to  $\tilde{C}_H \propto p_1 \cdot p_2 + M_W^2 - M_t^2$  and we have denoted by “reduced diagrams” all diagrams with at least one internal line less. The scalar product

$p_1 \cdot q_1$  survives as an irreducible one, showing the presence of scalar, vector and tensor  $V^H$ -type integrals, which appear in the combination of Eq.(77).

The reduction procedure is repeated iteratively on the reduced diagrams; as a matter of fact, the  $V^H$  topology generates a set of eight sub-topologies, including simple factorized topologies (products of one-loop functions) and two-loop vertices, self-energies and vacuum diagrams, as illustrated in Fig. 6.

During the reduction procedure, we devote special care to preserve the canonical routing of loop momenta defined in appendix A. In Fig. 7 we show an explicit example for reducing the scalar products of a  $V^G$ -family diagram. Note that this configuration can appear after performing the reduction of the  $V^H$  diagram using Eq.(77). In step (1a), the scalar product  $q_2 \cdot p_1$  is removed; this operation leads to the appearance of an additional integral belonging to the  $V^E$  family which does not possess the standard routing of momenta as defined in Fig. 27. The canonical routing of momenta is recovered in step (1b) through a shift in the loop momenta which acts also on the remaining scalar product  $q_1 \cdot p_2$  and generates a new reducible scalar product  $q_2 \cdot p_2$ . The latter is then removed in step (2), leading to an additional integral of the  $S^A$  family.

In some cases, only the scalar configuration survives after the projection procedure. An example is the  $V^K$  configuration in the left-hand side of Eq.(78), where the Higgs boson couples to two photons through a couple of  $Z$  bosons and a top-quark loop. After applying the projector  $P_D^{\mu\nu}$  and removing reducible scalar products, one obtains the decomposition

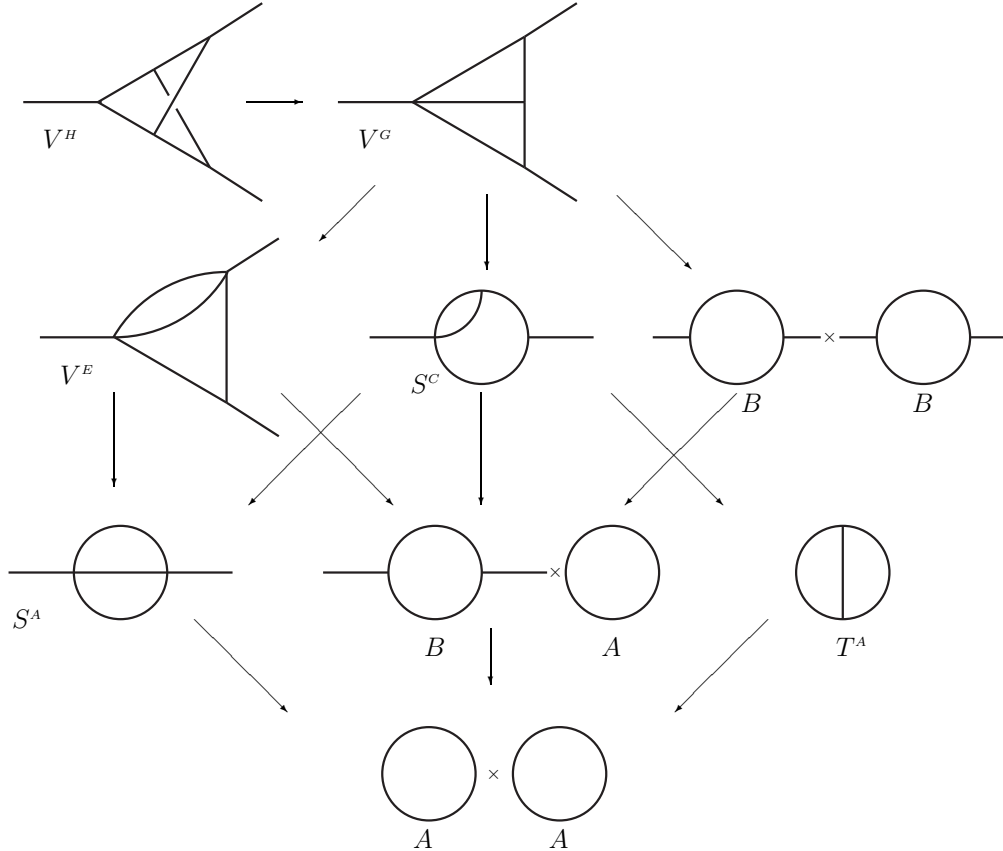


Figure 6: Generic child topologies of the  $V^H$  parent topology. The five-line  $V^G$  diagram is obtained by removing one line of the  $V^H$  diagram; the second line contains the child topologies of  $V^G$  ( $V^E$ ,  $S^C$  and  $B \times B$ ). The third line contains the topologies  $S^A$ ,  $B \times A$  and  $T^A$ , obtained by removing one line from the diagrams above. The arrows indicate the correspondences between parent and child topologies.

Figure 7: Reduction of scalar products for an example of the  $V^G$  family. The equations are valid for  $p_1^2 = p_2^2 = 0$ .

where the symbol  $\tilde{C}_K$  is proportional to  $\tilde{C}_K \propto 32(v_+^2 + v_-^2) M_t^2 (p_1 \cdot p_2 - M_Z^2 + 2 M_t^2) - 128 v_+ v_- M_t^2 (p_1 \cdot p_2 + 2 M_t^2)$ . Here,  $v_{\pm}$  are the  $V \pm A$  couplings  $Z\bar{t}t$ . Clearly, here no irreducible scalar products for the  $V^K$  topology remain, and only the scalar configuration survives.

## 4.2 Vacuum diagrams

The removal of scalar products illustrated in Fig. 6 shows that the vacuum diagram  $T^A$  appears after the reduction of the  $S^C$  self-energy. The explicit evaluation of  $T^A$  has been carried out in Ref. [71]. In addition, if the external momentum of the  $S^C$  integral corresponds to one of the photon momenta, the  $S^C$  integral is a vacuum integral with an increased power of one propagator. Furthermore, if additional loop-momentum dependent scalar products appear in the numerator of the  $S^C$  diagram, the integral has to be expanded in powers of the external momentum around zero; therefore, higher increased powers of the propagators can arise.

Vacuum integrals with increased powers of the propagators can be related to the  $T^A$  tadpole integral using the traditional IBP method. In particular, the relation between  $T^B$ , the tadpole diagram with one increased power of the third propagator (shown diagrammatically through a dot on the corresponding line) and  $T^A$  is given in Eq. (79) by

$$+ (2-n) \frac{m_1^2 - m_2^2 - m_3^2}{2 m_3^2 \lambda(m_1^2, m_2^2, m_3^2)} \textcircled{m_1} \textcircled{m_3} + (n-2) \frac{m_1^2 - m_2^2 + m_3^2}{2 m_3^2 \lambda(m_1^2, m_2^2, m_3^2)} \textcircled{m_2} \textcircled{m_3}, \quad (79)$$

with  $\lambda(x, y, z) = x^2 + y^2 + z^2 - 2xy - 2xz - 2yz$ .

After projecting the amplitude on the relevant form factors, it turns out that only the tadpole diagrams  $T^A$  and  $T^B$ , related to each other through Eq.(79), contribute to the amplitudes  $H \rightarrow \gamma\gamma$  and  $H \rightarrow gg$ .

### 4.3 Symmetrization of loop integrals

It is essential to exploit the symmetries of each diagram in order to reduce the number of integrals to be calculated and to identify equal configurations. We have taken into account the symmetries of the appearing one-loop and two-loop topologies, summarizing them in Tab. 1 and Tab. 2. In both tables, the first column denotes the topology and the second column enumerates the different symmetry transformations for a given topology; the third column contains the transformation of the loop momenta  $q_1$  and  $q_2$  and the fourth column the corresponding interchange of masses and external momenta. The identity transformation and the total reflection of all external momenta ( $p_1 \rightarrow -p_1$ ,  $p_2 \rightarrow -p_2$  and  $P \rightarrow -P$ , corresponding to the loop-momentum transformation  $q_1 \rightarrow -q_1$  and  $q_2 \rightarrow -q_2$ ), which leaves the loop integral unchanged, are not listed in Tab. 1 and Tab. 2. The largest number of symmetries can be observed for the  $V^H$  family.

$B$	(I)	$q \rightarrow -p - q'$	$m_1 \leftrightarrow m_2$
$C$	(I)	$q \rightarrow -p_1 - q'$	$m_1 \leftrightarrow m_2, -P \leftrightarrow p_2$
	(II)	$q \rightarrow -P - q'$	$m_1 \leftrightarrow m_3, p_1 \leftrightarrow p_2$
	(III)	$q \rightarrow -q'$	$m_2 \leftrightarrow m_3, -P \leftrightarrow p_1$
	(IV)	$q \rightarrow -P + q'$	$m_1 \rightarrow m_3, m_2 \rightarrow m_1, m_3 \rightarrow m_2,$ $p_1 \rightarrow -P, p_2 \rightarrow p_1, -P \rightarrow -p_2$
	(V)	$q \rightarrow -p_1 + q'$	$m_1 \rightarrow m_2, m_2 \rightarrow m_3, m_3 \rightarrow m_1,$ $p_1 \rightarrow p_2, p_2 \rightarrow -P, -P \rightarrow p_1$

Table 1: Symmetry transformations for one-loop topologies.

As an explicit simple example concerning the application of symmetry transformations, let us consider the case of the  $V^I$ -family integrals arising after the reduction of the  $V^K$ - and  $V^M$ -type Feynman diagrams shown in Fig. 8 (a) and (c). Note that the momenta routings of the two child  $V^I$ -family diagrams in Fig. 8 (b) and (d) are different; the application of symmetries aims to map the various integral representations onto a single one in order to allow for cancellations. The  $V^I$  family has three basic symmetry transformations, summarized in Tab. 2 and graphically illustrated in Fig. 9: here the first diagram corresponds to the standard integral representation of  $V^I$  as defined in appendix A; the symmetry transformation (I) amounts to exchanging the first and the second line of the self-energy insertion in the diagram; (II) corresponds to an exchange of the fourth and fifth lines (in this case also the external momenta are interchanged,  $p_1 \leftrightarrow -P$ ); symmetry (III) is a combination of symmetries (I) and (II). The two  $V^I$  child topologies in Fig. 8(b) and (d) are related through the symmetry transformation (III).

Finally, we stress that the procedures of reducing scalar products and symmetrizing loop integrals have been recursively performed in order to achieve a maximal simplification of the amplitude. Next, the remaining integrals are classified as scalar-, vector- and tensor-type integrals according to the number of irreducible scalar products in the numerators. The Lorentz structure of the loop integrals are expressed through the external momenta  $p_j$ , with  $j = 1, 2$ , and the metric tensor introducing suitable form factors. A FORTRAN code is generated and the form factors are then evaluated numerically employing the NAG library [72].

$T^A$	(I)	$q_1 \rightarrow q'_1,$	$q_2 \rightarrow q'_1 - q'_2$	$m_2 \leftrightarrow m_3$
	(II)	$q_1 \rightarrow -q'_1 + q'_2,$	$q_2 \rightarrow q'_2$	$m_1 \leftrightarrow m_2$
	(III)	$q_1 \rightarrow -q'_2,$	$q_2 \rightarrow -q'_1$	$m_1 \leftrightarrow m_3$
	(IV)	$q_1 \rightarrow -q'_1 + q'_2,$	$q_2 \rightarrow -q'_1$	$m_1 \rightarrow m_3, m_2 \rightarrow m_1, m_3 \rightarrow m_2$
	(V)	$q_1 \rightarrow -q'_2,$	$q_2 \rightarrow q'_1 - q'_2$	$m_1 \rightarrow m_2, m_2 \rightarrow m_3, m_3 \rightarrow m_1$
$S^A$	(I)	$q_1 \rightarrow -q'_2,$	$q_2 \rightarrow -q'_1$	$m_1 \leftrightarrow m_3$
	(II)	$q_1 \rightarrow -p - q'_1 + q'_2,$	$q_2 \rightarrow q'_2$	$m_1 \leftrightarrow m_2$
	(III)	$q_1 \rightarrow q'_1,$	$q_2 \rightarrow p + q'_1 - q'_2$	$m_2 \leftrightarrow m_3$
	(IV)	$q_1 \rightarrow -q'_2,$	$q_2 \rightarrow p + q'_1 - q'_2$	$m_1 \rightarrow m_2, m_2 \rightarrow m_3, m_3 \rightarrow m_1$
	(V)	$q_1 \rightarrow -p - q'_1 + q'_2,$	$q_2 \rightarrow -q'_1$	$m_1 \rightarrow m_3, m_2 \rightarrow m_1, m_3 \rightarrow m_2$
$S^C$	(I)	$q_1 \rightarrow -q'_1 + q'_2,$	$q_2 \rightarrow q'_2$	$m_1 \leftrightarrow m_2$
$S^D$	(I)	$q_1 \rightarrow -p - q'_1,$	$q_2 \rightarrow -p - q'_2$	$m_1 \leftrightarrow m_2, m_4 \leftrightarrow m_5$
$S^E$	(I)	$q_1 \rightarrow -q'_1 + q'_2,$	$q_2 \rightarrow q'_2$	$m_1 \leftrightarrow m_2$
	(II)	$q_1 \rightarrow q'_1,$	$q_2 \rightarrow q'_2$	$m_3 \leftrightarrow m_5$
	(III)	$q_1 \rightarrow -q'_1 + q'_2,$	$q_2 \rightarrow q'_2$	$m_1 \leftrightarrow m_2, m_3 \leftrightarrow m_5$
$V^E$	(I)	$q_1 \rightarrow -q'_1 + q'_2,$	$q_2 \rightarrow q'_2$	$m_1 \leftrightarrow m_2$
	(II)	$q_1 \rightarrow -q'_1,$	$q_2 \rightarrow -q'_2$	$m_3 \leftrightarrow m_4, p_2 \leftrightarrow -P$
	(III)	$q_1 \rightarrow q'_1 - q'_2,$	$q_2 \rightarrow -q'_2$	$m_1 \leftrightarrow m_2, m_3 \leftrightarrow m_4, -P \leftrightarrow p_2$
$V^I$	(I)	$q_1 \rightarrow -q'_1 + q'_2,$	$q_2 \rightarrow q'_2$	$m_1 \leftrightarrow m_2$
	(II)	$q_1 \rightarrow -q'_1,$	$q_2 \rightarrow -q'_2$	$m_4 \leftrightarrow m_5, -P \leftrightarrow p_1$
	(III)	$q_1 \rightarrow q'_1 - q'_2,$	$q_2 \rightarrow -q'_2$	$m_1 \leftrightarrow m_2, m_4 \leftrightarrow m_5, -P \leftrightarrow p_1$
$V^M$	(I)	$q_1 \rightarrow -q'_1 + q'_2,$	$q_2 \rightarrow q'_2$	$m_1 \leftrightarrow m_2$
	(II)	$q_1 \rightarrow -q'_1,$	$q_2 \rightarrow -q'_2$	$m_4 \leftrightarrow m_5, -P \leftrightarrow p_1$
	(III)	$q_1 \rightarrow q'_1 - q'_2,$	$q_2 \rightarrow -q'_2$	$m_1 \leftrightarrow m_2, m_4 \leftrightarrow m_5, -P \leftrightarrow p_1$
$V^G$	(I)	$q_1 \rightarrow -P - q'_2,$	$q_2 \rightarrow -P - q'_1$	$m_1 \leftrightarrow m_5, m_2 \leftrightarrow m_4, p_1 \leftrightarrow p_2$
$V^K$	(I)	$q_1 \rightarrow -P - q'_1,$	$q_2 \rightarrow -P - q'_2$	$m_1 \leftrightarrow m_2, m_4 \leftrightarrow m_6, p_1 \leftrightarrow p_2$
$V^H$	(I)	$q_1 \rightarrow p_2 - q'_1,$	$q_2 \rightarrow p_1 - q'_2$	$m_1 \leftrightarrow m_2, m_3 \leftrightarrow m_4, m_5 \leftrightarrow m_6$
	(II)	$q_1 \rightarrow -p_1 - q'_1 + q'_2,$	$q_2 \rightarrow q'_2$	$m_1 \leftrightarrow m_3, m_2 \leftrightarrow m_4, -P \leftrightarrow p_2$
	(III)	$q_1 \rightarrow q'_1,$	$q_2 \rightarrow -p_2 + q'_1 - q'_2$	$m_3 \leftrightarrow m_6, m_4 \leftrightarrow m_5, -P \leftrightarrow p_1$
	(IV)	$q_1 \rightarrow p_2 - q'_2,$	$q_2 \rightarrow p_1 - q'_1$	$m_1 \leftrightarrow m_6, m_2 \leftrightarrow m_5, p_1 \leftrightarrow p_2$
	(V)	$q_1 \rightarrow P + q'_1 - q'_2,$	$q_2 \rightarrow p_1 - q'_2$	$m_1 \leftrightarrow m_4, m_2 \leftrightarrow m_3, m_5 \leftrightarrow m_6, p_2 \leftrightarrow -P$
	(VI)	$q_1 \rightarrow p_2 - q'_1,$	$q_2 \rightarrow P - q'_1 + q'_2$	$m_1 \leftrightarrow m_2, m_3 \leftrightarrow m_5, m_4 \leftrightarrow m_6, p_1 \leftrightarrow -P$
	(VII)	$q_1 \rightarrow q'_2,$	$q_2 \rightarrow q'_1$	$m_1 \leftrightarrow m_5, m_2 \leftrightarrow m_6, m_3 \leftrightarrow m_4, p_1 \leftrightarrow p_2$
	(VIII)	$q_1 \rightarrow q'_2,$	$q_2 \rightarrow -p_2 - q'_1 + q'_2$	$m_1 \rightarrow m_4, m_2 \rightarrow m_3, m_3 \rightarrow m_5,$ $m_4 \rightarrow m_6, m_5 \rightarrow m_1, m_6 \rightarrow m_2,$ $p_1 \rightarrow p_2, p_2 \rightarrow -P, -P \rightarrow p_1$
	(IX)	$q_1 \rightarrow p_2 - q'_2,$	$q_2 \rightarrow P + q'_1 - q'_2$	$m_1 \rightarrow m_3, m_2 \rightarrow m_4, m_3 \rightarrow m_6,$ $m_4 \rightarrow m_5, m_5 \rightarrow m_2, m_6 \rightarrow m_1,$ $p_1 \rightarrow p_2, p_2 \rightarrow -P, -P \rightarrow p_1$
	(X)	$q_1 \rightarrow P - q'_1 + q'_2,$	$q_2 \rightarrow p_1 - q'_1$	$m_1 \rightarrow m_6, m_2 \rightarrow m_5, m_3 \rightarrow m_1,$ $m_4 \rightarrow m_2, m_5 \rightarrow m_4, m_6 \rightarrow m_3,$ $p_2 \rightarrow p_1, p_1 \rightarrow -P, -P \rightarrow p_2$
	(XI)	$q_1 \rightarrow -p_1 + q'_1 - q'_2,$	$q_2 \rightarrow q'_1$	$m_1 \rightarrow m_5, m_2 \rightarrow m_6, m_3 \rightarrow m_2,$ $m_4 \rightarrow m_1, m_5 \rightarrow m_3, m_6 \rightarrow m_4,$ $p_1 \rightarrow -P, p_2 \rightarrow p_1, -P \rightarrow p_2$

Table 2: Symmetry transformations for two-loop topologies.

## 5 Behavior of two-loop diagrams around a normal threshold

In this section we will discuss one of the main results of the paper: by carefully studying all singularities of Feynman diagrams we propose the two-loop implementation of a renormalization scheme which cures

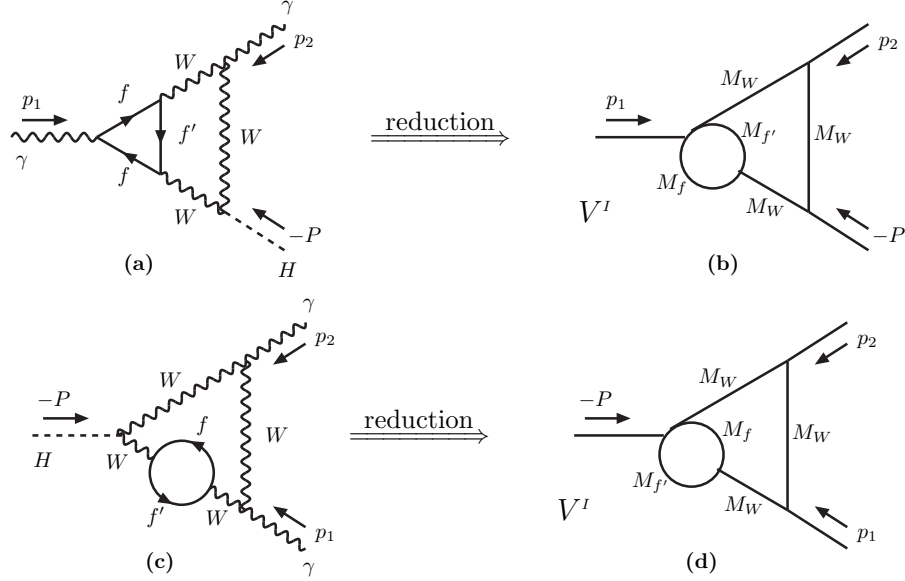


Figure 8: The  $V^K$ - and  $V^M$ -type Feynman diagrams (a) and (c), where  $f$  and  $f'$  stand for fermions of the same doublet, lead to the  $V^I$  integrals (b) and (d) after reduction of scalar products.

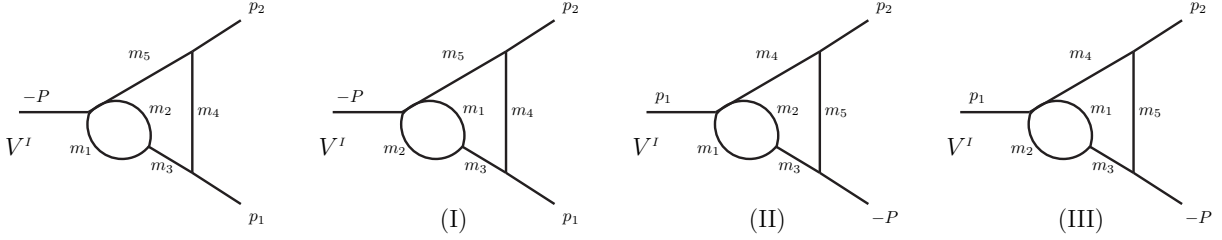


Figure 9: The symmetries of the  $V^I$  family enumerated in Tab. 2.

anomalous behaviors of the amplitude.

Feynman diagrams have a complicated analytical structure as functions of the external Mandelstam invariants and the internal masses. A frequently encountered singular behavior is associated with the so-called normal thresholds: the leading Landau singularities [73] of self-energy-like diagrams which can appear, in more complicated diagrams, as sub-leading singularities. In this section we discuss how the amplitudes for  $H \rightarrow \gamma\gamma$  and  $H \rightarrow gg$  behave around a normal threshold, with special emphasis to the problem of possible square-root and logarithmic singularities.

Without loss of generality, let us consider the case of the  $H \rightarrow \gamma\gamma$  decay in the setup where all light fermions are taken to be massless. As far as normal thresholds are concerned, we have the possibilities  $M_H = M_W, M_Z, 2M_W, 2M_Z, 2M_t$ , as illustrated in terms of cut diagrams in Fig. 10. Note that, as observed by the authors of Ref. [28], there is no cut at  $M_H = 0$  even in presence of massless fermions; indeed, the two-particle cut of the first diagram of Fig. 10 is zero because of the helicity structure of the diagram.

The  $M_H = M_W, M_Z$  cuts are identified by the configuration shown in the second and third diagrams of Fig. 10. Note that, for  $H \rightarrow \gamma\gamma$ , the imaginary part is not exactly zero below the single- $W$  threshold; this is due to the introduction of complex masses for vector bosons, as we will explain in detail in section 5.3. It is worth mentioning the behavior of the one-loop amplitude which is rapidly decreasing for small values of  $M_H$ , as shown in Fig. 11 for  $H \rightarrow gg$ . Here, once again, we use a complex  $W$  mass and, therefore, the imaginary part is different from zero even below the  $\bar{t}\bar{t}$  threshold. We have performed a dedicated analysis of the behavior of the amplitude around *single* thresholds which shows that regular behavior is a consequence

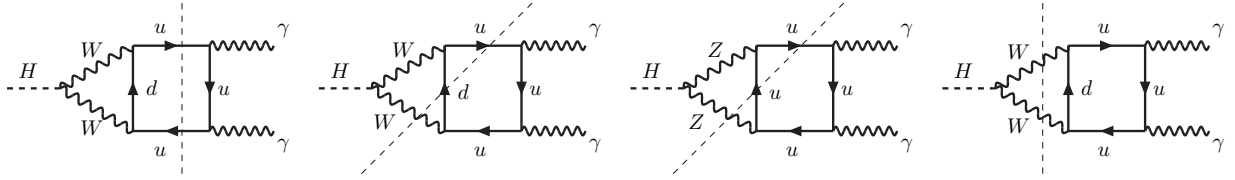


Figure 10: Sample two- and three-particle cut diagrams for  $H \rightarrow \gamma\gamma$ . The mass of the up and down quarks is neglected.

of a delicate mechanism of numerical cancellation among several diagrams, e.g.  $V^H, V^G$  doubly collinear and  $V^E$  simply collinear.

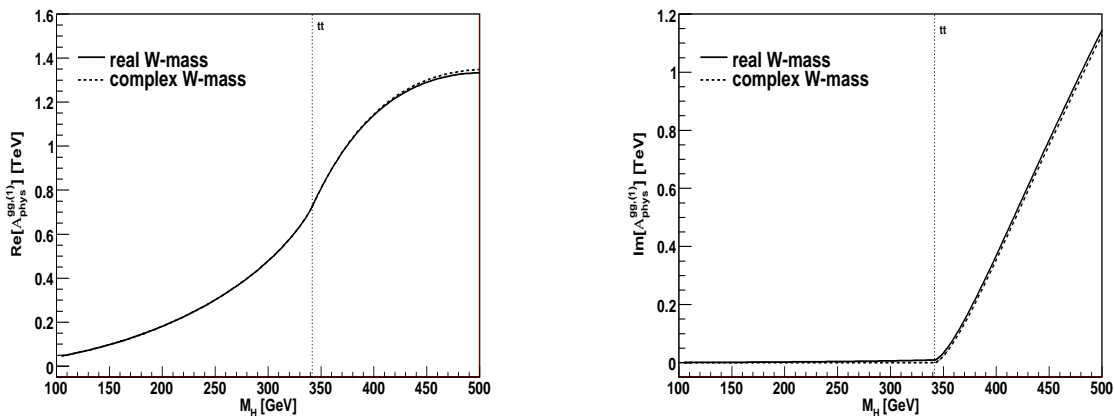


Figure 11: Real and imaginary parts of the one-loop  $H \rightarrow gg$  amplitude.

Having discussed the single vector-boson thresholds, we move to the double ones, identified for example by the cut of the fourth diagram of Fig. 10.

### 5.1 Square-root singularities

In this section we are interested in the problem of possible square-root singularities of the amplitude. When present, they are unphysical, although integrable; the solution to the apparent puzzle consists, as we will argue, in replacing real masses of unstable particles with their complex poles.

In order to illustrate the problem, let us consider the following integral, related to a generalized one-loop two-point function:

$$I_\alpha^n = \int_0^1 dx x^n (x^2 - x + \mu^2 - i0)^{-\alpha}, \quad (80)$$

where  $n$  is a non-negative integer. When  $\beta = 0$ , with  $\beta^2 = 1 - 4\mu^2$ , the integration contour is pinched between the two singular points  $x_\pm = (1 \pm \beta)/2$ , and the integral of Eq.(80) is singular, with a branch point of the two-particle cut  $\mu^2 = 1/4$ ; for  $\alpha \geq 1$  we find

$$I_\alpha^0 \sim \left(-\frac{\beta}{2}\right)^{1-2\alpha} B\left(\frac{1}{2}, \alpha - \frac{1}{2}\right), \quad \beta \rightarrow 0, \quad (81)$$

where  $B$  is the Euler beta function. To be more explicit, let us consider the UV decomposition of section 2 for the generalized one-loop two-point function with equal masses

$$B_0(k, l; s, m, m) = \sum_{i=-1}^1 B_0(k, l; s, m, m; i) F_i^1(s), \quad (82)$$

where  $k$  and  $l$  are the powers of the two propagators. Concerning the finite parts for the  $k = l = 1$  and  $k = 2, l = 1$  configurations, we obtain

$$B_0(1, 1; s, m, m; 0) = 2 - \ln \frac{m^2}{s + i0} - \beta L_\beta, \quad B_0(2, 1; s, m, m; 0) = -\frac{1}{\beta} L_\beta,$$

$$L_\beta = \ln \frac{\beta + 1}{\beta - 1}, \quad \beta^2 = 1 - 4 \frac{m^2}{s + i0}. \quad (83)$$

In general, for  $k + l > 2$ , we have

$$B_0(k, l; s, m, m; 0) \sim \beta^{5-2(k+l)}, \quad \beta \rightarrow 0, \quad (84)$$

and we can easily conclude that the generalized one-loop two-point function has an (unphysical) singularity at  $s = 4m^2 \forall k, l | k + l > 2$ . For practical applications, one has to distinguish between the above- and below-threshold regions,

$$\beta^2 = a^2 \geq 0, \quad L_\beta = \ln \frac{1+a}{1-a} - i\pi \sim -i\pi, \quad s \rightarrow 4m^2 |_+,$$

$$\beta^2 = -a^2 \leq 0, \quad L_\beta = i \left( \arctan \frac{2a}{1-a^2} + \pi \right) \sim i\pi, \quad s \rightarrow 4m^2 |_- . \quad (85)$$

Therefore, the generalized one-loop two point function with  $k + l = 3$  generates a square-root  $1/\beta$ -divergent behavior, with  $\beta^2 = 1 - 4M_W^2/M_H^2$  or  $\beta^2 = 1 - 4M_Z^2/M_H^2$ , associated with the normal threshold related to the two-particle cut (the leading Landau singularity).

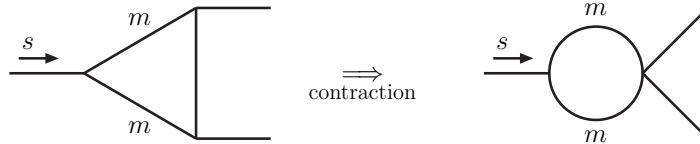


Figure 12: One-loop vertex with two equal masses and its sub-diagram giving the sub-leading square-root singularity.

Let us now consider three-point functions, and investigate the behavior of the vertex of Fig. 12 around the normal threshold located at  $s = 4m^2$ . The leading Landau singularity of the vertex is the so-called anomalous threshold; the normal threshold shows up as a sub-leading singularity. Since the sub-leading singularity for a graph is the leading one for any of the contracted sub-graphs, we easily conclude that the singular behavior of the one-loop vertex of Fig. 12 around  $s = 4m^2$  is due to the sub-graph where we shrink a line to a point; the singularity is a branch point in the complex  $s$ -plane.

The same argument can be repeated for all diagrams with any number of external legs where we can cut *two and only two* lines with mass  $m$ ; any normal threshold will be a sub-(sub-...) leading singularity, and a  $1/\beta$  behavior will show up only if the reduced sub-graph, responsible for the singularity, can be reduced to the generalized one-loop two-point function of Eq.(83),  $\dot{B}_0(s, m, m) = B_0(2, 1; s, m, m; 0)$ . A  $\dot{B}_0(s, m, m)$  function is related to the derivative of a  $B_0(1, 1; s, m, m)$  function and therefore emerges in the computation whenever we include WFR factors for the external legs or we perform finite renormalization of the mass of an internal particle, as depicted in Fig. 13. In the second case, generalized one-loop triangle functions appear, and it is known that they can always be reduced to  $\dot{B}_0$  functions using IBP identities (this is just another way to say that the normal threshold is a sub-leading singularity for a generalized three-point function).

Concerning genuine two-loop diagrams, we observe that a  $B_0$  configuration can only arise if we have a self-energy insertion in a two-loop diagram. A two-loop vertex containing a self-energy insertion, leading to a  $1/\beta$ -divergent behavior, is depicted in Fig. 14. For this diagram it is possible to find a representation where the singular part is completely written in terms of one-loop diagrams, as shown in the figure. The remainder can be cast in a form suited for numerical integration.

Note that the unphysical  $1/\beta$  behavior, generated by the diagram of Fig. 14, exactly cancels the one coming from mass finite renormalization. This is strictly true only in a complex renormalization scheme

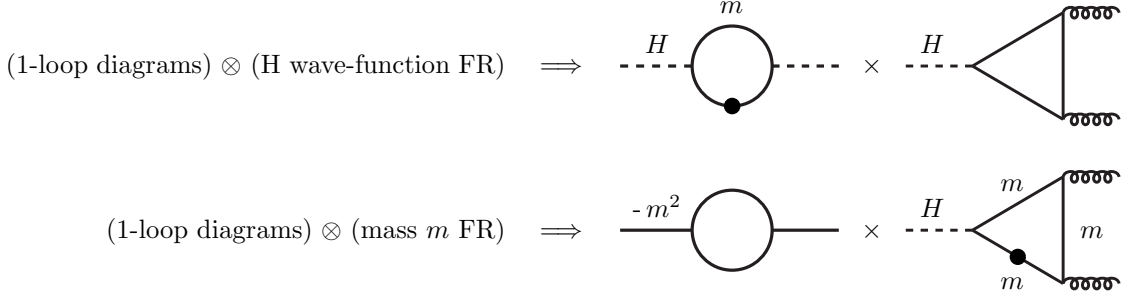


Figure 13: Singular  $\beta^{-1}$  behavior at the normal  $m$  threshold coming from WFR and mass finite renormalization.

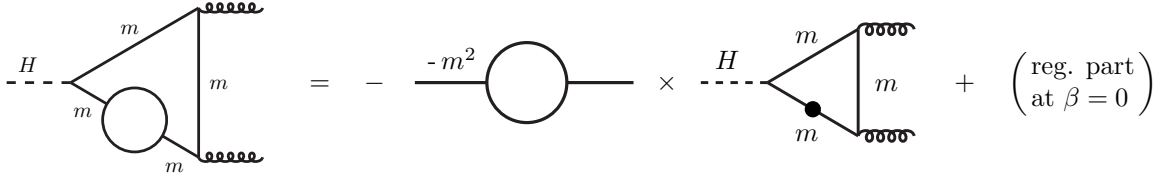


Figure 14: Singular  $\beta^{-1}$  behavior at the normal  $m$  threshold coming from self-energy insertions ( $V^M$  topology). The generalized one-loop triangle function in the right-hand side is related to the generalized one-loop self-energy of Eq.(83) through IBP identities.

because, for on-shell real masses, only the real part of the self-energy in Fig. 13 is taken and the cancellation does not take place for the corresponding imaginary part generated by the two-loop diagram of Fig. 14. This is not surprising at all: self-energy insertions, signaling the presence of an unstable particle, should not be there. They are the consequence of a misleading organization of the perturbative expansion; Dyson-resummed propagators should be used and complex poles should replace real on-shell masses. The remaining  $1/\beta$  singularity is therefore coming only from the wave-function renormalization of the Higgs boson. This unphysical behavior is strictly connected to the problem of defining a proper WFR for an unstable particle, as pointed out in section 3.1.

It is interesting to note that for the  $t\bar{t}$  threshold in  $H \rightarrow gg$  the  $\dot{B}_0$ -functions that are potentially dangerous always appear multiplied by  $\beta^2$ , as it happens for QCD corrections; the same is not true for pseudo-scalar Higgs decay, cfr. Fig. 4 of [9].

Finally, we observe that a more severe behavior associated with  $\beta \rightarrow 0$  should not show up; for instance, we have verified that  $1/\beta^2$  terms which appear as a consequence of the reduction procedure for the  $H \rightarrow \gamma\gamma$  decay are of the form  $F(M_H^2)/(M_H^2 - 4M_W^2)$ , with  $F(4M_W^2) = 0$ .

## 5.2 Logarithmic singularities

Let us consider the scalar two-loop diagram of the  $V^\kappa$  family shown in Fig. 15, and derive the corresponding integral in parametric space. We introduce the quadratic forms

$$\chi(x) = \left(x - \frac{1}{2}\right)^2 - \frac{1}{4}\beta^2, \quad \xi(x, y) = x(x-1)y^2 + \frac{1}{4}(1-\beta^2), \quad \beta^2 = 1 - \frac{4m^2}{s}, \quad (86)$$

where  $s = -P^2 > 0$  and  $m$  is the mass of the solid line (wavy lines correspond to massless particles). We obtain

$$V^\kappa = \frac{2}{s^2} \int_0^1 \frac{dx dy}{y \chi(x)} \left[ \text{Li}_2 \left( 1 - \frac{y \chi(x)}{\chi(xy)} \right) - \text{Li}_2 \left( 1 - \frac{y \chi(x)}{\xi(x, y)} \right) \right]. \quad (87)$$

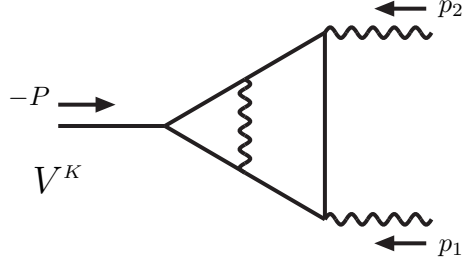


Figure 15: The irreducible scalar two-loop vertex diagram of the  $V^K$  family showing up a logarithmic divergence. Solid lines represent a massive particle with mass  $m$ , whereas wavy lines correspond to massless particles.

Since we are interested in the behavior around  $\beta \rightarrow 0$ , we split  $V^K$  into a singular and regular part,

$$V^K = V_{\text{sing}}^K + V_{\text{reg}}^K = \frac{2}{s^2} \int_0^1 \frac{dx dy}{y \chi(x)} \left[ \text{Li}_2 \left( 1 - \frac{y \chi(x)}{\chi(xy)} \right) - \zeta(2) \right] + V_{\text{reg}}^K. \quad (88)$$

The singular part  $V_{\text{sing}}^K$  will be written as [74]

$$V_{\text{sing}}^K = \frac{2}{s^2} \int_0^1 dt \frac{\ln t}{1-t} I(t), \quad I(t) = \int_0^1 dx dy \left[ (1-t)\chi(xy) + ty\chi(x) \right]^{-1} = \int_0^1 dx dy \left[ a(x-X)^2 + \lambda \right]^{-1}, \quad (89)$$

where we have introduced the short-hand notations

$$a = \tau y, \quad X = \frac{1}{2\tau}, \quad \lambda = \frac{t(1-t)}{4\tau} \left[ (1-y)^2 - \beta^2 (y+T) \left( y + \frac{1}{T} \right) \right], \quad (90)$$

with  $\tau = (1-t)y + t$  and  $T = t/(1-t) > 0$ .  $I(t)$  can be split into two parts,

$$I(t) = B\left(\frac{1}{2}, \frac{1}{2}\right) \int_{y_{\min}}^1 dy a^{-1/2} \lambda^{-1/2} - \frac{1}{2} \sum_{i=1,2} \int_0^1 dx dy (-1)^i X_i x^{-1/2} (aX_i^2 + \lambda x)^{-1}. \quad (91)$$

Here  $X_1 = -X$ ,  $X_2 = 1 - X$  and  $B(x, y)$  is the Euler beta function. The second term of Eq.(91) is regular for  $\beta = 0$ ; the first term, instead, shows a singularity due to the fact that  $\lambda \sim (1-y)^2$  for  $\beta \rightarrow 0$ . However, we have a singular behavior only if  $0 \leq X \leq 1$ , which requires  $y \geq y_{\min} = \max\{0, (t-1/2)/(t-1)\}$ . Being interested in the leading behavior for  $\beta \rightarrow 0$ , we can extend the integration domain in the first term to  $[0, 1]$  without modifying the divergent behavior of the diagram. The singular part is then given by

$$I_{\text{sing}}(t) = \frac{2\pi}{\sqrt{t(1-t)}} \int_0^1 dy y^{-1/2} \left[ (1-y)^2 - \beta^2 (1+Ty) \left( 1 + \frac{y}{T} \right) \right]^{-1/2} = \frac{2\pi}{\sqrt{t(1-t)}} J(t),$$

$$\begin{aligned} J(t) &= \frac{1}{2\pi i} \int_{-i\infty}^{+i\infty} ds B\left(s, \frac{1}{2} - s\right) (-\beta^2 - i0)^{s-1/2} \int_0^1 dy y^{-1/2} (1-y)^{-2s} (1+Ty)^{s-1/2} \left( 1 + \frac{y}{T} \right)^{s-1/2} \\ &= \frac{1}{2\pi i} \int_{-i\infty}^{+i\infty} ds \frac{\Gamma(s) \Gamma(1/2-s) \Gamma(1-2s)}{\Gamma(3/2-2s)} (-\beta^2 - i0)^{s-1/2} F_1\left(\frac{1}{2}, \frac{1}{2}-s, \frac{1}{2}-s, \frac{3}{2}-2s; -T, -\frac{1}{T}\right), \end{aligned} \quad (92)$$

where  $0 < \text{Res} < 1/2$  and  $F_1$  denotes the first Appell function. In order to obtain the expansion corresponding to  $\beta \rightarrow 0$ , we close the integration contour over the right-hand complex half-plane at infinity. The leading (double) pole is at  $s = 1/2$ ; therefore, we obtain

$$J(t) = -\frac{1}{2} \ln(-\beta^2 - i0) + \mathcal{O}(1), \quad \beta \rightarrow 0. \quad (93)$$

Inserting the result into Eq.(89) and using  $\int_0^1 dt t^{-1/2} (1-t)^{-3/2} \ln t = -2\pi$ , we get

$$V_{\text{sing}}^\kappa = \frac{4\pi^2}{s^2} \ln(-\beta^2 - i0) + \mathcal{O}(1), \quad \beta \rightarrow 0. \quad (94)$$

If the massive loop in Fig. 15 is made of top quarks, the contribution of the  $V^\kappa$  integral to the amplitude behaves like  $\beta^2 V^\kappa$  and, therefore, the logarithmic singularity is  $\beta^2$ -protected at threshold; however, the same is not true for a  $W$ -loop. Our result of Eq.(94) is confirmed by the evaluation of  $V^\kappa$  of Ref. [10] in terms of generalized log-sine functions. Starting from Eq. (6.34) of Ref. [10] and using the results of Ref. [75] we expand around  $\theta = \pi$ , where  $x = e^{i\theta} = (\beta - 1)(\beta + 1)$ , with  $0 < \theta < \pi$ . This gives for the leading behavior of  $V^\kappa$  below threshold  $(\pi^2/2) \ln(\theta - \pi)$ , where  $\ln(-\beta^2) = \ln(\theta - \pi)^2 - \ln 2$ . The same behavior can also be extracted from the results of Ref. [9].

Logarithmic singularities of the kind discussed in this section are a remnant of the one-loop Coulomb singularity of one-loop sub-diagrams. An alternative approach that automatically resums large Coulomb singularities at threshold has been pursued in Ref. [76]. The reader should be aware that in the pseudo-scalar decay the real and imaginary parts of the form factor may be significantly different from the lowest order perturbative ones<sup>1</sup>.

### 5.3 Complex masses

In this section we set up and discuss our implementation of a consistent and gauge-invariant treatment of unstable particles in NNLO radiative corrections.

Our two-loop renormalization scheme has been described in details in section 3 where counterterms have been introduced, different choices of IPSs considered and finite renormalization of lagrangian parameters discussed. In short, this represents the so-called

- RM - scheme

where masses are the real on-shell ones; it gives the extension of the generalized minimal subtraction scheme up to two loop level. The analysis of section 5 has shown the presence of pathological features and the cure proceeds in two steps. Our first, pragmatcal, solution to the problems induced by unstable internal particles has been presented in Ref. [38] (for an alternative approach to the problem of unphysical threshold singularities connected to WFR factors, see Ref. [77]); the corresponding scheme will be termed minimal complex mass scheme (hereafter MCM), the first emergency kit.

- MCM - scheme

To evaluate the amplitude we start by removing the Re label in those terms that, coming from finite renormalization, violate WSTIs. For instance, when we compute the doubly contracted WSTI for the full two-loop amplitude in  $H \rightarrow \gamma\gamma$  we obtain the result of Eq.(75): pure two-loop contribution to the WSTI gives  $\Sigma_H^{(1)}(-M_H^2)$  while finite renormalization gives its real part  $\text{Re} \Sigma_H^{(1)}(-M_H^2)$ . Therefore, the WSTI is violated above the  $WW$  threshold, as shown in section 3.4.3.

Furthermore, we decompose the amplitude for  $H \rightarrow \gamma\gamma$  according to

$$\mathcal{A}_{\text{phys}} = \left(\sqrt{2} G_F M_W^2\right)^{1/2} \frac{\alpha}{2\pi} A_{\text{phys}}, \quad A_{\text{phys}} = A_{\text{ex}}^{(1)} + \frac{G_F M_W^2}{2\sqrt{2}\pi^2} \left[ \frac{A_R^{(2)}}{\beta} + A_L^{(2)} \ln(-\beta^2 - i0) + A_{\text{rem}}^{(2)} \right], \quad (95)$$

and prove that, as expected,  $A_R^{(2)}$ ,  $A_L^{(2)}$  and  $A_{\text{rem}}^{(2)}$  separately satisfy the WSTI. The latter fact allows us to minimally modify  $A_{R,L}^{(2)}$  by working in the complex-mass scheme of Ref. [60]: we include complex masses in the gauge-invariant leading part of the two-loop amplitude as well as in the one-loop part.

The decomposition of Eq.(95) deserves a further comment. As we stressed in section 5.1, there are three sources of  $1/\beta$  terms: a) pure two-loop diagrams of the  $V_M$  family, i.e. bubble insertions on the internal lines of the one-loop triangle; b)  $W$ -mass renormalization, i.e. on-shell  $W$  self-energy  $\times$  the mass-squared

<sup>1</sup>A discussion with M. Spira on the last two points is gratefully acknowledged.

derivative of the one-loop  $W$  triangle (the latter giving rise to  $1/\beta$ ); c) Higgs wave-function renormalization factor  $\times$  lowest order (the former giving rise to  $1/\beta$ ). One can easily prove that only c) survives in MCM and a,b), which are separately singular, add up to a finite contribution ( $\beta \rightarrow 0$ ); their divergence is an artifact of expanding Dyson-resummed propagators in the on-shell approach.

The  $\ln\beta$ -dependent term originates from pure two-loop diagrams of the  $V_\kappa$  family and it is a remnant of the one-loop Coulomb singularity of one-loop sub-diagrams.

The amplitude for  $H \rightarrow gg$  is different in some points, for instance we have no  $V^\kappa$  diagram with a logarithmic behavior. Also the violation of WSTIs, described above, is specific to  $H \rightarrow \gamma\gamma$  since we have no one-loop bosonic triangle. Further details have been presented in Ref. [78].

The one-loop  $H \rightarrow \gamma\gamma$  amplitude, with a complex  $W$  mass, is shown in Fig. 16 around the  $WW$  threshold including a comparison with the real- $W$ -mass amplitude. We have also analyzed the effect of (artificially)

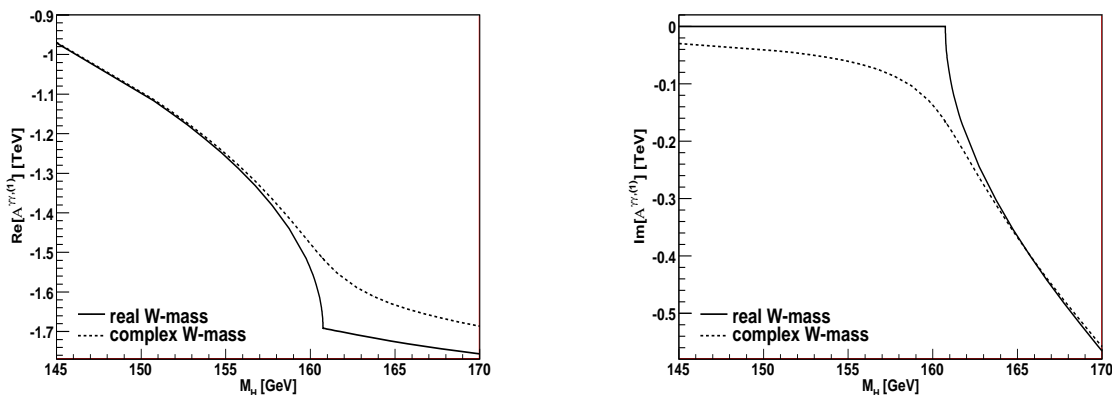


Figure 16: Real and imaginary parts of the one-loop  $H \rightarrow \gamma\gamma$  amplitude with real and complex  $W$ -boson mass. Note the sizable difference with Fig. 11.

varying the imaginary part of the  $W$ -boson complex mass (more details can be found in Ref. [78]), showing that our *complex* result reproduces the *real* one (with a complex Higgs-mass renormalization condition) in the limit  $\Gamma_W \rightarrow 0$ . Here, a comment is needed: we introduce complex masses as poles on the second Riemann sheet, a fact that requires a careful analytical continuation of loop integrals.

Let us consider the decay  $H \rightarrow \gamma\gamma$  in the RM scheme; on-shell renormalization spoils the complete cancellation between pure two-loop diagrams and  $W$ -mass renormalization mentioned before. As a consequence the RM scheme badly fails to approximate the complex mass results above the  $WW$  threshold; here RM is not the smooth limit  $\Gamma_W \rightarrow 0$  of MCM and we understand the reason, RM is missing a cancellation which is instrumental in building a consistent theory of unstable particles. If RM scheme is further modified by arbitrarily forcing this cancellation the corresponding result is the smooth limit just mentioned. Thus we have an additional argument to reject RM; at two-loop this scheme is wholly inconsistent.

It is worth noting that cancellation between mass renormalization for some internal line and bubble insertion in the same line, as far as divergent terms are concerned, is a strict consequence of Dyson resummation with complex poles, see Eq. (195) of Ref. [44] and consequent discussion.

Finally, we mention the fact that MCM can be forced to agree with RM in the limit  $\Gamma_W \rightarrow 0$  only if we adopt the unjustified approach of continuing the  $W$  self-energy in different Riemann sheets depending on its origin, irreducible two-loop diagrams or finite renormalization.

In a nutshell, the MCM scheme has been designed to cure the unphysical infinities of two-loop amplitudes, namely those points where the amplitude is artificially infinite; it does not deal with cusps associated with the crossing of normal-thresholds present in  $A_{\text{rem}}^{(2)}$ , as described in detail in Ref. [78]. Note that this is not only an aesthetical issue but also a concrete problem in assessing the impact of electroweak NLO corrections on, say, Higgs production via gluon gluon fusion: observing the effect of NNLO QCD corrections with respect to NLO ones one is lead to understand possible sources of additional large corrections. Electroweak

corrections, typically around the  $WW$  threshold, can reach a 10% in the MCM scheme due to a magnified cusped behavior.

- CM - scheme

Further to the last point, we have undertaken the task of introducing the (complete) complex-mass scheme (CM), based on Ref. [60], as explained for a two-loop calculation in Sect. 10 of [44]. This means that all two-loop diagrams must be computed with complex  $M_W, M_Z$  masses, whereas the top quark mass is the on-shell mass; note, however, that we keep the external Higgs boson on-shell and do not perform the ultimate step of introducing a (complex) pole residue and the associated partial width for the decaying Higgs boson.

For  $H \rightarrow \gamma\gamma$  (in  $R_\xi$  gauge) we have a bosonic triangle at one loop, which contains a factor  $m_H$  (from the  $H - \phi - \phi$  vertex, see Fig. 4), which needs to be renormalized through the replacement of the renormalized Higgs mass with the physical Higgs-boson mass. This fact introduces the real parts of  $B_0$  functions, which lead to a violation of the WST identities above the  $WW$  threshold, as described in Eq.(75) (note that wave-function renormalization factors never pose similar problem); also in the CM scheme the corresponding real label is removed, even if the external Higgs boson is assumed to be an on-shell particle (see comment above).

As a final note one can say that CM scheme is the default for our results, the other schemes being assigned to the role of benchmark.

## 6 Extraction of collinear singularities

In this section we discuss the problem of collinear singularities showing up in the calculation of a given (pseudo-)observable. Any method that aims to produce theoretical predictions for (pseudo-)observable quantities organizes the calculation of the corresponding  $S$ -matrix element into several building blocks, and the analytical structure of the total amplitude will not necessarily be the same of the single components. From this point of view, collinear singularities are a clear example: sometimes, a collinear-free amplitude is split into components which are separately divergent in the collinear regime. Therefore, singularities must be regularized and singular terms have to be extracted.

It is worth noting that no numerical evaluation can be attempted before two basic steps have been performed. On the one hand, all singular terms (ultraviolet, infrared, collinear) of the amplitude have to be extracted, and their cancellation or absorption into parton distribution functions have to be explicitly checked. On the other hand, all enhanced terms have to be isolated, such that numerical integration is only limited to *smooth* remainders; at this level there is no need to worry about the length of the remainders.

Focusing our attention on electroweak processes, several methods aimed to deal with collinear singularities have been developed and presented in the literature, as in Ref. [79], for one-loop leading logarithms in electroweak radiative corrections, and in Ref. [80], for two-loop electroweak NLO logarithmic corrections to massless and massive fermionic processes.

Concerning electroweak corrections to the decay of the Higgs boson into two photons or two gluons, collinear divergencies are related to the coupling between photons or gluons with light fermions. Therefore, there is no substantial difference between the two processes and in the following, without loss of generality, we will concentrate on the process  $H \rightarrow \gamma\gamma$ . On the contrary, the QCD corrections generate special types of divergencies in the gluonic decay, because of the three-gluon coupling.

A common approach to the problem of collinear divergencies is to consider all light fermions of the theory as massless states; dimensional regularization is then used to control the collinear behavior of single components of the amplitude. In our approach, we prefer to keep the physical light-fermion masses to act as regulators, and to express the collinear behavior in terms of logarithms of these masses. After analytically checking that singular parts cancel in the total, we can safely get rid of the regularization parameter and include all collinear-free remainders into the total amplitude. These finite parts will be cast in a form which is functional to numerical integration.

At two-loop level we encounter three different situations illustrated in Fig. 17: 1) one and only one of the two external photons is coupled to a light-fermion current (second, third diagram and fourth heavy- $f'$

diagram); 2) both photons are coupled to the same light-fermion current in a loop (first diagram); 3) one photon is coupled to a light-fermion current in one loop, the other photon in the other loop (fourth diagram with light  $f'$ ).

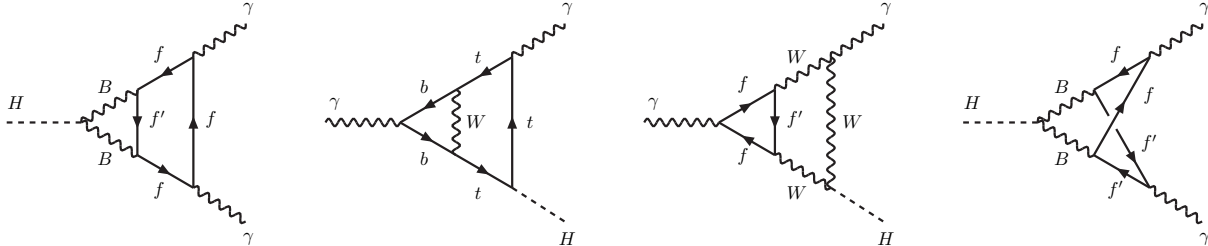


Figure 17: Complete list of diagrams with photons coupled to light fermions ( $f$ ). In the figure  $f'$  denotes any fermion (light or not, equal to  $f$  or not). The capital  $B$  indicates a boson which can be either a  $Z$  or a  $W$ .

The treatment of the above-mentioned configurations simplifies when taking into account the reduction  $\otimes$  symmetrization procedure described in section 4. This aspect is considered in section 6.1 where we show that all diagrams of type 2) cancel. Diagrams of type 1) and 3) are then discussed in section 6.2 and in section 6.3, where we analytically extract the coefficients of the collinear logarithms. In section 6.4 the special case of the  $V^M$  configuration is considered; divergencies which are peculiar of the QCD corrections to  $H \rightarrow gg$  are shortly reviewed in appendix C.

## 6.1 Collinear behavior and tensor reduction

In this section we address a general question which has important consequences in classifying those collinear configurations which are actually needed for the calculation. For the  $H \rightarrow \gamma\gamma$  process, the diagrams where photons couple to light fermions belong to the  $V^K$  and  $V^H$  families with the mass patterns depicted in Fig. 17. Two naive approaches to the treatment of collinear singularities would consist on the one hand in evaluating all the possible tensor integrals associated to these families; on the other hand, to express them in terms of some set of Master Integrals (hereafter MIs) using IBP identities.

The first option is not very convenient, since it requires to evaluate explicitly a large set of integrals. However, also a blind application of reduction through IBP identities has a drawback: the MIs representing the basis integrals cannot be a priori predicted (e.g. by using the standard Laporta algorithm [81]; constructive approaches can be found in Ref. [82]), and complicated collinear-divergent MIs could show up in the final answer. In this section we show that our approach, based on the reduction  $\otimes$  symmetrization procedure of section 4, represents the optimal solution: it identifies the smallest set of collinear-divergent integrals whose structure is simple enough to allow for an analytical extraction of all collinear singularities.

To introduce our argument, we start considering an  $N$ -point one-loop function with external momenta  $p_1, \dots, p_N$  and with scalar products in the numerator. After introducing  $P_0^\mu = 0$  and  $P_i^\mu = p_1^\mu + \dots + p_i^\mu$ , we consider the integral

$$S_{n;N}(f) = \frac{\mu^\epsilon}{i\pi^2} \int d^n q \frac{f(q, \{p\})}{\prod_{i=0}^{N-1} [i]}, \quad [i] = (q + P_i)^2 + m_i^2, \quad (96)$$

and we perform a standard-reduction procedure to simpler functions; taking for instance four-point functions, it is a well-known fact that

$$S_{n;4}(f) = \sum_i b_i B_0(P_i^2) + \sum_{i,j} c_{ij} C_0(P_i^2, P_j^2) + \sum_{i,j,k} d_{ijk} D_0(P_i^2, P_j^2, P_k^2) + R, \quad (97)$$

where  $B_0$ ,  $C_0$  and  $D_0$  are scalar two-, three- and four-point functions and  $R$  is the so-called rational term. Let us consider, in particular, the following example:

$$S_{n;4}(q \cdot p_1) = \frac{\mu^\epsilon}{i\pi^2} \int d^n q \frac{q \cdot p_1}{\prod_{i=0}^3 [i]} = - \sum_{i=1}^3 D_{1i} H_{1i}, \quad (98)$$

where the matrix  $H$  is given by  $H_{ij} = -p_i \cdot p_j$ ,  $G = \det H$  is the Gram determinant associated with the four-point function and  $D_{1i}$  are standard form factors [51]. In standard reduction, one goes on expressing the  $D_{1i}$  form factors in terms of  $D_0$  and of three-point functions, with inverse powers of  $G$ . However, a more careful application of the method will make use of

$$D_{1i} = -\frac{1}{2} H_{ij}^{-1} d_j, \quad d_i = D_0^{(i+1)} - D_0^{(i)} - 2 K_i D_0, \quad K_i = \frac{1}{2} (P_i^2 - P_{i-1}^2 + m_i^2 - m_{i-1}^2), \quad (99)$$

where  $D_0^{(i)}$  is the scalar triangle obtained by removing the propagator  $i$  from the box. Therefore, we obtain

$$S_{n;4}(q \cdot p_1) = \frac{1}{2} \sum_{i,j=1}^3 H_{ij}^{-1} H_{1i} d_j = \frac{1}{2} d_1, \quad (100)$$

without explicit factors involving  $G$ . Furthermore, from Eq.(99), we see that the coefficient of  $D_0$  in the reduction is  $(m_0^2 - m_1^2 - p_1^2)/2$ . Note that at the leading Landau singularity of the box, corresponding to the anomalous threshold [83], we must have

$$q^2 + m_0^2 = 0, \quad (q + P_i)^2 + m_i^2 = 0 \quad \rightarrow \quad q \cdot p_1 = \frac{1}{2} (m_0^2 - m_1^2 - p_1^2), \quad (101)$$

which is equal to the coefficient of the  $D_0$  function. This is a general property: a careful application of standard reduction to an  $N$ -point function with any scalar product gives as coefficient for the scalar  $N$ -point integral the value of the scalar product at the anomalous threshold.

To summarize, in standard reduction for a  $N$ -point function each reducible scalar product in the numerator is replaced by a difference of propagators plus a  $K$  factor, predicted by factorization properties at the anomalous threshold. The procedure can be continued and one finds  $(N-1)$ -point functions with reducible and also irreducible scalar products; for the latter inverse powers of Gram determinants will remain.

Imagine now that our  $N$ -point one-loop function is a sub-diagram (with loop momentum  $q_2$ ) of a two-loop diagram (with momenta  $q_1, q_2$ ). The numerator will contain, in general, reducible and irreducible scalar products. If only reducible scalar products are present and if, after algebraic reduction  $N \rightarrow N-1$  (as we said earlier, no inverse Gram determinants), the coefficients of the corresponding scalar, vector or tensor one-loop diagrams turn out to be zero, then the two-loop diagram will not appear in the final result and only its reduced child diagrams will do. In particular, if the original two-loop diagram is collinear divergent, the singular behavior can be read off from its sub-diagrams, which is a simpler problem because one propagator less is involved.

This is what happens with the first diagram in Fig. 17; as described in appendix B, the physical content of the diagrams for the process  $H \rightarrow \gamma\gamma$  can be extracted contracting the tensor in the amplitude by means of the projector  $P_D^{\mu\nu} = D_{3;\mu\nu}$  of Eq.(236). After the standard reduction 6legs  $\rightarrow$  5legs is applied (see section 4), when  $m_f \rightarrow 0$  and for arbitrary  $M_B$  and  $m_{f'}$ , we obtain <sup>2</sup>:

$$\text{Diagram} \otimes P_D^{\mu\nu} = C_K^{\text{dc}} (m_{f'}^2 - M_B^2 + 2 q_1 \cdot p_1) \text{Diagram} + (\text{reduced diagrams}), \quad (102)$$

<sup>2</sup>In this section we use low-case letters for denoting the masses of *light* particles, which will be neglected after proving the cancellation of collinear logarithms.

where the coefficient  $C_K^{\text{dc}}$  is  $\propto (n-4)P^2$ . Since the scalar and vector  $V^K$  are UV finite, we can take the limit  $n \rightarrow 4$ ; therefore, as we anticipated, six-propagator terms disappear from the projected  $V^K$  and only reduced diagrams with at most one photon coupled to light-fermion lines survive. Concerning reduced diagrams, the collinear-divergent ones are always of the type  $V^E$  and  $V^G$ , collected in Fig. 18. Note that for the  $V^E$  type only the scalar configuration survives, while for  $V^G$  we have to deal with tensor integrals up to rank two.

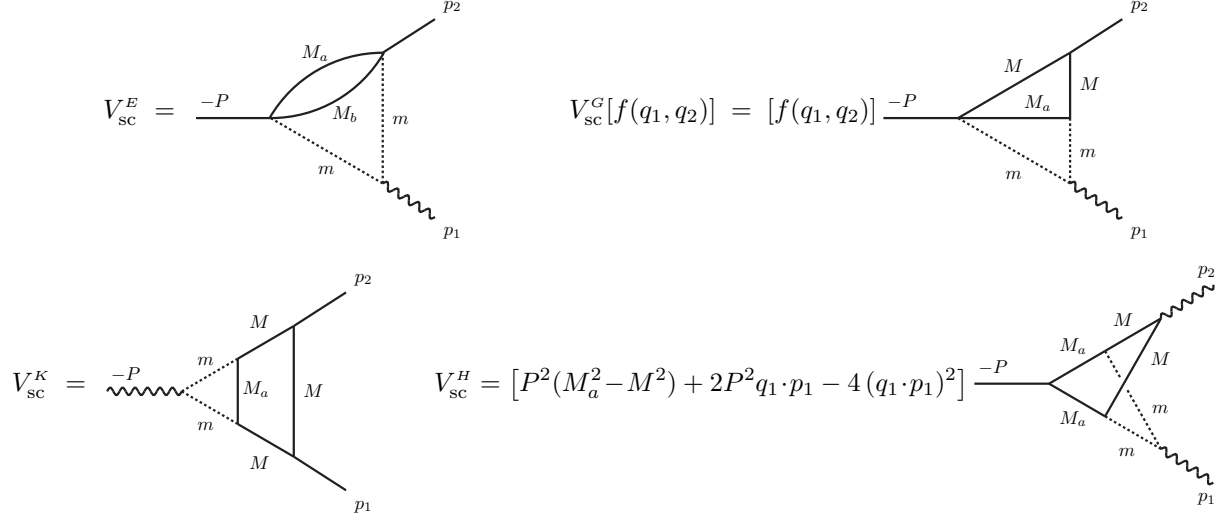


Figure 18: Definition of all MIs with one external massless particle coupled to a light particle for the process  $H \rightarrow \gamma\gamma$ . The dot-lines indicate light particles of mass  $m$ , the wavy line a massless particle and the solid lines whatever particles. The mass  $M$  is strictly heavy, while  $M_a$  and  $M_b$  can also be light.

The same procedure will then be applied to the second and third diagram of Fig. 17. In these cases the coefficient of  $V^K$  does not vanish; in the end, however, only scalar configurations survive,

$$\begin{aligned}
\begin{array}{c} \text{Diagram 1} \\ \nu \text{ wavy } p_1 \text{ wavy } p_2 \text{ wavy } \mu \\ \text{solid lines } t, b, w \\ \text{dotted lines } t, b \\ \text{external } -P \end{array} \otimes P_D^{\mu\nu} &= C_{K,1}^{\text{sc}} \begin{array}{c} \text{Diagram 2} \\ \nu \text{ wavy } p_1 \text{ wavy } p_2 \text{ wavy } \mu \\ \text{solid lines } M_t, M_w \\ \text{dotted lines } m_b, m_t \\ \text{external } -P \end{array} + \left( \text{reduced diagrams} \right), \\
\begin{array}{c} \text{Diagram 3} \\ \nu \text{ wavy } p_1 \text{ wavy } p_2 \text{ wavy } \mu \\ \text{solid lines } f, f', w \\ \text{dotted lines } f, f' \\ \text{external } -P \end{array} \otimes P_D^{\mu\nu} &= C_{K,2}^{\text{sc}} \begin{array}{c} \text{Diagram 4} \\ \nu \text{ wavy } p_1 \text{ wavy } p_2 \text{ wavy } \mu \\ \text{solid lines } M_w, M_f \\ \text{dotted lines } m_f, m_f \\ \text{external } -P \end{array} + \left( \text{reduced diagrams} \right). \quad (103)
\end{aligned}$$

The coefficients  $C_{K,1}^{\text{sc}}$  and  $C_{K,2}^{\text{sc}}$  are independent from the loop momenta. The collinear-divergent reduced diagrams belong to the families  $V_{\text{sc}}^E$  and  $V_{\text{sc}}^G$  depicted in Fig. 18; the new object to be computed is the scalar diagram  $V_{\text{sc}}^K$ , also defined in Fig. 18.

For the last diagram of Fig. 17 we have to distinguish two cases, with  $f'$  heavy (i.e.  $f'$  is the top quark) or light. In both cases, the coefficients of the tensor  $V^H$  do not vanish, but some universal structure in  $q_1$

and  $q_2$  can be identified, irrespective of the coupling between the boson  $B$  and the fermions  $f$  and  $f'$ . In the case of light  $f'$ , the reduced diagrams show also a doubly collinear behavior of the  $V^G$  type, characterized by a universal structure in the loop momenta. Indeed we obtain

$$\begin{aligned}
 \text{Left Diagram} \otimes P^{\mu\nu} &= C_H^{\text{sc}} V_{\text{sc}}^H + \text{r.d.}, \\
 \text{Right Diagram} \otimes P^{\mu\nu} &= C_H^{\text{dc}} V_{\text{dc}}^H + C_G^{\text{dc}} V_{\text{dc}}^G + \text{r.d.}, \quad (104)
 \end{aligned}$$

where the coefficients  $C_H^{\text{sc}}$ ,  $C_H^{\text{dc}}$  and  $C_G^{\text{dc}}$  depend on the coupling between the boson  $B$  and the fermions. The diagram  $V_{\text{sc}}^H$  is defined in Fig. 18, while  $V_{\text{dc}}^H$  and  $V_{\text{dc}}^G$  are shown Fig. 19; the reduced diagrams (r.d.) are again of the form  $V_{\text{sc}}^E$  and  $V_{\text{sc}}^G$  of Fig. 18.

$$\begin{aligned}
 V_{\text{dc}}^H &= [P^2 M^2 + 2P^2 q_1 \cdot p_1 - 4(q_1 \cdot p_1)^2]^{-P} \text{Diagram} \\
 V_{\text{dc}}^G &= [M^2 - 4(M^2 + P^2 + q_1 \cdot p_2) \frac{q_2 \cdot p_1}{P^2}]^{-P} \text{Diagram}
 \end{aligned}$$

Figure 19: Definition of all MIs with two external massless particles coupled to a light particle for the process  $H \rightarrow \gamma\gamma$ . The dot-lines indicate light particles of mass  $m$  or  $m'$  ( $m'$  can be equal to  $m$  or not), the wavy line a massless particle and the solid lines a heavy particle of mass  $M$ .

Summarizing, we can say that the reduction  $\otimes$  symmetrization procedure allows us to identify the smallest sub-set of all diagrams with collinear divergencies, collected in Fig. 18 and Fig. 19; they can be taken as MIs for the set of simply and doubly collinear configurations. The extraction of the corresponding collinear logarithms will be treated in the next two sections.

## 6.2 Vertices with one photon coupled to light fermions

In this section we extract the coefficients of the collinear logarithms for the MIs shown in Fig. 18 and compute the associated collinear-finite parts. For the  $V_{\text{sc}}^E$  configuration (first diagram in Fig. 18), we use the result derived in section 5.1 of Ref. [47], and evaluate the limits  $p_1^2 \rightarrow 0$  and  $m_3 = m_4 = m \rightarrow 0$ ,

$$\begin{aligned}
 V_{\text{sc}}^E &= -2 \left[ F_{-2}^2(s) - F_{-1}^2(s) \left( \ln \frac{m^2}{s} - \frac{1}{2} \right) \right] - \frac{1}{2} \ln^2 \frac{m^2}{s} - \ln \frac{m^2}{s} \int_0^1 dx dz \ln \frac{\chi_E}{s} \\
 &+ \int_0^1 dx dz \left[ \frac{1}{2} \ln^2 \frac{\chi_E}{s} + \ln \frac{z}{x(1-x)} \ln \frac{\chi_E}{s} - \text{Li}_2 \left( \frac{p_2^2 xz(1-x)}{\chi_E} \right) \right] - \frac{1}{2} \zeta(2) + \frac{3}{2}, \quad (105)
 \end{aligned}$$

where  $\chi_E = P^2 x(1-x)(1-z) + p_2^2 xz(1-x) + M_a^2(1-x) + M_b^2 x$  and the two-loop UV factors  $F_{-i}^2$ , with  $i = 1, 2$ , have been defined in Eq.(3). We readily identify  $\chi_E$  with the polynomial associated with the Feynman-parameter representation of the one-loop two-point function  $B_0(1, 1, (1-z)P^2 + zp_2^2, M_a, M_b)$  ( $x$  is the Feynman parameter). In particular, the coefficient of the collinear logarithm can be written through the one-fold integral representation of a one-loop function,

$$V_{\text{sc}}^E = \text{Diagram} = \ln \frac{m^2}{s} \left[ 1 - \frac{\epsilon}{2} \Delta_{UV}(s) - \frac{\epsilon}{4} \ln \frac{m^2}{s} \right] \int_0^1 dz \text{Diagram} + V_{\text{sc,fin}}^E, \quad (106)$$

where  $\Delta_{UV}$  can be read in Eq.(1) and  $V_{\text{sc,fin}}^E$  denotes the collinear-free remainder (see Eq.(105)). This simple result shows a feature that we will encounter also in more-complicated configurations: collinear singularities can be represented through objects with well-known analytical properties, and the cancellation of all collinear logarithms at the amplitude level can be analytically verified.

It will be shown in the following that the collinear behavior of the remaining three vertices of Fig. 18 is also embedded in a one-loop integration. The key observation is that all these configurations contain the product of two propagators of the same type:

$$\frac{1}{(q^2 + m^2)[(q + p)^2 + m^2]}, \quad \text{with} \quad \begin{cases} p = p_1, & q = q_1 & \text{for } V_{\text{sc}}^G \\ p = P, & q = q_1 & \text{for } V_{\text{sc}}^K \\ p = -p_1, & q = q_2 & \text{for } V_{\text{sc}}^H \end{cases}. \quad (107)$$

In particular, let us consider the scalar configurations  $V_{\text{sc}}^G[1]$  and  $V_{\text{sc}}^K$  (scalar configurations of the second and third diagrams in Fig. 18); we define  $J_N$  as the scalar sub-loop containing  $q$ , where  $N$  denotes the number of  $q$ -dependent propagators in addition to those of Eq.(107). For  $V_{\text{sc}}^G[1]$  and  $V_{\text{sc}}^K$  we have  $N = 1$  and consider

$$J_1 = \frac{\mu^{4-n}}{i\pi^2} \int d^n q \frac{1}{(q^2 + m^2)[(q + p)^2 + m^2][(q - q_2)^2 + M_a^2]}. \quad (108)$$

Next, we introduce Feynman parameters  $z$  and  $y$ , integrate over  $q$  and set  $n = 4$ , obtaining

$$J_1 = \int_0^1 dz \int_0^z dy \frac{1}{V}, \quad V = [A - y(q_2 + p)^2]y + m^2(1 - y), \quad A = (q_2 + pz)^2 + M_a^2. \quad (109)$$

The result shows that the singularity for  $m = 0$  is generated, in parametric space, at the point  $y = 0$ ; we introduce  $V_0 = Ay + m^2$ , a simple polynomial having the same collinear properties of  $V$ , and add and subtract  $1/V_0$  at the integrand level, getting

$$J_1 = \int_0^1 \frac{dz}{A} \ln \frac{Az - m^2}{s} + \int_0^1 dz \int_0^z \frac{dy}{y} \left[ \frac{1}{A - y(q_2 + p)^2} - \frac{1}{A} \right] + \mathcal{O}(m^2), \quad (110)$$

where the first term is the collinear-divergent part of  $J_1$ . The complete expressions for  $V_{\text{sc}}^G[1]$  and  $V_{\text{sc}}^K$ , and the related coefficients of the collinear logarithms, are obtained inserting the result for  $J_1$  in the  $q_2$  integrals,

$$\begin{aligned} V_{\text{sc}}^G[1] &= \frac{1}{i\pi^2} \ln \frac{m^2}{s} \int_0^1 dz \int \frac{d^4 q_2}{[(q_2 + p_1 z)^2 + M_a^2][(q_2 + p_1)^2 + M^2][(q_2 + P)^2 + M^2]} + V_{\text{sc,fin}}^G[1], \\ V_{\text{sc}}^K &= \frac{1}{i\pi^2} \ln \frac{m^2}{s} \int_0^1 dz \int \frac{d^4 q_2}{[(q_2 + Pz)^2 + M_a^2](q_2^2 + M^2)[(q_2 + p_1)^2 + M^2][(q_2 + P)^2 + M^2]} + V_{\text{sc,fin}}^K, \end{aligned} \quad (111)$$

with the following diagrammatical correspondences,

$$\begin{aligned} V_{\text{sc}}^G[1] &= \begin{array}{c} p_2 \\ \diagup \\ M \\ \diagdown \\ m \\ \diagup \\ m \\ \diagdown \\ p_1 \end{array} = \ln \frac{m^2}{s} \int_0^1 dz \begin{array}{c} p_2 \\ \diagup \\ M \\ \diagdown \\ z p_1 \\ \diagup \\ M_a \\ \diagdown \\ (1-z)p_1 \end{array} + V_{\text{sc,fin}}^G[1], \\ V_{\text{sc}}^K &= \begin{array}{c} p_2 \\ \diagup \\ m \\ \diagdown \\ m \\ \diagup \\ m \\ \diagdown \\ p_1 \end{array} = \ln \frac{m^2}{s} \int_0^1 dz \begin{array}{c} -(1-z)P \\ \diagup \\ M \\ \diagdown \\ -zP \\ \diagup \\ M_a \\ \diagdown \\ p_1 \end{array} + V_{\text{sc,fin}}^K. \end{aligned} \quad (112)$$

The computation of the collinear-finite parts  $V_{\text{sc,fin}}^G[1]$  and  $V_{\text{sc,fin}}^K$  will be described in more detail in section 6.2.1 and section 6.2.2.

The  $V_{\text{sc}}^H$  configuration (fourth diagram in Fig. 18) shows two additional  $q$ -dependent propagators; we consider the generalization of Eq.(108),

$$J_N = \frac{\mu^{4-n}}{i\pi^2} \int \frac{d^n q}{(q^2 + m^2)[(q+p)^2 + m^2]} \prod_{i=1}^N \frac{1}{(q+k_i)^2 + m_i^2}, \quad (113)$$

and later we will specialize to the  $V_{\text{sc}}^H$  case, setting  $N = 2$ ,  $k_1 = -q_2 - p_1$ ,  $k_2 = -q_1 + p_2$  and  $m_1 = m_2 = M_a$ . We start introducing a Feynman parametrization,

$$\prod_{i=1}^N \frac{1}{(q+k_i)^2 + m_i^2} = \Gamma(N) \int dS_{N-1}(\{x\}) \frac{1}{[(q+K)^2 + \mu^2]^N},$$

$$\mu^2 = \sum_{i=1}^N (x_{i-1} - x_i)(m_i^2 + k_i^2) - K^2, \quad K = \sum_{i=1}^N (x_{i-1} - x_i) k_i, \quad x_0 = 1, \quad x_N = 0. \quad (114)$$

Next, we combine the resulting three propagators of Eq.(113) with variables  $z$  and  $y$  and perform the  $q$  integration. Since the  $V_{\text{sc}}^H$  configuration in Fig. 18 is UV finite, we can set  $n = 4$  and obtain

$$J_N = \Gamma(N) \int_0^1 dz \int_0^z dy \int dS_{N-1}(\{x\}) \frac{y^{N-1}}{V^N}, \quad V = [A - y(K-p)^2]y + m^2(1-y), \quad A = (K-pz)^2 + \mu^2. \quad (115)$$

Subtracting and adding at the integrand level  $1/V_0^N$ , with  $V_0 = Ay + m^2$ , we can extract the collinear logarithm through the  $y$  integration,

$$J_N = -\Gamma(N) \int dS_{N-1}(\{x\}) \int_0^1 dz \left\{ \frac{1}{A^N} \left( \ln \frac{m^2}{s} - \ln \frac{Az}{s} + \sum_{n=1}^{N-1} \frac{1}{n} \right) - \int_0^1 dy \frac{[A - y(K-p)^2]^{-N}}{y} \Big|_+ \right\} + \mathcal{O}(m^2), \quad (116)$$

where the '+' distribution has been defined in Eq.(8). The coefficient of the collinear logarithm can be further simplified if we move back to momentum space integrating over all Feynman variables  $\{x\}$ ,

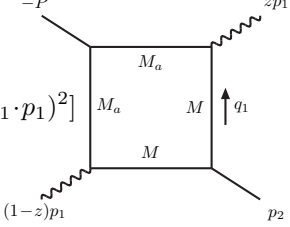
$$\Gamma(N) \int dS_{N-1}(\{x\}) \frac{1}{A^N} = \prod_{i=1}^N \frac{1}{(k_i - pz)^2 + m_i^2}. \quad (117)$$

Formally, we have reconstructed the product of  $N$  propagators on the right-hand side of Eq.(113), replacing the loop momentum  $q$  by  $-pz$ . Eq.(116) has been derived under rather-general assumptions, and it can be used for extracting the collinear behavior of any two-loop scalar (respect to  $q$ ) UV-finite diagram with one external massless particle coupled to one light particle; its graphical representation reads

$$\text{Diagram} = \ln \frac{m^2}{s} \int_0^1 dz \text{Diagram} + \text{coll. fin.}, \quad (118)$$

where the bubble denotes a generic one-loop diagram involving a tensor structure  $q_a^{\mu_1} \dots q_a^{\mu_m}$ ,  $q_a$  is the loop momentum, the wavy line represents the external massless particle ( $p^2 = 0$ ) and the dotted one is the light particle with mass  $m$ .

The result of Eq.(118) can be immediately applied to the  $V_{\text{sc}}^H$  configuration of Fig. 18; note that we do not confine ourselves to the scalar configuration, but we consider the full  $q_1$ -dependent structure appearing in the coefficient of the diagram. We obtain

$$V_{\text{sc}}^H = \ln \frac{m^2}{s} \int_0^1 dz \left[ P^2(M_a^2 - M^2) + 2P^2 q_1 \cdot p_1 - 4(q_1 \cdot p_1)^2 \right] \text{Diagram} + V_{\text{sc,fin}}^H. \quad (119)$$


The procedure for dealing with the collinear-finite part  $V_{\text{sc,fin}}^H$  will be described in section 6.2.3.

Finally, let us discuss the extraction of the collinear logarithms for generic tensor and/or UV-divergent two-loop integrals. We introduce

$$J_N^{\nu_1 \dots \nu_r} = \frac{\mu^{4-n}}{i\pi^2} \int \frac{d^n q q^{\nu_1} \dots q^{\nu_r}}{(q^2 + m^2)[(q+p)^2 + m^2]} \prod_{i=1}^N \frac{1}{(q+k_i)^2 + m_i^2}, \quad (120)$$

and use a Feynman parametrization analogous to the one used for deriving Eq.(115). In particular, before performing the  $q$  integration, we have

$$J_N^{\nu_1 \dots \nu_r} = \frac{\mu^{4-n} \Gamma(N+2)}{i\pi^2} \int_0^1 dz \int_0^z dy \int dS_{N-1}(\{x\}) y^{N-1} \int d^n q \prod_{i=1,r} q^{\nu_i} \mathcal{V}^{-N-2},$$

$$\mathcal{V} = q^2 + 2q \cdot \mathcal{K} + \mathcal{M}^2, \quad \mathcal{K} = zp + y(K-p), \quad \mathcal{M}^2 = (\mu^2 + K^2)y + m^2(1-y), \quad (121)$$

where  $K$  and  $\mu^2$  have been defined in Eq.(114). The  $q$  integration is performed according to

$$\begin{aligned} \int d^n q \prod_{i=1,r} q^{\nu_i} \mathcal{V}^{-N-2} &= \left(-\frac{1}{2}\right)^r \frac{\Gamma(N+2-r)}{\Gamma(N+2)} \prod_{i=1,r} \frac{\partial}{\partial \mathcal{K}^{\nu_i}} \int d^n q \mathcal{V}^{-N-2+r} \\ &= i\pi^{2-\epsilon/2} \left(-\frac{1}{2}\right)^r \frac{\Gamma(N-r+\epsilon/2)}{\Gamma(N+2)} \prod_{i=1,r} \frac{\partial}{\partial \mathcal{K}^{\nu_i}} V^{-N+r-\epsilon/2}, \end{aligned} \quad (122)$$

where  $V = \mathcal{M}^2 - \mathcal{K}^2 = [A - y(K-p)^2]y + m^2(1-y)$  is the same of Eq.(115).

The first derivative in Eq.(122) decreases the power of  $V$  by one unit and generates an extra factor  $\mathcal{K}$ . The second derivative acts on both  $\mathcal{K}$  and  $V$ , producing two terms: one where the power of  $V$  does not change and the metric tensor appears; another one where the power of  $V$  decreases by one unit and an additional factor  $\mathcal{K}$  is generated. After taking all  $r$  derivatives, we find a term containing  $V^{-N-\epsilon/2}$ : the one where all derivatives have acted on  $V$ , generating a factor  $\mathcal{K}^{\nu_1} \dots \mathcal{K}^{\nu_r}$ . All other terms in the result will contain at least one power of the metric tensor, and for each of them the power of  $V$  will be greater than  $-N - \epsilon/2$ , because at least one derivative has not acted on  $V$ .

We can show the following result: if the power of  $V$  is greater than  $-N - \epsilon/2$  then no collinear logarithm is generated. We cast the  $y$  integral of Eq.(121) as

$$\int_0^z dy \frac{y^\beta}{V^\alpha} = \int_0^z dy \frac{y^\beta}{(Ay + m^2)^\alpha} + \int_0^z dy y^\beta \left( \frac{1}{V^\alpha} - \frac{1}{V_0^\alpha} \right), \quad (123)$$

where we have added and subtracted in the integrand  $V_0^{-\alpha}$ , with  $V_0 = Ay + m^2$ . From Eq.(121), Eq.(122) and the subsequent discussion we can argue that: 1)  $\alpha \leq N + \epsilon/2$  for all terms; 2)  $\beta \geq N - 1$ , since powers of  $y$  in addition to the  $y^{N-1}$  term of Eq.(121) can be embedded in the  $\mathcal{K}$  factors. Therefore, being  $\beta - \alpha \geq -1 - \epsilon/2$  in all cases, the second integral in Eq.(123) is always finite in the limit  $m \rightarrow 0$ : indeed

$$\int_0^z dy y^\beta \left( \frac{1}{V^\alpha} - \frac{1}{V_0^\alpha} \right) = \int_0^z dy y^{\beta-\alpha} \left\{ \frac{1}{[A - y(K-p)^2]^\alpha} - \frac{1}{A^\alpha} \right\} + \mathcal{O}(m^2), \quad \text{if } \beta - \alpha > -2. \quad (124)$$

The first term in Eq.(123), instead, is collinear finite only if  $\beta - \alpha > -1$ ; in this case indeed

$$\int_0^z dy \frac{y^\beta}{(Ay + m^2)^\alpha} = \frac{1}{(\beta - \alpha + 1)A^\alpha} + \mathcal{O}(m^2). \quad (125)$$

Therefore, for all terms where the power of  $V$  is greater or equal to  $-N - \epsilon/2 + 1$ , we have  $\beta - \alpha \geq -\epsilon/2$ , Eq.(124) and Eq.(125) simultaneously hold and no collinear logarithm is generated.

As a result, we can extract the collinear behavior of  $J_N^{\nu_1 \dots \nu_r}$  replacing Eq.(122) in Eq.(121), and considering only the term where all  $r$  derivatives have acted on  $V$ ; in this way we obtain

$$J_N^{\nu_1 \dots \nu_r} = (-1)^r \Gamma\left(N + \frac{\epsilon}{2}\right) \left(\frac{\mu^2}{\pi}\right)^{\epsilon/2} \int_0^1 dz \int_0^z dy \int dS_{N-1}(\{x\}) y^{N-1} \prod_{i=1,r} \mathcal{K}^{\nu_i} V^{-N-\epsilon/2} + \text{coll. fin.} \quad (126)$$

The expression for  $\mathcal{K}$  given in Eq.(121) contains a term proportional to  $y$ ; it cannot produce a collinear logarithm in Eq.(126) because it increases the power of  $y$  and leads to the above-mentioned condition  $\beta - \alpha \geq -\epsilon/2$ . Therefore, the collinear-divergent piece of  $J_N^{\nu_1 \dots \nu_r}$  is simply given by

$$J_N^{\nu_1 \dots \nu_r} = \Gamma\left(N + \frac{\epsilon}{2}\right) \left(\frac{\mu^2}{\pi}\right)^{\epsilon/2} \int_0^1 dz \int_0^z dy \int dS_{N-1}(\{x\}) y^{N-1} (-z)^r \prod_{i=1,r} p^{\nu_i} V^{-N-\epsilon/2} + \text{coll. fin.} \quad (127)$$

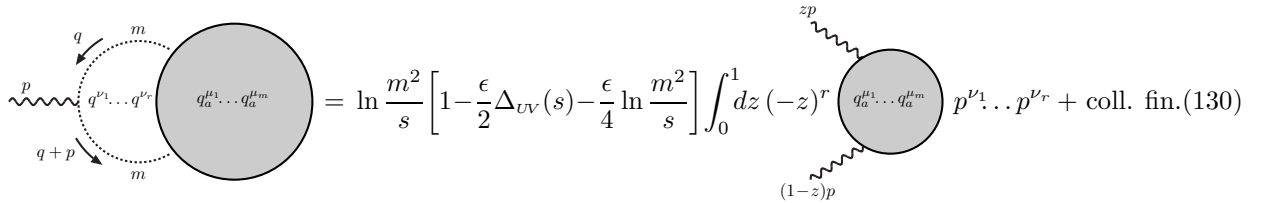
Now we add and subtract  $V_0^{-N-\epsilon/2}$ , integrate in  $y$  the added term and absorb in the collinear-finite remainder the subtracted one. The  $y$  integration gives

$$\int_0^z dy \frac{y^{N-1}}{(Ay + m^2)^{N+\epsilon/2}} = -\frac{\Gamma(N)\Gamma(1+\epsilon/2)}{\Gamma(N+\epsilon/2)} \frac{1}{A^N} \ln\left(\frac{m^2}{s}\right) \sum_{k=0}^{\infty} \frac{1}{(k+1)!} \left(-\frac{\epsilon}{2} \ln \frac{m^2}{s}\right)^k + \text{coll. fin.} \quad (128)$$

Inserting the result in Eq.(127) and using Eq.(117), we finally extract the collinear logarithm for  $J_N^{\nu_1 \dots \nu_r}$ ,

$$J_N^{\nu_1 \dots \nu_r} = \left(\frac{\mu^2}{s\pi}\right)^{\epsilon/2} \Gamma\left(1 + \frac{\epsilon}{2}\right) \sum_{k=0}^{\infty} \frac{(\epsilon/2)^k}{(k+1)!} \left(-\ln \frac{m^2}{s}\right)^{k+1} \int_0^1 dz (-z)^r \prod_{j=1,r} p^{\nu_j} \prod_{i=1}^N \frac{1}{(k_i - pz)^2 + m_i^2} + \text{coll. fin.} \quad (129)$$

We are now able to compute the coefficient of the collinear logarithm for a two-loop diagram with a generic tensor structure in the configuration where only one external massless particle is coupled to a light internal one,



It is important to mention the striking correspondence with the special result derived for the simple configuration in Eq.(106).

### 6.2.1 The collinear-finite part of $V_{\text{sc}}^G$

In order to compute the collinear-finite parts of the diagrams belonging to the  $V_{\text{sc}}^G$  family, we slightly modify our approach. We use a complete Feynman parametrization before extracting the collinear logarithms; they are then discarded and the collinear-finite remainder is written in a way that allows for direct numerical integration. We follow the parametrization procedure described in section 7 of Ref. [47] for the scalar cases;

the corresponding parametrization for tensor integrals can be found in section 9 of Ref. [49]. Extracting the UV poles from these expressions and performing some changes of variables, we get

$$\begin{aligned}
V_{\text{sc}}^G &= - \int_0^1 dx_1 dx_2 dy_1 \int_0^{y_1} dy_2 (1-x_2) W_G^{-1}, \\
V_{\text{sc}}^G[q_i^\mu] &= \int_0^1 dx_1 dx_2 dy_1 \int_0^{y_1} dy_2 (1-x_2) p_{G,i}^\mu W_G^{-1}, \quad p_{G,i}^\mu = \sum_{h=1}^2 a_{G,i}^h p_h^\mu, \\
V_{\text{sc}}^G[q_i^\mu q_j^\nu] &= - \int_0^1 dx_1 dx_2 dy_1 \int_0^{y_1} dy_2 (1-x_2) p_{G,i}^\mu p_{G,j}^\nu W_G^{-1} + \Delta_{G,ij}^{\text{sc}} \delta^{\mu\nu},
\end{aligned} \tag{131}$$

where we have defined auxiliary quantities,  $\chi_G = p_2^2 y_1 (1-y_1) + M^2$  and

$$\begin{aligned}
W_G &= x_2 (1-x_2) A_G + y_2 [x_2 M_a^2 + (1-x_2) m^2], & A_G &= (1-y_1) [P^2 x_1 y_2 + p_2^2 (y_1 - x_1 y_2)] + M^2, \\
a_{G,1}^1 &= 1 - x_1 [1 - x_2 (1-y_2)], & a_{G,1}^2 &= x_2 (1-y_1), & a_{G,2}^1 &= 1 - x_1 y_2, & a_{G,2}^2 &= 1 - y_1, \\
\Delta_{G,11}^{\text{sc}} &= -\frac{1}{2} \left\{ F_{-2}^2(s) + F_{-1}^2(s) \left( \frac{3}{4} - \int_0^1 dy_1 \ln \frac{\chi_G}{s} \right) + \frac{5}{16} + \frac{1}{4} \zeta(2) \right. \\
&\quad \left. + \frac{1}{2} \int_0^1 dy_1 \left[ \ln^2 \frac{\chi_G}{s} - (\ln y_1 + 2) \ln \frac{\chi_G}{s} - 2 \int_0^1 dx_1 dx_2 \int_0^{y_1} dy_2 \left( x_2 \ln \frac{W_G}{s} + \frac{1-x_2}{y_2} \ln \frac{W_G}{W_G|_{y_2=0}} \right) \right] \right\}, \\
\Delta_{G,12}^{\text{sc}} &= \frac{1}{2} \left[ -\frac{1}{2} F_{-1}^2(s) + \frac{7}{8} + \int_0^1 dx_1 dx_2 dy_1 \int_0^{y_1} dy_2 \ln \frac{W_G}{s} \right], \\
\Delta_{G,22}^{\text{sc}} &= -\frac{1}{2} \left[ F_{-2}^2(s) + F_{-1}^2(s) \left( \frac{3}{4} - \ln \frac{m^2}{s} \right) + \frac{7}{16} + \frac{\zeta(2)}{4} + \frac{1}{2} \ln^2 \frac{m^2}{s} - \frac{3}{4} \ln \frac{m^2}{s} - \int_0^1 dx_1 dx_2 dy_1 \int_0^{y_1} dy_2 \frac{1}{x_2} \ln \frac{W_G}{W_G|_{x_2=0}} \right].
\end{aligned} \tag{132}$$

In order to get the collinear-finite parts, we have to extract and discard the collinear logarithms  $\ln(m^2/s)$ . Concerning the coefficients of the metric tensor, only  $\Delta_{G,22}^{\text{sc}}$  has a collinear-divergent behavior;  $\Delta_{G,11}^{\text{sc}}$  and  $\Delta_{G,12}^{\text{sc}}$  are in a form suited for numerical integration, and there we simply set  $m = 0$ . For  $\Delta_{G,22}^{\text{sc}}$ , some of the collinear logarithms are already explicit and we can discard them; the last term of  $\Delta_{G,22}^{\text{sc}}$  in Eq.(133), instead, requires a further step. Introducing  $W_{G,0} = x_2 A_G + x_2 y_2 M_a^2 + y_2 m^2$  and  $W_{G,1} = A_G + y_2 M_a^2$ , we have

$$\begin{aligned}
\int_0^1 \frac{dx_2}{x_2} \ln \frac{W_G}{W_G|_{x_2=0}} &= \int_0^1 \frac{dx_2}{x_2} \left( \ln \frac{W_G}{W_{G,0}} + \ln \frac{W_{G,0}}{W_G|_{x_2=0}} \right) \\
&= \int_0^1 \frac{dx_2}{x_2} \ln \frac{(1-x_2) A_G + y_2 M_a^2}{A_G + y_2 M_a^2} - \text{Li}_2 \left( -\frac{W_{G,1}}{y_2 m^2} \right) + \mathcal{O}(m^2) \\
&= \frac{1}{2} \ln^2 \frac{m^2}{s} + \ln \frac{m^2}{s} \ln \frac{y_2 s}{W_{G,1}} - \text{Li}_2 \left( \frac{A_G}{W_{G,1}} \right) + \frac{1}{2} \ln^2 \frac{y_2 s}{W_{G,1}} + \zeta(2) + \mathcal{O}(m^2).
\end{aligned} \tag{133}$$

The integrals in Eq.(131) containing  $W_G^{-1}$  show a collinear-divergent behavior for  $m \rightarrow 0$  at the point  $x_2 = 0$ ; therefore, terms where  $W_G^{-1}$  is multiplied by  $x_2$  are not singular and there we can simply set  $m = 0$ . If no factor  $x_2$  is present, instead, we write

$$\begin{aligned}
\int_0^1 dx_2 \frac{1}{W_G} &= \int_0^1 dx_2 \frac{1}{W_{G,0}} + \int_0^1 dx_2 \left( \frac{1}{W_G} - \frac{1}{W_{G,0}} \right) \\
&= \frac{1}{A_G + y_2 M_a^2} \ln \frac{A_G + y_2 (M_a^2 + m^2)}{y_2 m^2} + \int_0^1 \frac{dx_2}{x_2} \left[ \frac{1}{(1-x_2) A_G + y_2 M_a^2} - \frac{1}{A_G + y_2 M_a^2} \right] + \mathcal{O}(m^2) \\
&= \frac{1}{W_{G,1}} \left( -\ln \frac{m^2}{s} + \ln \frac{M_a^2}{s} + 2 \ln \frac{W_{G,1}}{y_2 M_a^2} \right) + \mathcal{O}(m^2).
\end{aligned} \tag{134}$$

Now all collinear logarithms have been extracted and can be discarded. The finite remainder, however, can not be directly integrated numerically, because of the presence of denominators which can vanish inside the

integration region. On the other hand, these denominators are always linear in the variable  $y_2$ , being both  $A_G$  and  $W_G$  linear in  $y_2$ , and all terms generated from  $W_G^{-1}$  have the following dependence on  $y_2$ :

$$\frac{y_2^n}{a y_2 + b}, \quad \frac{y_2^n}{a y_2 + b} \ln \frac{a y_2 + b}{c}, \quad y_2^n \frac{\ln y_2}{a y_2 + b}. \quad (135)$$

For them we write

$$\begin{aligned} \frac{\ln(a y_2 + b)}{a y_2 + b} &= \frac{1}{a} \partial_{y_2} \left[ \frac{1}{2} \ln^2 \left( 1 + \frac{a}{b} y_2 \right) + \ln b \ln \left( 1 + \frac{a}{b} y_2 \right) \right], \\ \frac{\ln y_2}{a y_2 + b} &= \frac{1}{a} \partial_{y_2} \left[ \ln y_2 \ln \left( 1 + \frac{a}{b} y_2 \right) + \text{Li}_2 \left( -\frac{a}{b} y_2 \right) \right], \quad \frac{1}{a y_2 + b} = \frac{1}{a} \partial_{y_2} \ln \left( 1 + \frac{a}{b} y_2 \right). \end{aligned} \quad (136)$$

The crucial point in Eq.(136) is that in the right-hand side the  $1/a$  is always multiplied by a regulator function which goes to zero when the  $a$  vanishes. The  $-i0$  prescription associated to each mass ensures the validity of these expressions and can be used to produce the right imaginary parts of the logarithms. After integrating by parts in  $y_2$ , we get for the collinear-finite parts

$$\begin{aligned} V_{\text{sc,fin}}^G &= I_{\text{sc}}^G[0, 1, 0, 0, 1, 1], \quad V_{\text{sc,fin}}^G[q_i^\mu] = - \sum_{h=1}^2 p_h^\mu I_{\text{sc}}^G[b_{G,i}^h, c_{G,i}^h, d_{G,i}^h, \bar{d}_{G,i}^h, e_{G,i}^h, \bar{e}_{G,i}^h], \\ V_{\text{sc,fin}}^G[q_i^\mu q_j^\nu] &= \Delta_{G,ij}^{\text{fin}} \delta^{\mu\nu} + \sum_{h,k=1}^2 p_h^\mu p_k^\nu I_{\text{sc}}^G[b_{G,ij}^{hk}, c_{G,ij}^{hk}, d_{G,ij}^{hk}, \bar{d}_{G,ij}^{hk}, e_{G,ij}^{hk}, \bar{e}_{G,ij}^{hk}], \end{aligned} \quad (137)$$

where the auxiliary function  $I_{\text{sc}}^G$  depends on six parameters, symbolically denoted by  $\{b\}_6$ :

$$\begin{aligned} I_{\text{sc}}^G[\{b\}_6] &= \int_0^1 dx_1 dx_2 dy_1 dy_2 \left\{ \frac{b_1}{\rho_G} \ln \left( 1 + \frac{y_1 y_2 \rho_G}{x_2 \chi_G} \right) + \frac{b_2}{\rho_G} \ln \left( 1 + \frac{y_1 \rho_G}{x_2 \chi_G} \right) \right. \\ &\quad - \frac{b_3}{\eta_G} \left[ \ln^2 \left( 1 + \frac{y_1 y_2 \eta_G}{\chi_G} \right) + \left( \ln \frac{M_a^2}{s} + 2 \ln \frac{\chi_G}{y_1 y_2 M_a^2} \right) \ln \left( 1 + \frac{y_1 y_2 \eta_G}{\chi_G} \right) \right] + \frac{2b_4}{\eta_G} \ln \left( 1 + \frac{y_1 y_2 \eta_G}{\chi_G} \right) \\ &\quad \left. - \frac{b_5}{\eta_G} \left[ \ln^2 \left( 1 + \frac{y_1 \eta_G}{\chi_G} \right) + \left( \ln \frac{M_a^2}{s} + 2 \ln \frac{\chi_G}{y_1 M_a^2} \right) \ln \left( 1 + \frac{y_1 \eta_G}{\chi_G} \right) \right] + \frac{2b_6}{\eta_G} \text{Li}_2 \left( -\frac{y_1 \eta_G}{\chi_G} \right) \right\}. \end{aligned} \quad (138)$$

We recall that  $\chi_G = p_2^2 y_1 (1 - y_1) + M^2$ ; in addition, we have introduced the polynomials:

$$\rho_G = x_1 x_2 (1 - y_1) (P^2 - p_2^2) - x_2 M^2 + M_a^2, \quad \eta_G = x_1 (1 - y_1) (P^2 - p_2^2) - M^2 + M_a^2. \quad (139)$$

Concerning the coefficients of the metric tensor, we have defined  $\Delta_{G,11}^{\text{fin}} = \Delta_{G,11}^{\text{sc}}|_{m=0}$ ,  $\Delta_{G,12}^{\text{fin}} = \Delta_{G,12}^{\text{sc}}|_{m=0}$ , since they are collinear free; for  $\Delta_{G,22}^{\text{fin}}$ , we start from Eq.(133) and insert the result of Eq.(133),

$$\Delta_{G,22}^{\text{fin}} = - \frac{1}{2} \left\{ F_{-2}^2(s) + \frac{3}{4} F_{-1}^2(s) + \frac{7}{16} - \frac{\zeta(2)}{4} + \int_0^1 dx_1 dy_1 \int_0^{y_1} dy_2 \left[ \text{Li}_2 \left( \frac{A_G}{A_G + y_2 M_a^2} \right) - \frac{1}{2} \ln^2 \frac{A_G + y_2 M_a^2}{y_2 s} \right] \right\}. \quad (140)$$

Finally, we show the explicit expressions for the arguments of the vector integrals (second equation in Eq.(137)),

$$\begin{aligned} b_{G,1}^1 &= -x_1 x_2 y_1, & b_{G,1}^2 &= 0, & b_{G,2}^1 &= x_1 y_1, & b_{G,2}^2 &= 0, \\ c_{G,1}^1 &= 1 - x_1 - x_1 x_2 (1 - y_1), & c_{G,1}^2 &= -x_2 (1 - y_1), & c_{G,2}^1 &= 1 - x_1 y_1, & c_{G,2}^2 &= 1 - y_1, \\ d_{G,1}^1 &= 0, & d_{G,1}^2 &= 0, & d_{G,2}^1 &= x_1 y_1, & d_{G,2}^2 &= 0, \\ e_{G,1}^1 &= 1 - x_1, & e_{G,1}^2 &= 0, & e_{G,2}^1 &= 1 - x_1 y_1, & e_{G,2}^2 &= 1 - y_1, \\ \bar{e}_{G,1}^1 &= 1 - x_1, & \bar{e}_{G,1}^2 &= 0, & \bar{e}_{G,2}^1 &= 1, & \bar{e}_{G,2}^2 &= 1 - y_1, \end{aligned} \quad (141)$$

and for those of the tensor integrals (third equation in Eq.(137)),

$$\begin{aligned}
b_{G,11}^{11} &= -2 x_1 x_2 y_1 \{1 - x_1 [x_2 + y_1 y_2 (1 - x_2)]\}, & b_{G,11}^{12} &= b_{G,11}^{21} = -x_1 x_2 y_1 (1 - x_2) (1 - y_1), \\
b_{G,11}^{22} &= 0, & b_{G,12}^{11} &= x_1 y_1 (1 - x_1 - x_2 - x_1 x_2 + 2 x_1 x_2 y_1 y_2), \\
b_{G,12}^{12} &= b_{G,12}^{21} = -x_1 x_2 y_1 (1 - y_1), & b_{G,12}^{22} &= 0, \\
b_{G,22}^{11} &= 2 x_1 y_1 (1 - x_1 y_1 y_2), & b_{G,22}^{12} &= b_{G,22}^{21} = x_1 y_1 (1 - y_1), \\
b_{G,22}^{22} &= 0, & c_{G,11}^{11} &= [1 - x_1 - x_1 x_2 (1 - y_1)]^2 - x_1^2 x_2 (1 - y_1)^2, \\
c_{G,11}^{12} &= c_{G,11}^{21} = -x_2 (1 - y_1) \{1 - x_1 [1 - (1 - x_2) (1 - y_1)]\}, & c_{G,11}^{22} &= -x_2 (1 - x_2) (1 - y_1)^2, \\
c_{G,12}^{11} &= (1 - x_1 y_1) [1 - x_1 - x_1 x_2 (1 - y_1)], & c_{G,12}^{12} &= (1 - y_1) [1 - x_1 - x_1 x_2 (1 - y_1)], \\
c_{G,12}^{21} &= -x_2 (1 - y_1) (1 - x_1 y_1), & c_{G,12}^{22} &= -x_2 (1 - y_1)^2, \\
c_{G,22}^{11} &= (1 - x_1 y_1)^2, & c_{G,22}^{12} &= c_{G,22}^{21} = (1 - y_1) (1 - x_1 y_1), \\
c_{G,22}^{22} &= (1 - y_1)^2, & d_{G,11}^{ij} &= \bar{d}_{G,11}^{ij} = 0, \\
d_{G,12}^{11} &= \bar{d}_{G,12}^{11} = x_1 y_1 (1 - x_1), & d_{G,12}^{12} &= d_{G,12}^{21} = d_{G,12}^{22} = \bar{d}_{G,12}^{12} = \bar{d}_{G,12}^{21} = \bar{d}_{G,12}^{22} = 0, \\
d_{G,22}^{11} &= 2 x_1 y_1 (1 - x_1 y_1 y_2), & d_{G,22}^{12} &= \bar{d}_{G,22}^{12} = 0, \\
d_{G,22}^{12} &= d_{G,22}^{21} = \bar{d}_{G,22}^{12} = \bar{d}_{G,22}^{21} = x_1 y_1 (1 - y_1), & d_{G,22}^{22} &= \bar{d}_{G,22}^{22} = 0, \\
e_{G,11}^{11} &= \bar{e}_{G,11}^{11} = (1 - x_1)^2, & e_{G,11}^{12} &= e_{G,11}^{21} = e_{G,11}^{22} = \bar{e}_{G,11}^{12} = \bar{e}_{G,11}^{21} = \bar{e}_{G,11}^{22} = 0, \\
e_{G,12}^{11} &= (1 - x_1) (1 - x_1 y_1), & \bar{e}_{G,12}^{11} &= 1 - x_1, \\
e_{G,12}^{12} &= \bar{e}_{G,12}^{12} = (1 - x_1) (1 - y_1), & e_{G,12}^{2j} &= \bar{e}_{G,12}^{2j} = 0, \\
e_{G,22}^{11} &= (1 - x_1 y_1)^2, & \bar{e}_{G,22}^{11} &= 1, \\
e_{G,22}^{12} &= e_{G,22}^{21} = (1 - y_1) (1 - x_1 y_1), & \bar{e}_{G,22}^{12} &= \bar{e}_{G,22}^{21} = 1 - y_1, \\
e_{G,22}^{22} &= \bar{e}_{G,22}^{22} = (1 - y_1)^2. & & 
\end{aligned} \tag{142}$$

### 6.2.2 The collinear-finite part of $V_{\text{sc}}^K$

In this section we consider the  $V_{\text{sc}}^K$  configuration, using the Feynman parametrization of Ref. [48]. For the needed UV-finite scalar configuration we set  $\epsilon = 0$  in Eq. (159) of Ref. [48], perform the  $y_3$  integration and make the appropriate change of variables in order to simplify the integral. In the collinear configuration we obtain

$$V_{\text{sc}}^K = - \int_0^1 dx_1 dx_2 dy_1 \int_0^{y_1} dy_2 x_1 (1 - x_2) y_2 \sum_{i=a,b} \frac{1}{W_{K,i} U_{K,i}}, \tag{143}$$

where we have defined

$$\begin{aligned}
W_{K,a} &= x_2 (1 - x_2) A_{K,a} + y_2 [m^2 (1 - x_2) + M_a^2 x_2], & U_{K,a} &= A_{K,a} + y_2 M^2, \\
A_{K,a} &= (1 - y_1) [p_1^2 (y_1 - x_1 y_2) + p_2^2 x_1 y_2] + (1 - y_2) M^2, & & \\
W_{K,b} &= W_{K,a} (p_1 \leftrightarrow p_2), & U_{K,b} &= U_{K,a} (p_1 \leftrightarrow p_2).
\end{aligned} \tag{144}$$

The integrand behaves as  $1/x_2$  for  $m = 0$ , revealing the presence of a collinear divergence. In order to extract the collinear logarithm, we introduce the polynomial  $W_{K,a0} = x_2 A_{K,a} + y_2 (m^2 + M_a^2 x_2)$  (similarly for  $W_{K,b}$ ). Then, we perform the integration over  $x_2$ ,

$$\begin{aligned}
\int_0^1 dx_2 \frac{1 - x_2}{W_{K,a}} &= \int_0^1 dx_2 \left[ \frac{1}{W_{K,a0}} + \left( \frac{1}{W_{K,a}} - \frac{1}{W_{K,a0}} \right) \Big|_{m=0} - \frac{x_2}{W_{K,a}} \Big|_{m=0} \right] + \mathcal{O}(m^2) \\
&= \frac{1}{A_{K,a} + y_2 M_a^2} \left( -\ln \frac{m^2}{s} + \ln \frac{M_a^2}{s} + 2 \ln \frac{A_{K,a} + y_2 M_a^2}{y_2 M_a^2} \right) - \frac{1}{A_{K,a}} \ln \frac{A_{K,a} + y_2 M_a^2}{y_2 M_a^2} + \mathcal{O}(m^2).
\end{aligned} \tag{145}$$

All the polynomials involved in the computation are linear in  $y_2$ ; therefore, an additional analytical integration is possible. First, we perform two splittings,

$$\frac{y_2}{U_{K,a} (A_{K,a} + y_2 M_a^2)} = \frac{1}{M^2 - M_a^2} \left( \frac{1}{A_{K,a} + y_2 M_a^2} - \frac{1}{U_{K,a}} \right), \quad \frac{y_2}{U_{K,a} A_{K,a}} = \frac{1}{M^2} \left( \frac{1}{A_{K,a}} - \frac{1}{U_{K,a}} \right). \tag{146}$$

Secondly, we carry on the  $y_2$  integration by means of the relations introduced in Eq.(136) and of the identity

$$\frac{\ln(cy_2+b)}{ay_2+b} = \frac{1}{a} \partial_{y_2} \left[ \frac{1}{2} \ln^2 \left( 1 + \frac{a}{b} y_2 \right) + \ln b \ln \left( 1 + \frac{a}{b} y_2 \right) + \text{Li}_2 \left( -\frac{a}{b} y_2 \right) + \text{Li}_2 \left( \frac{(a-c)y_2}{ay_2+b} \right) - \text{Li}_2 \left( -\frac{c}{b} y_2 \right) \right]. \quad (147)$$

Note that for  $a \rightarrow 0$  the content of the squared bracket vanishes; the complete result reads

$$V_{\text{sc,fin}}^K = \int_0^1 dx_1 dy_1 \frac{x_1}{M^2} \left\{ \frac{1}{\rho_K} L_K(y_1 \rho_K, y_1 M_a^2, y_1 M_a^2; 0) - \frac{2 M^2}{(M^2 - M_a^2) \eta_K} L_K(y_1 \eta_K, 0, y_1 M_a^2; 1) \right. \\ \left. - \frac{1}{(p_1^2 - p_2^2) y_1} \left[ L_K(y_1 \omega_K, \mu_K, (1-y_1) M_a^2; 0) - \frac{2 M^2}{M^2 - M_a^2} L_K(y_1 \omega_K, \mu_K, (1-y_1) M_a^2; 1) \right] \right\}, \quad (148)$$

where we have introduced

$$L_K(A, B, C; \alpha) = \text{Li}_2 \left( \frac{-B}{\chi_K + A} \right) - \text{Li}_2 \left( \frac{A+B}{-\chi_K} \right) + \frac{1}{2} \ln^2 \left( 1 + \frac{A}{\chi_K} \right) + \left( \ln \frac{\chi_K}{C} + \frac{\alpha}{2} \ln \frac{M_a^2}{s} \right) \ln \left( 1 + \frac{A}{\chi_K} \right). \quad (149)$$

Here  $\chi_K = y_1(1-y_1)p_2^2 + M^2$  and the polynomials appearing in the arguments of  $L_K$  are given by

$$\eta_K = \omega_K + M_a^2 - M^2, \quad \rho_K = \omega_K - M^2, \quad \omega_K = x_1(1-y_1)(p_1^2 - p_2^2), \quad \mu_K = (1-y_1)(M^2 - M_a^2). \quad (150)$$

### 6.2.3 The collinear-finite part of $V_{\text{sc}}^H$

As previously done for  $V_{\text{sc}}^C$  and  $V_{\text{sc}}^K$ , we specify here the parametrization of the diagram, following the procedure outlined in section 10.4 of Ref. [47]. Setting the UV regulator  $\epsilon$  to zero and performing some trivial change of variables, we can cast the collinear configuration of  $V_{\text{sc}}^H$  as

$$V_{\text{sc}}^H = -P^2 \int dC_5(x, y, \{z\}) x y (1-x) (1-y) \frac{a_H}{W_H^2}, \quad (151)$$

where we have defined the following quantities:

$$\begin{aligned} W_H &= y(1-y) A_H + y B_H + (1-y) x (1-x) m^2, & A_H &= x(1-x)(1-z_2 - z_3)(1-z_1 - z_2) P^2, \\ B_H &= x \chi_H + (1-x) M^2, & \chi_H &= P^2 z_2 (1-z_2) + M_a^2, \\ a_H &= M_a^2 - M^2 - P^2 \mathcal{Z}_H (1 - \mathcal{Z}_H), & \mathcal{Z}_H &= z_1 + x(1-y)(1-z_1 - z_2). \end{aligned} \quad (152)$$

Since the collinear singularity for  $m \rightarrow 0$  shows up at the point  $y = 0$ , we extract the collinear logarithm according to

$$\int_0^1 dy \frac{y(1-y)}{W_H^2} = \int_0^1 dy y \left[ \frac{1}{W_{H,0}^2} + \left( \frac{1-y}{W_H^2} - \frac{1}{W_{H,0}^2} \right) \right] = \frac{1}{W_{H,0}^2} \left[ \ln \frac{W_{H,0}}{x(1-x)s} - \ln \frac{m^2}{s} - 1 \right] + \int_0^1 dy \left( \frac{1-y}{y} \left( \frac{1-y}{W_H^2} - \frac{1}{W_{H,0}^2} \right) \right) + \mathcal{O}(m^2), \\ \int_0^1 dy \frac{y^{n+2}(1-y)}{W_H^2} = \int_0^1 dy \frac{y^n(1-y)}{W_H^2} + \mathcal{O}(m^2), \quad n \geq 0, \quad (153)$$

where we have introduced  $W_{H,0} = y W_{H,0} + x(1-x) m^2$ ,  $W_H = (1-y)A_H + B_H$  and  $W_{H,0} = A_H + B_H$ . We notice that all polynomials involved in the computation are combinations of the quantities  $A_H$  and  $B_H$ , both linear in  $z_1$ ; therefore, for the terms involving  $W_{H,0}^{-2}$  or  $W_H^{-2}$ , we perform an integration by parts in  $z_1$  using the following relations:

$$\int_0^1 dz_1 z_1^n \frac{\ln(az_1+b)}{(az_1+b)^2} = \int_0^1 dz_1 \left[ \frac{z_1^n}{(az_1+b)^2} + n z_1^{n-1} \frac{\ln(az_1+b)}{a(az_1+b)} \right] - \frac{\ln(a+b)}{a(a+b)} + \delta_{n,0} \frac{\ln b}{ab}, \\ \int_0^1 dz_1 \frac{z_1^n}{(az_1+b)^2} = -\frac{n}{b} \int_0^1 dz_1 \frac{z_1^n}{az_1+b} + \frac{1}{b(a+b)}. \quad (154)$$

Let now be  $\mathcal{P}$  and  $\mathcal{Q}$  two generic polynomials in the Feynman variables. The result after this step can be formally written as a sum of terms of the form  $1/\mathcal{Q}\mathcal{P}$  or  $\ln\mathcal{P}/\mathcal{Q}\mathcal{P}$ . These polynomials are directly related to  $W_H$  and  $W_{H,0}$  and therefore are linear in  $z_3$ , as one can easily prove by direct computation. Therefore, we can use the following relations, with  $\Delta = ad - bc$ :

$$\begin{aligned} \frac{1}{(az_3 + b)(cz_3 + d)} &= \frac{1}{\Delta} \partial_{z_3} \left[ \ln(az_3 + b) - \ln(cz_3 + d) \right], \\ \frac{\ln(cz_3 + d)}{(az_3 + b)(cz_3 + d)} &= \frac{1}{\Delta} \partial_{z_3} \left[ \ln \frac{\Delta}{a} \ln \frac{az_3 + b}{cz_3 + d} - \text{Li}_2 \left( \frac{\Delta}{a(cz_3 + d)} \right) - \ln \frac{\Delta}{a(cz_3 + d)} \ln \left( 1 - \frac{\Delta}{a(cz_3 + d)} \right) \right]. \end{aligned} \quad (155)$$

After performing the integration over  $z_3$ , the remaining integrands can be cast as

$$\frac{1}{\omega_H} \ln^n \left( 1 + \frac{\omega_H}{\mathcal{P}} \right) \left[ 1, \ln \frac{\mathcal{Q}}{s} \right], \quad \frac{1}{\omega_H} \text{Li}_2 \left( \frac{\omega_H}{\mathcal{P}} \right), \quad \frac{1}{\omega_H} \ln \frac{\mathcal{P}}{s} \left[ 1, \ln x, \ln(1-x), \ln \frac{\omega_H}{s} \right], \quad (156)$$

with  $n = 1, 2$ , where we have defined  $\omega_H = x \chi_H + (1-x) M^2$ . The first two cases in Eq.(156) can be numerically integrated; the last, instead, requires further manipulations. In particular, for the terms with  $1/y$ , coming from the last integral of the first relation contained in Eq.(153), we have always the combination

$$\frac{1}{\omega_H} \int_0^1 \frac{dy}{y} \ln \frac{\mathcal{P}'(1-y) - \omega_H}{\mathcal{P}' - \omega_H} = -\frac{1}{\omega_H} \text{Li}_2 \left( \frac{\mathcal{P}'}{\mathcal{P}' - \omega_H} \right) = \frac{1}{\omega_H} \left[ \text{Li}_2 \left( \frac{\omega_H}{\mathcal{P}' - \omega_H} \right) + \ln \frac{\omega_H}{\mathcal{P}' - \omega_H} \ln \left( 1 - \frac{\omega_H}{\mathcal{P}' - \omega_H} \right) - \zeta(2) \right]. \quad (157)$$

In the last expression, the terms with  $\zeta(2)$  cancel out and the others are suited for numerical integration. For the other terms of the type  $\omega_H^{-1} \ln(\mathcal{P}/s)$ , we explicitly write the  $i0$  Feynman prescription and get

$$\frac{1}{\omega_H} \ln \frac{\mathcal{P}}{s} = \frac{1}{\omega_H} \ln \frac{(\mathcal{P} + \omega_H) - \omega_H - i0}{s} = \frac{1}{\omega_H} \left[ \ln \left( 1 - \frac{\omega_H}{\mathcal{P} + \omega_H - i0} \right) + \ln \left( \frac{\mathcal{P} + \omega_H}{s} - i0 \right) \right], \quad (158)$$

where the first logarithm regulates the zero of the denominator  $\omega_H$ , while the second is always of the following form:

$$\ln \left( \frac{\mathcal{P} + \omega_H}{s} - i0 \right) = \ln \left( x(1-x) \frac{\mathcal{P}'}{s} - i0 \right) = \ln x + \ln(1-x) + \ln \left( \frac{\mathcal{P}'}{s} - i0 \right). \quad (159)$$

Here  $\mathcal{P}'$  does not depend on  $x$ . As a consequence, for the terms containing this logarithm, we can integrate by parts in  $x$ , since  $\omega_H$  is linear in  $x$ , using the three relations of Eq.(136) (replacing  $y_2$  with  $x$ ).

Collecting all pieces, we derive the final result for  $V_{\text{sc,fin}}^H$ ,

$$\begin{aligned} V_{\text{sc,fin}}^H &= \sum_{n=1}^3 \int dC_4(x, y, \{z\}) \left\{ \frac{2b_{H,n}}{\omega_H} \left[ 2 \text{Li}_2 \left( \frac{\omega_H}{\omega_n} \right) + \left( \ln \frac{x(1-x)\omega_H}{s} - 2 \ln \frac{\omega_n}{s} \right) \ln \left( 1 - \frac{\omega_H}{\omega_n} \right) \right] \right. \\ &\quad \left. + \frac{c_{H,n}}{\omega_H} \ln \left( 1 - \frac{\omega_H}{\omega_{n,y}} \right) \right\} + \int_0^1 dx dz_1 dz_2 \frac{1}{\bar{\omega}_H} \left\{ \Theta_1 \text{Li}_2 \left( -\frac{\bar{\omega}_H}{M^2} \right) + \left( \Theta_2 \ln \frac{M^2}{s} + \Theta_3 \right) \ln \left( 1 + \frac{\bar{\omega}_H}{M^2} \right) \right. \\ &\quad \left. + \Theta_4 \left[ \frac{1}{2} \ln \left( 1 + \frac{x\bar{\omega}_H}{M^2} \right) + \ln \frac{M^2}{xs} - 2 \right] \ln \left( 1 + \frac{x\bar{\omega}_H}{M^2} \right) + (\Theta_5 + \Theta_6 \ln x) \ln \left( 1 - \frac{x\bar{\omega}_H}{\chi_H} \right) \right\}, \end{aligned} \quad (160)$$

where, in addition to  $\omega_H$  introduced after Eq.(156), we have defined auxiliary quantities in term of  $\chi_H$  of Eq.(152),

$$\begin{aligned} \bar{\omega}_H &= \chi_H - M^2, \quad \omega_n = \omega_H + P^2 x(1-x) \sigma_n, \quad \omega_{n,y} = \omega_H + P^2 x(1-x)(1-y) \sigma_n, \\ \sigma_1 &= (1-z_2)^2, \quad \sigma_2 = -z_2(1-z_2), \quad \sigma_3 = (1-z_2)(1-z_1-z_2), \end{aligned} \quad (161)$$

$$\Theta_n = 2 d_{H,n} \ln \left( \frac{P^2}{s} (1-z_1-z_2) - i0 \right) + i \pi e_{H,n} \text{sign}(P^2). \quad (162)$$

The coefficients appearing in Eq.(160) and Eq.(162) read as

$$\begin{aligned}
b_{H,1} &= M^2 - M_a^2 + \frac{P^2}{4}(4z_2^2 - 6z_2 + 1), & b_{H,2} &= M_a^2 - M^2 - \frac{P^2}{4}[(4z_2^2 - 6z_2 + 3)x - 2], \\
b_{H,3} &= P^2(1-x)[1 - 2z_2 - 2(1-x)(1-z_1-z_2)], & c_{H,1} &= -2P^2x(1-z_2)[1 - x(1-z_2)(2-y)], \\
c_{H,2} &= P^2x[1 - \frac{x}{2}(2-y)(4z_2^2 - 6z_2 + 3)], & c_{H,3} &= -2P^2x[1 - 2z_2 - 2(2-2x+xy)(1-z_1-z_2)], \\
d_{H,1} &= P^2(1-2z_1), & d_{H,2} &= 0, \\
d_{H,3} &= P^2(z_1 - z_2), & d_{H,4} &= P^2[1 - 2z_2 - 4(1-x)(1-z_1-z_2)], \\
d_{H,5} &= -P^2[1 - 2z_2 - 2x(1-z_1-z_2)], & d_{H,6} &= -P^2[1 - 2z_2 - 4x(1-z_1-z_2)], \\
e_{H,1} &= 4(M^2 - M_a^2) + \frac{P^2}{2}(4z_2^2 - 6z_2 + 1), & e_{H,2} &= 2(M_a^2 - M^2) - \frac{P^2}{2}(4z_2^2 - 6z_2 + 1), \\
e_{H,3} &= \frac{P^2}{4}(12z_2^2 - 18z_2 + 5), & e_{H,4} &= -P^2[1 - x(4z_2^2 - 6z_2 + 3)], \\
e_{H,5} &= P^2[x - 2(2-x)(1-z_2)(1-2z_2)], & e_{H,6} &= P^2[1 - (1-x)(4z_2^2 - 6z_2 + 3)].
\end{aligned} \tag{163}$$

### 6.3 Vertices with two photons coupled to light fermions

In this section we extract the coefficients of the collinear logarithms for the MIs illustrated in Fig. 19, where both photons are attached to light-fermion lines. In general the two light masses  $m$  and  $m'$  are different and both vanishing small: therefore, we need to extract both collinear logarithms,  $L = \ln(m^2/M^2)$  and  $L' = \ln(m'^2/M^2)$ .

#### 6.3.1 The Master Integral $V_{dc}^G$

We apply to  $V_{dc}^G$  the parametrization introduced for  $V^H$  in section 10.4 of Ref. [47]. We first combine the  $q_1$  and  $q_2$  propagators with  $z_1$  and  $z_2$  Feynman parameters; the resulting expression contains the product of three propagators, the first in  $q_1$ , the second in  $q_1 - q_2$  and the last in  $q_2$ ,

$$\begin{aligned}
V_{dc}^G &= \frac{1}{P^2} \frac{\mu^{2\epsilon}}{\pi^4} \int d^n q_1 d^n q_2 \int_0^1 dz_1 dz_2 \frac{P^2 M^2 - 4(M^2 + P^2 + q_1 \cdot p_2) q_2 \cdot p_1}{[12]^2 [3] [45]^2}, \\
[12] &= q_1^2 + 2z_1 q_1 \cdot p_1 + m'^2, \quad [3] = (q_1 - q_2)^2 + M^2, \quad [45] = q_2^2 + 2q_2 \cdot (p_1 + z_2 p_2) + z_2 P^2 + m^2.
\end{aligned} \tag{164}$$

The terms [12] and [3] are then combined with a variable  $x$  and the  $q_1$  integration is performed generating a new  $q_2$  propagator; the resulting two  $q_2$ -dependent propagators are then combined with a new variable  $y$ , so that the integration in  $q_2$  can be carried on. After extracting the UV simple pole in  $\epsilon$ , the result simply reads

$$\begin{aligned}
V_{dc}^G &= \frac{1}{2} F_{-1}^2(M^2) - \frac{7}{8} - \int dC_4(x, y, \{z\}) (1-y) \left[ \ln \frac{U_G}{M^2} + (1-x) \frac{c_G}{U_G} \right], \\
c_G &= M^2 [1 + 2z_2(1-y)] + P^2 z_2(1-y) \{1 + z_1[1 - x(1-y)]\}, \\
U_G &= z_1 z_2 x y (1-x)(1-y) P^2 + x y M^2 + x(1-x)(1-y) m^2 + y(1-x) m'^2.
\end{aligned} \tag{165}$$

Only the term containing  $U_G^{-1}$  is singular for a vanishing fermion mass; indeed, for  $m \rightarrow 0$  ( $m' \rightarrow 0$ ), a term  $y^{-1}(x^{-1})$  can be factorized out of  $U_G^{-1}$ , leading to a divergent integral. Therefore, if  $U_G^{-1}$  is multiplied by the product  $xy$ , we can simply set the fermion masses to zero, while if  $U_G^{-1}$  is multiplied by  $x$  or  $y$  we have to perform a subtraction,

$$\frac{x}{U_G} = x \left( \frac{1}{U_G} - \frac{1}{U_{G,y}} \right) + \frac{x}{U_{G,y}}, \quad \frac{y}{U_G} = y \left( \frac{1}{U_G} - \frac{1}{U_{G,x}} \right) + \frac{y}{U_{G,x}}, \tag{166}$$

where the subscripts  $x$  and  $y$  indicate that inside  $U_G$  we have set  $x^2 = 0$  and  $y^2 = 0$ . The first bracket in both equations is collinear free while the last term of the first (second) formula generates the collinear logarithm  $L$  ( $L'$ ), after an explicit integration in  $y$  ( $x$ ). For terms where the coefficient of  $U_G^{-1}$  contains neither  $x$  nor  $y$  a double subtraction is needed,

$$\frac{1}{U_G} = \left( \frac{1}{U_G} - \frac{1}{U_{G,x}} - \frac{1}{U_{G,y}} + \frac{1}{U_{G,xy}} \right) + \left( \frac{1}{U_{G,x}} - \frac{1}{U_{G,xy}} \right) + \left( \frac{1}{U_{G,y}} - \frac{1}{U_{G,xy}} \right) + \frac{1}{U_{G,xy}}, \tag{167}$$

with  $x^2 = y^2 = 0$  in the polynomial with the subscript  $xy$ . The first bracket of Eq.(167) contains no singularity; in the second (third) bracket, we integrate in  $x$  ( $y$ ) generating the collinear logarithm  $L'$  ( $L$ ). Finally, in the last term, both integrations in  $x$  and  $y$  are performed and the product  $LL'$  appears. Having extracted the collinear logarithms, we can now set the fermion masses to zero, obtaining

$$V_{\text{dc}}^G = \frac{1}{2} F_{-1}^2(M^2) + \frac{3}{8} + \int dC_4(x, y, \{z\}) (\mathcal{I}_G LL' + \mathcal{I}_G^y L + \mathcal{I}_G^x L' + \mathcal{I}_G^{xy}), \quad (168)$$

where we have introduced

$$\begin{aligned} \mathcal{I}_G &= -\alpha_{G,1} \xi_{G,0}^{-1}, & \mathcal{I}_G^u &= \alpha_{G,1} \left( \frac{\xi_{G,u}^{-1}}{u} \Big|_+ + \xi_{G,0}^{-1} \ln \frac{\xi_{G,0}}{M^2} \right) - \alpha_{G,u} \xi_{G,u}^{-1}, & u &= x, y, \\ \mathcal{I}_G^{xy} &= -\alpha_{G,1} \left\{ \frac{\xi_G^{-1}}{xy} \Big|_{++} + \sum_{u=x,y} \frac{\xi_{G,u}^{-1} [\ln(\xi_{G,u}/M^2) - 1]}{u} \Big|_+ + \xi_{G,0}^{-1} \left[ \ln^2 \frac{\xi_{G,0}}{M^2} + \zeta(2) \right] - \xi_{G,x}^{-1} \frac{\ln(1-x)}{x} \right\} \\ &+ \sum_{u=x,y} \alpha_{G,u} \xi_{G,u}^{-1} \left( 2 \ln \frac{\xi_{G,u}}{M^2} - 1 \right) - \alpha_{G,x} \xi_{G,x}^{-1} \ln(1-x) - \alpha_G \xi_G^{-1} - (1-y) \ln \frac{\xi_G}{M^2}. \end{aligned} \quad (169)$$

Here the  $'+$  and  $'++$  distributions have been defined in Eq.(8) and Eq.(9); the  $\alpha_G$  coefficients and the  $\xi_G$  functions are given by

$$\begin{aligned} \alpha_G &= P^2 z_2 \{ (2-y)[1 + z_1(2-x)] + z_1(1-x)(1-y)^2 \} + M^2 [1 + 2z_2(2-y)], & \xi_G &= P^2 z_1 z_2 (1-x)(1-y) + M^2, \\ \alpha_{G,y} &= \alpha_G(x=1), & \alpha_{G,x} &= \alpha_G(y=1), & \alpha_{G,1} &= \alpha_G(x=1=y), \\ \xi_{G,y} &= \xi_G(x=0), & \xi_{G,x} &= \xi_G(y=0), & \xi_{G,0} &= \xi_G(x=0=y). \end{aligned} \quad (170)$$

Since the  $\xi_G$  functions are linear in the four integration variables, all integrations can be analytically performed. Introducing  $\omega = -P^2/M^2$  and  $l_\omega = \ln(1-\omega)$ , the result is

$$\begin{aligned} V_{\text{dc}}^G &= \frac{1}{2} F_{-1}^2(M^2) - \frac{43}{8} - \frac{1}{\omega^2} \left\{ LL' [2\omega + (1-\omega)(2-\omega)l_\omega] + L [2\omega(1+\omega) + 2(1-\omega)l_\omega - (1-\omega)(2-\omega)l_\omega^2 \right. \\ &+ \omega(1-\omega)\text{Li}_2(\omega)] + L' [6\omega + (1-\omega)(4-\omega)l_\omega - (1-\omega)(2-\omega)l_\omega^2 + (\omega^2 - 2\omega + 2)\text{Li}_2(\omega)] \\ &+ \left[ \frac{19}{2} + 4\zeta(2) \right] \omega + \left[ \frac{3}{2} (5+\omega) + 2(2-\omega)\zeta(2) \right] (1-\omega)l_\omega - (1-\omega)(6-\omega)l_\omega^2 + \frac{4}{3} (1-\omega)(2-\omega)l_\omega^3 \\ &\left. - (\omega^2 - 4\omega + 2)\text{Li}_2(\omega) + 2(1-\omega)(2-\omega)l_\omega\text{Li}_2(\omega) - 2\omega\text{Li}_3(\omega) - 2(3\omega - 2)S_{1,2}(\omega) \right\}, \end{aligned} \quad (171)$$

where  $\text{Li}_n(\omega)$  and  $S_{1,2}(\omega)$  are Nielsen poly-logarithms.

### 6.3.2 The Master Integral $V_{\text{dc}}^H$

We parametrize  $V_{\text{dc}}^H$  following section 10.4 of Ref. [47]. After combining the  $q_1$ ,  $q_1 - q_2$  and  $q_2$  propagators with Feynman parameters  $z_1$ ,  $z_2$  and  $z_3$ , we obtain

$$\begin{aligned} V_{\text{dc}}^H &= \frac{\mu^{2\epsilon}}{\pi^4} \int d^n q_1 d^n q_2 \int dC_3(\{z\}) \frac{P^2 M^2 + 2P^2 q_1 \cdot p_1 - 4(q_1 \cdot p_1)^2}{[12]^2 [34]^2 [56]^2}, & [12] &= q_1^2 - 2z_1 q_1 \cdot p_2 + m^2, \\ [34] &= (q_1 - q_2)^2 + 2(q_1 - q_2) \cdot (p_1 - z_2 P) + M^2, & [56] &= q_2^2 - 2(1-z_3) q_2 \cdot p_1 + m'^2. \end{aligned} \quad (172)$$

Afterwards, [12] and [34] are combined with an additional variable  $x$ ; we integrate in  $q_1$  and obtain a new  $q_2$  propagator which is combined with [56] using a variable  $y$ . Finally, the  $q_2$  integration is performed. The MI  $V_{\text{dc}}^H$  is UV finite; after setting  $\epsilon = 0$ , we obtain

$$V_{\text{dc}}^H = - \int dC_5(x, y, \{z\}) xy(1-x)(1-y) \frac{c_H}{U_H^2},$$

$$\begin{aligned}
c_H &= P^2 M^2 + P^4 [z_1 - x(1-y)(z_1-z_2)][1 - z_1 + x(1-y)(z_1-z_2)], \\
U_H &= xy(1-x)(1-y)(z_1-z_2)(1-z_2-z_3)P^2 + xy\chi + y(1-x)m^2 + x(1-x)(1-y)m'^2, \quad (173)
\end{aligned}$$

where we have introduced  $\chi = z_2(1-z_2)P^2 + M^2$ .

The collinear-singular behavior corresponding to  $m \rightarrow 0$  ( $m' \rightarrow 0$ ) shows up at  $x = 0$  ( $y = 0$ ). In fact, in this limit, the global  $xy$  factor combines with the  $1/x^2$  ( $1/y^2$ ) term coming from  $U_H^{-2}$  and produces a global  $x^{-1}$  ( $y^{-1}$ ) divergent integral. Subtraction terms are evidently not needed when the coefficient of  $U_H^{-2}$  contains the product  $x^2y^2$ ; for terms where  $U_H^{-2}$  is multiplied by either  $x^2y$ ,  $xy^2$  or  $xy$ , we apply the following subtraction formulae:

$$x^2y(1-x)(1-y)U_H^{-2} = x^2y(1-x)[(1-y)U_H^{-2} - U_{H,y}^{-2}] + x^2y(1-x)U_{H,y}^{-2}, \quad (174)$$

$$xy^2(1-x)(1-y)U_H^{-2} = xy^2(1-y)[(1-x)U_H^{-2} - U_{H,x}^{-2}] + xy^2(1-y)U_{H,x}^{-2}, \quad (175)$$

$$\begin{aligned}
xy(1-x)(1-y)U_H^{-2} &= xy[(1-x)(1-y)U_H^{-2} - (1-y)U_{H,x}^{-2} - (1-x)U_{H,y}^{-2} + U_{H,xy}^{-2}] \\
&\quad + xy[(1-y)U_{H,x}^{-2} - U_{H,xy}^{-2}] + xy[(1-x)U_{H,y}^{-2} - U_{H,xy}^{-2}] + xyU_{H,xy}^{-2}. \quad (176)
\end{aligned}$$

The subscripts  $x$ ,  $y$  and  $xy$  for  $U_H$  indicate that we have set  $x^2 = 0$ ,  $y^2 = 0$  and  $x^2 = y^2 = 0$  respectively.

The first squared brackets in all three Eqs.(174-176) are collinear free. In the second (third) squared bracket of Eq.(176) and in the last term of Eq.(175) (Eq.(174)), the integration in  $x$  ( $y$ ) generates the collinear logarithms  $L$  ( $L'$ ). In the last term of Eq.(176) we perform both integrations in  $x$  and  $y$  obtaining the product  $LL'$ . At this point, the collinear-divergent behavior is explicit and we can set  $m = m' = 0$  inside all polynomials, getting

$$V_{\text{dc}}^H = \int dC_5(x, y, \{z\}) (\mathcal{I}_H L L' + \mathcal{I}_H^y L + \mathcal{I}_H^x L') + V_{\text{dc,fin}}^H, \quad (177)$$

$$\mathcal{I}_H = -\beta_H \xi_{H,0}^{-2}, \quad \mathcal{I}_H^u = \beta_H \left[ \frac{(1-u)\xi_{H,u}^{-2}}{u} \Big|_+ + \xi_{H,0}^{-2} \left( \ln \frac{\xi_{H,0}}{M^2} - 1 \right) \right] + \alpha_{H,u} \xi_{H,u}^{-2}, \quad u = x, y. \quad (178)$$

Here  $V_{\text{dc,fin}}^H$  reads

$$\begin{aligned}
V_{\text{dc,fin}}^H &= \int dC_5(x, y, \{z\}) \left\{ \alpha_H (1-y)\xi_H^{-2} - \alpha_{H,x} \left[ \frac{(1-y)\xi_{H,y}^{-2}}{y} \Big|_+ + \xi_{H,x}^{-2} \left( \ln \frac{\xi_{H,x}}{(1-x)M^2} - 1 \right) \right] - \beta_H \left[ \frac{(1-x)(1-y)\xi_H^{-2}}{xy} \Big|_{++} \right. \right. \\
&\quad \left. \left. + \sum_{u=x,y} \frac{(1-u)\xi_{H,u}^{-2} (\ln(\xi_{H,u}/M^2) - 1)}{u} \Big|_+ + \xi_{H,0}^{-2} \left( \ln^2 \frac{\xi_{H,0}}{M^2} - 2 \ln \frac{\xi_{H,0}}{M^2} + \zeta(2) \right) - (1-x)\xi_{H,x}^{-2} \frac{\ln(1-x)}{x} \right] \right\}, \quad (179)
\end{aligned}$$

where the  $\alpha_H$  and  $\beta_H$  coefficients and the  $\xi_H$  functions are given by

$$\begin{aligned}
\alpha_H &= P^4 (1-x)(1-z_1-z_2) \{ (1-z_1-z_2)[1-x(2-y)] - z_1 + z_2 \}, \quad \beta_H = P^2 [P^2 z_1(1-z_1) + M^2], \\
\xi_H &= P^2 [(1-z_1)(1-z_2)(1-z_3) + z_1 z_2 z_3] (1-x)(1-y) + P^2 z_2(1-z_2)(x+y-xy) + M^2, \\
\alpha_{H,y} &= \alpha_H(x=1) = 0, \quad \alpha_{H,x} = \alpha_H(y=1), \quad \xi_{H,y} = \xi_H(x=0), \quad \xi_{H,x} = \xi_H(y=0), \quad \xi_{H,0} = \xi_H(x=0=y). \quad (180)
\end{aligned}$$

We consider now the coefficients  $\mathcal{I}_H$ ,  $\mathcal{I}_H^x$  and  $\mathcal{I}_H^y$ , written in Eq.(178), of the collinear logarithms of Eq.(177), and express them in terms of one-loop functions. After changing  $y \rightarrow x$  in  $\mathcal{I}_H^y$ , we observe that the coefficients of  $L$  and  $L'$  are integrals in  $x$ ,  $z_1$ ,  $z_2$  and  $z_3$ . Then, we use the following trick to get rid of  $\ln(\xi_{H,0}/M^2)$ ,

$$\xi_{H,0}^{-2} \left( \ln \frac{\xi_{H,0}}{M^2} - 1 \right) = \xi_{H,0}^{-2} \ln \frac{P^2 z_2(1-z_2) + M^2}{M^2} + \int_0^1 dx \frac{(1-x)\xi_{H,x}^{-2}}{x} \Big|_+. \quad (181)$$

Since  $\beta_H$  and  $\alpha_{H,x}$  do not depend on  $z_3$  and  $\xi_{H,x}$  is linear in  $z_3$ , the  $z_3$  integration can be easily performed, leading to

$$V_{\text{dc}}^H = \int_0^1 dx dz_1 dz_2 (\mathcal{J}_H^{ff'} L L' + \mathcal{J}_H^f L + \mathcal{J}_H^{f'} L') + V_{\text{dc,fin}}^H, \quad \mathcal{J}_H^{ff'} = -\beta_H \eta_{H,0}^{-1} \rho_{H,0}^{-1},$$



In Eq.(189) the triangle of loop momentum  $q$  is to be intended in the graphical representation given in appendix A.

For the collinear-finite part  $V_{\text{dc,fin}}^H$  we do not need an analytical expression, since it will be enough to put it in a form suited for numerical evaluation. The situation is similar to the one for  $V_{\text{sc,fin}}^H$ , computed in section 6.2.3; all terms of Eq.(179) have the following structure, with respect to  $z_1$  and  $z_3$ :

$$f(n, m) = z_1^n \frac{\ln^m \xi}{\xi^2}, \quad \xi = a z_1 z_3 + b z_1 + c z_3 + d, \quad n, m = 0, 1, 2. \quad (190)$$

Therefore, we can integrate by parts in  $z_1$  after inserting

$$\frac{\ln^2 \xi}{\xi^2} = -\frac{2}{az_3+b} \partial_{z_1} \left[ \frac{1}{\xi} \left( 1 + \ln \xi + \frac{1}{2} \ln^2 \xi \right) \right], \quad \frac{\ln \xi}{\xi^2} = -\frac{1}{az_3+b} \partial_{z_1} \left[ \frac{1}{\xi} \left( 1 + \ln \xi \right) \right], \quad \frac{1}{\xi^2} = -\frac{1}{az_3+b} \partial_{z_1} \frac{1}{\xi}, \quad (191)$$

obtaining the result

$$\begin{aligned} V_{\text{dc,fin}}^H = \int dC_5(x, y, \{z\}) & \left\{ (1-x) \left[ \frac{1-y}{\xi_A} \left( \frac{\alpha_1}{\xi_B} - \frac{\alpha_z}{\xi} \right) + \left( \frac{1-y}{y\xi_A} \left( \frac{z_1 \alpha_{xz}}{\xi} - \frac{\alpha_{x1}}{\xi_B} \right) \right) \right] \Big|_{-} \frac{\ln(1-x)}{\xi_{xA}} \left( \frac{z_1 \alpha_{xz}}{\xi_x} - \frac{\alpha_{x1}}{\xi_{xB}} \right) \right] \\ & + \frac{1}{\xi_2} \left( \frac{\alpha_{x1}}{\xi_{xB}} \ln \frac{\xi_{xB}}{M^2} - \frac{\alpha_{x0}}{\xi_{xA}} \ln \frac{\xi_{xA}}{M^2} - \frac{\alpha_{xz}}{\xi_x} \ln \frac{\xi_x}{M^2} \right) + \left[ \frac{(1-x)(1-y)}{xy\xi_A} \left( \frac{z_1 \beta_z}{\xi} - \frac{\beta_0}{\xi_B} \right) \right] \Big|_{++} \\ & + \frac{1}{\xi_2} \sum_{u=x,y} \left[ \frac{1}{u} \left( \frac{\beta_0}{\xi_{uB}} \ln \frac{\xi_{uB}}{M^2} - \frac{\beta_0}{\xi_{uA}} \ln \frac{\xi_{uA}}{M^2} - \frac{\beta_z}{\xi_u} \ln \frac{\xi_u}{M^2} \right) \right] \Big|_{+} + \frac{1}{\xi_2} \left( \frac{\beta_0}{\xi_{0B}} \ln^2 \frac{\xi_{0B}}{M^2} - \frac{\beta_0}{\xi_{0A}} \ln^2 \frac{\xi_{0A}}{M^2} \right. \\ & \left. - \frac{\beta_z}{\xi_0} \ln^2 \frac{\xi_0}{M^2} \right) + \frac{\zeta(2)}{\xi_{0A}} \left( \frac{z_1 \beta_z}{\xi_0} - \frac{\beta_0}{\xi_{0B}} \right) - \frac{1-x}{x\xi_{xA}} \ln(1-x) \left( \frac{z_1 \beta_z}{\xi_x} - \frac{\beta_0}{\xi_{xB}} \right) \right\}, \quad (192) \end{aligned}$$

where we have used the following short-hand notations for the  $\xi$  functions,

$$\begin{aligned} \xi &= \xi_H, & \xi_x &= \xi_{H,x}, & \xi_y &= \xi_{H,y}, & \xi_0 &= \xi_{H,0}, & \xi_2 &= P^2 (z_2 + z_3 - 1), \\ \xi_A &= \xi(z_1 = 0), & \xi_{xA} &= \xi_x(z_1 = 0), & \xi_{yA} &= \xi_y(z_1 = 0), & \xi_{0A} &= \xi_0(z_1 = 0), \\ \xi_B &= \xi(z_1 = 1), & \xi_{xB} &= \xi_x(z_1 = 1), & \xi_{yB} &= \xi_y(z_1 = 1), & \xi_{0B} &= \xi_0(z_1 = 1), \end{aligned} \quad (193)$$

and for the  $\alpha$  and  $\beta$  coefficients,

$$\begin{aligned} \alpha_z &= P^4 z_1 \{ 1 - 2(1-z_1-z_2) [1-x(2-y)] - 2(1-z_1) \}, & \alpha_1 &= P^4 z_2 [1-xz_2(2-y)], \\ \alpha_{xz} &= P^4 [1-2(1-x)(1-z_1-z_2) - 2(1-z_1)], & \alpha_{x1} &= P^4 z_2 (1-xz_2), \\ \alpha_{x0} &= P^4 (1-z_2) [1-x(1-z_2)], & \beta_z &= P^4 (1-2z_1), & \beta_0 &= P^2 M^2. \end{aligned} \quad (194)$$

The result contains terms having the following structures in  $z_3$ :  $1/\mathcal{QP}$  and  $1/\mathcal{QP} \ln^n \mathcal{P}$ , with  $n = 1, 2$ , where  $\mathcal{Q}$  and  $\mathcal{P}$  are linear in  $z_3$ . The integration in  $z_3$  can be performed using Eq.(155) for the first two cases and the following relation for the last one, with  $\Delta = ad - bc$ :

$$\begin{aligned} \frac{\ln^2(cz_3+d)}{(az_3+b)(cz_3+d)} &= \frac{1}{\Delta} \partial_{z_3} \left\{ \ln^2 \frac{\Delta}{a} \left[ \ln(az_3+b) - \ln(cz_3+d) \right] - 2\text{Li}_3 \left( \frac{\Delta}{a(cz_3+d)} \right) \right. \\ & \left. - 2\ln(cz_3+d) \text{Li}_2 \left( \frac{\Delta}{a(cz_3+d)} \right) - \left[ \ln^2 \frac{\Delta}{a} - \ln^2(cz_3+d) \right] \ln \left( 1 - \frac{\Delta}{a(cz_3+d)} \right) \right\}. \quad (195) \end{aligned}$$

We also integrate analytically the '+' distributions and use the properties of the dilogarithms to cast the result in one of the following forms:

$$\frac{\mathcal{F}}{\chi} \ln^n \left( 1 - \frac{\chi}{\mathcal{P}} \right), \quad n = 1, 2; \quad \frac{\mathcal{F}}{\chi} \text{Li}_2 \left( \frac{\chi}{\mathcal{P}} \right); \quad \frac{\mathcal{F}}{\chi} \text{Li}_3 \left( \frac{\chi}{\mathcal{P}} \right); \quad \frac{\mathcal{F}}{\chi} S_{1,2} \left( \frac{\chi}{\mathcal{P}} \right); \quad \frac{1}{\chi} \ln \frac{\mathcal{P}}{M^2} \ln^k \frac{\chi}{M^2}, \quad k = 0, 1, 2, \quad (196)$$

where  $\mathcal{F}$  is a polynomial or a logarithm of polynomials. The first four forms are ready for numerical integration, since the zeros of  $\chi$  are compensated by a regulator function. For the last case, we observe that the polynomial  $\mathcal{P}$  is always of a special form: making explicit the  $i0$  Feynman prescription we have

$$\frac{1}{\chi} \ln \frac{\mathcal{P}}{M^2} = \frac{1}{\chi} \left[ \ln \left( 1 - \frac{\chi}{\mathcal{P} + \chi - i0} \right) + \ln \left( \frac{\mathcal{P} + \chi}{M^2} - i0 \right) \right], \quad \mathcal{P} + \chi = \pm a P^2 (1 - z_1 - z_2)^n, \quad n = 0, 1, \quad (197)$$

where  $a$  is the product of non-negative factors  $(1-x)$ ,  $(1-y)$ ,  $z_2$  and  $(1-z_2)$  which can be extracted from the logarithm. Our procedure has generated a regulator function for the zeros of  $\chi$  and we obtain a simple remainder which can be integrated in one variable (in our case  $z_1$ ).

Let us consider now terms without a regulator function: thanks to the special form of  $V_{\text{dc}}^H$ , the integration generates a factor  $\chi$  in the numerator, which cancels the  $\chi$  in the denominator. Note that this cancellation was anyway expected: if  $V_{\text{dc}}^H$  is a master integral, then it must have the right threshold properties of the original diagram. From the beginning (see section 5), we do not expect threshold singularities in  $V^H$  and a non-regulated  $1/\chi$  factor, having a  $1/\sqrt{1-4M^2/s}$  threshold behavior, is not allowed. The final expression for  $V_{\text{dc}}^H$  reads then

$$\begin{aligned} V_{\text{dc,fin}}^H = & \int dC_4(x, y, \{z\}) \frac{P^2}{\chi} \sum_{i=1}^3 \left\{ \frac{\beta_{a,i}}{2} \ln \left( 1 - \frac{\chi}{\xi_{a,i}} \right) + \frac{\beta_{b,i}}{2} \left[ 2 \text{Li}_2 \left( \frac{\chi}{\xi_{b,i}} \right) - \left( 2 \ln \frac{\xi_{b,i}}{M^2} - \ln \frac{(1-x)\chi}{M^2} \right) \ln \left( 1 - \frac{\chi}{\xi_{b,i}} \right) \right] \right. \\ & - 2\beta_{c,i} \left[ 2S_{1,2} \left( \frac{\chi}{\xi_{c,i}} \right) - 6\text{Li}_3 \left( \frac{\chi}{\xi_{c,i}} \right) + 2 \left( \ln \left( 1 - \frac{\chi}{\xi_{c,i}} \right) - 3 \ln \frac{\xi_{c,i}}{M^2} + \ln \frac{\chi}{M^2} \right) \text{Li}_2 \left( \frac{\chi}{\xi_{c,i}} \right) - \ln \frac{\xi_{c,i}}{\chi} \ln^2 \left( 1 - \frac{\chi}{\xi_{c,i}} \right) \right. \\ & \left. \left. + \left( 3 \ln \frac{\xi_{c,i}}{M^2} - 2 \ln \frac{\chi}{M^2} \right) \ln \frac{\xi_{c,i}}{M^2} \ln \left( 1 - \frac{\chi}{\xi_{c,i}} \right) \right] \right\} - 2i\pi \text{sign}(P^2) \int_0^1 dz_2 \left[ \ln^2 \frac{\chi}{M^2} - 2\zeta(2) \right], \quad (198) \end{aligned}$$

where the polynomial in the denominator is  $\chi = z_2(1-z_2)P^2 + M^2$ . The  $\xi$  functions and the  $\beta$  coefficients are given by

$$\begin{aligned} \xi_{a,1} &= z_2[1-z_2-(1-x)(1-y)(1-z_1-z_2)]P^2 + M^2, & \xi_{b,1} &= z_2[z_1-x(1-z_1-z_2)]P^2 + M^2, \\ \xi_{c,1} &= z_1z_2P^2 + M^2, & \xi_{a,2} &= z_2[1-z_2(x+y-xy)]P^2 + M^2, \\ \xi_{b,2} &= z_2(1-xz_2)P^2 + M^2, & \xi_{c,2} &= z_2P^2 + M^2, \\ \xi_{a,3} &= z_2(1-z_2)[1-y(1-x)]P^2 + M^2, & \xi_{b,3} &= xz_2(1-z_2)P^2 + M^2, \\ \xi_{c,3} &= M^2, & & \end{aligned} \quad (199)$$

$$\begin{aligned} \beta_{a,1} &= 4[1-2(2-2x+xy)(1-z_1-z_2)], & \beta_{b,1} &= 4[1-2(1-z_1)-2(1-x)(1-z_1-z_2)], & \beta_{c,1} &= 1-2z_1, \\ \beta_{a,2} &= -4z_2(1-2xz_2+xyz_2), & \beta_{b,2} &= -4z_2(1-xz_2), & \beta_{c,2} &= -M^2/P^2, \\ \beta_{a,3} &= 2-x(1-2z_2+4z_2^2)(1+y), & \beta_{b,3} &= 2-x+2xz_2(1-2z_2), & \beta_{c,3} &= M^2/P^2. \end{aligned} \quad (200)$$

#### 6.4 The special case of the $V^M$ family

The computation of the amplitude for  $H \rightarrow \gamma\gamma$  has been performed keeping the light-fermion masses during the whole generation  $\otimes$  simplification procedure; they have been set to zero just after the extraction of the collinear logarithms. Therefore, at intermediate steps, we have diagrams multiplied by a small mass which, in general, will disappear when the fermion mass goes to zero. However, some of these diagrams belong to the  $V^M$  family, and develop a  $1/m^2$  behavior. They are shown in Fig. 20 and they would in general lead to a residual contribution when their coefficient is proportional to  $m^2$ . It is worth noting that, concerning the  $H \rightarrow \gamma\gamma$  amplitude, only the scalar  $V^M$  function remains after the reduction  $\otimes$  symmetrization procedure; in fact, all tensor structures have been reduced to simpler topologies.

We parametrize the  $V_i^M$  ( $i = a, b$ ) integrals shown in Fig. 20 following section 8 of Ref. [47] and obtain

$$V_i^M = - \left( \frac{\mu^2}{\pi} \right)^\epsilon \Gamma(2+\epsilon) \int_0^1 dx dy \int_0^y dz_1 \int_0^{z_1} dz_2 [x(1-x)]^{-\frac{\epsilon}{2}} (1-y)^{\frac{\epsilon}{2}-1} (y-z_1) \chi_i(x, y, z_1, z_2)^{-2-\epsilon},$$

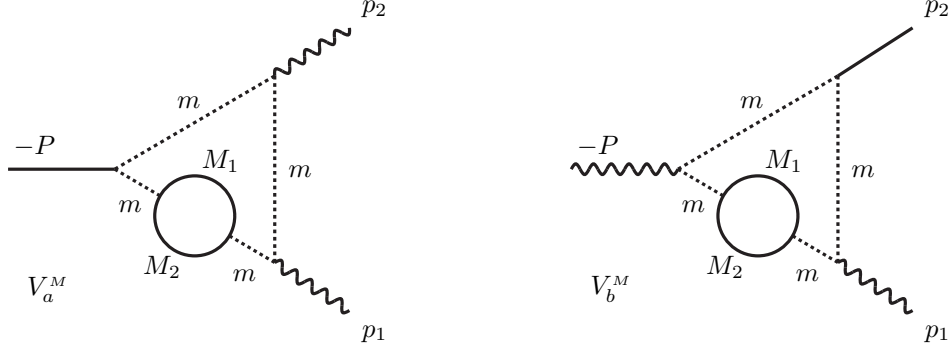


Figure 20: The  $V^M$  family, characterized by a  $1/m^2$  behavior in the  $m \rightarrow 0$  limit. Dot-lines have a small mass  $m$ ; wavy lines are massless.

$$\chi_a = m_x^2(1-y) + P^2 z_2(1-z_1) + m^2 y, \quad \chi_b = m_x^2(1-y) + p_2^2 z_2(z_1 - z_2) + m^2 y, \quad (201)$$

with  $m_x^2 = [M_1^2(1-x) + M_2^2 x]/[x(1-x)]$ . In order to extract the aforementioned  $1/m^2$  behavior, we apply a Bernstein-Sato-Tkachov algorithm [84] on  $\chi_i$ ,

$$\begin{aligned} \chi_a(x, y, z_1, z_2)^{-2-\epsilon} &= \frac{1}{m^2} \left\{ 1 + \frac{1}{1+\epsilon} \left[ (y-1)\partial_y + \frac{1}{2}(z_1-1)\partial_{z_1} + \frac{1}{2}z_2\partial_{z_2} \right] \right\} \chi_a(x, y, z_1, z_2)^{-1-\epsilon}, \\ \chi_b(x, y, z_1, z_2)^{-2-\epsilon} &= \frac{1}{m^2} \left\{ 1 + \frac{1}{1+\epsilon} \left[ (y-1)\partial_y + \frac{1}{2}z_1\partial_{z_1} + \frac{1}{2}z_2\partial_{z_2} \right] \right\} \chi_b(x, y, z_1, z_2)^{-1-\epsilon}. \end{aligned} \quad (202)$$

After integration by parts the poles are extracted. Analyzing the behavior at small  $m$ , we find that, in addition to the  $1/m^2$  behavior, also  $\ln m^2$  terms are present. The structure of the remaining integrals is simple enough to allow for a direct integration in all variables. The result yields

$$\begin{aligned} m^2 \times \text{Diagram } V_a^M &= -\frac{1}{P^2} \left[ 2F_{-1}^2(s) - \ln\left(-\frac{m^2}{P^2}\right) + \hat{\rho}(-P^2, M_1^2, M_2^2) + 1 \right] \\ &\quad + \mathcal{O}(\epsilon) + \mathcal{O}(m^2), \quad s = -P^2, \quad (203) \\ m^2 \times \text{Diagram } V_b^M &= -\frac{1}{p_2^2} \left\{ -2F_{-1}^2(s) \left[ \ln\left(-\frac{m^2}{p_2^2}\right) + 2 + i\pi \right] + \ln^2\left(-\frac{m^2}{p_2^2}\right) \right. \\ &\quad \left. + \ln\left(-\frac{m^2}{p_2^2}\right) \left[ 1 + i\pi - \hat{\rho}(-p_2^2, M_1^2, M_2^2) \right] - 2 - i\pi + \frac{\pi^2}{6} \right. \\ &\quad \left. - (2 + i\pi) \hat{\rho}(-p_2^2, M_1^2, M_2^2) \right\} + \mathcal{O}(\epsilon) + \mathcal{O}(m^2), \quad s = -p_2^2, \quad (204) \end{aligned}$$

and with  $\hat{\rho}(x, y, z) = [y \ln(y/x) - z \ln(z/x)]/(z-y)$ . Therefore, before taking the massless limit in the terms of the amplitude generated by the  $V^M$  family, we introduce the results of Eq.(203) and Eq.(204).

It turns out that all terms coming from these kinds of  $V^M$  diagrams, where the Higgs boson and the two photons are coupled to light fermions, are either zero or cancel analytically one another. As expected, they

lead to a total vanishing contribution; we would have obtained the same result treating them as massless diagrams from the very beginning. Note that diagrams with leptons, up and down quarks of the first and second generations and bottom quarks cancel separately.

Summarizing, in this section we have discussed an algorithm which allows to express the coefficients of all collinear logarithms in terms of one-loop integrals. In order to verify their cancellation, we then reduce all one-loop diagrams to scalar integrals with propagators raised to a canonical power one; this last step requires the standard reduction of Ref. [51] and the IBP identities of Ref. [41]. Each collinear-divergent diagram contributes to the total result with its collinear-free part which is manipulated as described above and then computed numerically.

## 7 Evaluation of massive diagrams

For the evaluation of massive two-loop diagrams, we follow the methods of Refs. [45,46] for self-energies and of Refs. [47,48,49] for vertices. For the three vertex families  $V^G$ ,  $V^K$  and  $V^H$ , we modify our approach, since two external massless particles appear and simpler results can be derived. Since the massive diagrams do not lead to collinear logarithms, the techniques described in this section can also be applied in the case of external light particles (setting their squared momenta to zero).

$V^G$  family. Let us consider the scalar, vector and tensor integrals of the  $V^G$  family, in the configuration where collinear divergences are absent and one of the two external squared momenta  $p_1^2$  and  $p_2^2$  vanishes. Setting without loss of generality  $p_2^2 = 0$ , we follow the parametrizations described in section 7 of Ref. [47] and in section 9 of Ref. [49], in close analogy with the procedure already described in section 6.2.1. The extraction of the UV poles is trivial; after an appropriate change of variables, we can write the  $V^G$  functions in parametric space as

$$\begin{aligned} V^G|_{p_2^2=0} &= - \int_0^1 dx_1 dx_2 dy_1 \int_0^{y_1} dy_2 (1-x_2) Y_G^{-1}, \\ V^G[q_i^\mu]_{p_2^2=0} &= \int_0^1 dx_1 dx_2 dy_1 \int_0^{y_1} dy_2 (1-x_2) p_{G,i}^\mu Y_G^{-1}, \quad p_{G,i}^\mu = \sum_{h=1}^2 a_{G,i}^h p_h^\mu, \\ V^G[q_i^\mu q_j^\nu]_{p_2^2=0} &= - \int_0^1 dx_1 dx_2 dy_1 \int_0^{y_1} dy_2 (1-x_2) p_{G,i}^\mu p_{G,i}^\nu Y_G^{-1} + \Delta_{G,ij} \delta^{\mu\nu}, \end{aligned} \quad (205)$$

where  $Y_G$  reads

$$\begin{aligned} Y_G &= a_G y_1 + b_G, \quad a_G = (1-x_2) \sigma_G, \quad \sigma_G = x_2 [x_1 y_2 (p_1^2 - P^2) + m_4^2 - m_5^2], \\ b_G &= x_1 x_2 y_2 (1-x_2) [P^2 - p_1^2 (1-x_1+y_2-x_2 y_2)] + x_2 (1-x_2) (m_5^2 - m_4^2 y_2) + y_2 (1-x_2) \chi_{G,x} + m_3^2 x_2 y_2, \\ \chi_{G,x} &= p_1^2 x_1 (1-x_1) + m_1^2 x_1 + m_2^2 (1-x_1), \end{aligned} \quad (206)$$

the coefficients of the tensor structures involving the external momenta are given by

$$a_{G,1}^1 = 1 - x_1 [1 - x_2 (1-y_2)], \quad a_{G,1}^2 = x_2 (1-y_1), \quad a_{G,2}^1 = 1 - x_1 y_2, \quad a_{G,2}^2 = 1 - y_1, \quad (207)$$

and the coefficients of the Kronecker delta are

$$\begin{aligned} \Delta_{G,11} &= -\frac{1}{2} F_{-2}^2(s) + \frac{1}{2} F_{-1}^2(s) \left( \int_0^1 dy_1 \ln \frac{m_{45}^2}{s} - \frac{3}{4} \right) - \frac{5}{32} - \frac{1}{8} \zeta(2) - \frac{1}{4} \int_0^1 dy_1 \ln^2 \frac{m_{45}^2}{s} \\ &\quad + \frac{1}{4} \int_0^1 dy_1 (\ln y_1 + 2) \ln \frac{m_{45}^2}{s} + \frac{1}{2} \int_0^1 dx_1 dx_2 dy_1 \int_0^{y_1} dy_2 \left( x_2 \ln \frac{Y_G}{s} + \frac{1-x_2}{y_2} \ln \frac{Y_G}{Y_G|_{y_2=0}} \right), \\ \Delta_{G,12} &= -\frac{1}{4} F_{-1}^2(s) + \frac{7}{16} + \frac{1}{2} \int_0^1 dx_1 dx_2 dy_1 \int_0^{y_1} dy_2 \ln \frac{Y_G}{s}, \end{aligned}$$

$$\begin{aligned}\Delta_{G,22} = & -\frac{1}{2}F_{-2}^2(s) + \frac{1}{2}F_{-1}^2(s) \left( \int_0^1 dx_1 \ln \frac{\chi_{G,x}}{s} - \frac{3}{4} \right) - \frac{7}{32} - \frac{1}{8}\zeta(2) - \frac{1}{4} \int_0^1 dx_1 \ln^2 \frac{\chi_{G,x}}{s} \\ & + \frac{3}{8} \int_0^1 dx_1 \ln \frac{\chi_{G,x}}{s} + \frac{1}{2} \int_0^1 dx_1 dx_2 dy_1 \int_0^{y_1} dy_2 \frac{1}{x_2} \ln \frac{Y_G}{Y_G|_{x_2=0}},\end{aligned}\quad (208)$$

with  $m_{45}^2 = m_4^2 y_1 + m_5^2(1-y_1)$  and  $s = -P^2$ .

The terms proportional to  $\delta^{\mu\nu}$  in Eq.(208) can be directly integrated numerically; for those terms in Eq.(205) containing  $Y_G^{-1}$  we observe that the polynomial  $Y_G$  is linear in  $y_1$  and integrate by parts,

$$\int_{y_2}^1 dy_1 \frac{y_1^n}{Y_G} = \frac{1}{a_G} \left[ \ln \left( 1 + \frac{a_G}{b_G} \right) - y_2^n \ln \left( 1 + \frac{a_G y_2}{b_G} \right) - n \int_{y_2}^1 dy_1 y_1^{n-1} \ln \left( 1 + \frac{a_G y_1}{b_G} \right) \right]. \quad (209)$$

Therefore, the expressions of Eq.(205) can be written in terms of simpler integral representations,

$$\begin{aligned}V^G|_{p_2^2=0} &= - \int_0^1 dx_1 dx_2 dy_2 \frac{1}{\sigma_G} \left[ \ln \left( 1 + \frac{a_G}{b_G} \right) - \ln \left( 1 + \frac{a_G y_2}{b_G} \right) \right], \\ V^G[q_i^\mu]_{p_2^2=0} &= \int_0^1 dx_1 dx_2 dy_1 dy_2 \left\{ \frac{\alpha_{G,i}^1}{\sigma_G} p_1^\mu \left[ \ln \left( 1 + \frac{a_G}{b_G} \right) - \ln \left( 1 + \frac{a_G y_2}{b_G} \right) \right] \right. \\ &\quad \left. + \alpha_{G,i}^2 p_2^\mu \left[ \frac{y_1}{\bar{a}_G} \ln \left( 1 + \frac{\bar{a}_G y_1}{\bar{b}_G} \right) - \frac{1-y_2}{\sigma_G} \ln \left( 1 + \frac{a_G y_2}{b_G} \right) \right] \right\}, \\ V^G[q_i^\mu q_j^\nu]_{p_2^2=0} &= \Delta_{G,ij} \delta^{\mu\nu} - \int_0^1 dx_1 dx_2 dy_1 dy_2 \left\{ \alpha_{G,i}^1 \alpha_{G,j}^1 p_1^\mu p_1^\nu \left[ \ln \left( 1 + \frac{a_G}{b_G} \right) - \ln \left( 1 + \frac{a_G y_2}{b_G} \right) \right] \right. \\ &\quad \left. + (\alpha_{G,i}^1 \alpha_{G,j}^2 p_1^\mu p_2^\nu + \alpha_{G,i}^2 \alpha_{G,j}^1 p_2^\mu p_1^\nu) \left[ \frac{y_1}{\bar{a}_G} \ln \left( 1 + \frac{\bar{a}_G y_1}{\bar{b}_G} \right) - \frac{1-y_2}{\sigma_G} \ln \left( 1 + \frac{a_G y_2}{b_G} \right) \right] \right. \\ &\quad \left. + \alpha_{G,i}^2 \alpha_{G,j}^2 p_2^\mu p_2^\nu \left[ \frac{2y_1(1-y_1)}{\bar{a}_G} \ln \left( 1 + \frac{\bar{a}_G y_1}{\bar{b}_G} \right) - \frac{(1-y_2)^2}{\sigma_G} \ln \left( 1 + \frac{a_G y_2}{b_G} \right) \right] \right\},\end{aligned}\quad (210)$$

where we have introduced short-hand notations related to Eq.(206) and Eq.(207),

$$\bar{a}_G = a_G|_{y_2 \rightarrow y_1 y_2}, \quad \bar{b}_G = b_G|_{y_2 \rightarrow y_1 y_2}, \quad \alpha_{G,1}^1 = a_{G,1}^1, \quad \alpha_{G,1}^2 = x_2, \quad \alpha_{G,2}^1 = a_{G,2}^1, \quad \alpha_{G,2}^2 = 1. \quad (211)$$

Looking at Eq.(210) we see that the zeros of  $\sigma_G$  in the denominator are smoothly compensated by logarithms that vanish for  $\sigma_G = 0$  ( $a_G$  is proportional to  $\sigma_G$ ). However, in the process under consideration we have  $m_4 = m_5$ , and we can encounter some numerical instability; in this case,  $\sigma_G$  is proportional to  $x_2 y_2$  and  $b_G$  vanishes for  $x_2 = y_2 = 0$ . Since the zero of  $b_G$  is of lower order with respect to the zero of  $\sigma_G$ , the instability can be cured by a sector decomposition of the unit square [85],

$$\int_0^1 dx_2 dy_2 f(x_2, y_2) = \left( \int_0^1 dx_2 \int_0^{x_2} dy_2 + \int_0^1 dy_2 \int_0^{y_2} dx_2 \right) f(x_2, y_2) = \int_0^1 dx_2 dy_2 \left[ x_2 f(x_2, x_2 y_2) + y_2 f(x_2 y_2, y_2) \right]. \quad (212)$$

$V^\kappa$  family. We analyze here the  $V^\kappa$  configurations with  $P^2 = 0$  and  $p_1^2 = p_2^2 = 0$ , focusing on the scalar diagram, since it is the only one which survives after the reduction procedure described in section 4.1. Note that the method explained here can be applied, with a straightforward generalization, also to tensor integrals. We set  $\epsilon = 0$  in Eq. (159) of Ref. [48], perform the  $y_3$  integration and make some change of variables simplifying the integral,

$$V^\kappa = \int_0^1 dx_1 dx_2 dy_1 \int_0^{y_1} dy_2 x_1 x_2 \sum_{i=a,b} \frac{1}{\mathcal{B}_{\kappa,i}} \left[ \frac{x_2(1-x_2)}{x_2(1-x_2)\mathcal{A}_{\kappa,i} + y_2 \mathcal{B}_{\kappa,i}} - \frac{1}{\mathcal{A}_{\kappa,i}} \right], \quad (213)$$

$$\begin{aligned}
\mathcal{A}_{\kappa,a} &= P^2 x_1 y_2 (y_1 - x_1 y_2) + (y_1 - x_1 y_2) [p_1^2 (1 - y_1) + m_4^2] + x_1 y_2 [p_2^2 (1 - y_1) + m_6^2] + (1 - y_1) m_5^2, \\
\mathcal{B}_{\kappa,a} &= P^2 x_2^2 x_1 (1 - x_1) + x_2 [m_1^2 (1 - x_1) + m_2^2 x_1] + (1 - x_2) m_3^2 - x_2 (1 - x_2) [m_4^2 (1 - x_1) + m_6^2 x_1], \\
\mathcal{A}_{\kappa,b} &= \mathcal{A}_{\kappa,a} (m_1 \leftrightarrow m_2, m_4 \leftrightarrow m_6, p_1 \leftrightarrow p_2), \quad \mathcal{B}_{\kappa,b} = \mathcal{B}_{\kappa,a} (m_1 \leftrightarrow m_2, m_4 \leftrightarrow m_6, p_1 \leftrightarrow p_2). \quad (214)
\end{aligned}$$

Note that the zeros of  $\mathcal{B}_{\kappa,a}$  and of  $\mathcal{B}_{\kappa,b}$  in Eq.(213) are compensated by a corresponding zero in the squared bracket. The general procedure described in Ref. [47] writes the integral in  $y_1$  and  $y_2$  as a one-loop  $C$  function; however, after setting  $P^2 = 0$  or  $p_1^2 = p_2^2 = 0$ , we observe that  $\mathcal{A}_{\kappa,a}$  and  $\mathcal{A}_{\kappa,b}$  are linear in  $y_2$  and  $y_1$ , respectively, thus allowing for an integration by parts where we use the last relation of Eq.(136). For the case  $P^2 = 0$  we obtain

$$\begin{aligned}
V^\kappa|_{P^2=0} &= \int_0^1 dx_1 dx_2 dy_1 \frac{x_2}{\mathcal{B}_{\kappa,a}} \left[ \frac{x_1 c_\kappa}{x_1 c_\kappa a_{\kappa,a} + \mathcal{B}_{\kappa,a}} \ln \left( 1 + \frac{x_1 c_\kappa a_{\kappa,a} + \mathcal{B}_{\kappa,a}}{c_\kappa b_{\kappa,a}} y_1 \right) - \frac{1}{a_{\kappa,a}} \ln \left( 1 + \frac{x_1 y_1 a_{\kappa,a}}{b_{\kappa,a}} \right) \right] + \left\{ \begin{array}{l} m_1 \leftrightarrow m_2 \\ m_4 \leftrightarrow m_6 \\ p_1 \leftrightarrow p_2 \end{array} \right\} \\
a_{\kappa,a} &= (p_2^2 - p_1^2)(1 - y_1) + m_6^2 - m_4^2, \quad b_{\kappa,a} = p_1^2 y_1 (1 - y_1) + m_4^2 y_1 + m_5^2 (1 - y_1), \quad c_\kappa = x_2 (1 - x_2). \quad (215)
\end{aligned}$$

A similar result holds for the configuration where  $p_1^2 = p_2^2 = 0$ ,

$$\begin{aligned}
V^\kappa|_{p_1^2=p_2^2=0} &= \int_0^1 dx_1 dx_2 dy_2 \frac{x_1 x_2}{\alpha_{\kappa,a} \mathcal{B}_{\kappa,a}} \left[ \ln \left( 1 + \frac{\gamma_\kappa \mathcal{B}_{\kappa,a}}{\alpha_{\kappa,a} + \beta_{\kappa,a}} \right) - \ln \left( 1 + \frac{\gamma_\kappa \mathcal{B}_{\kappa,a}}{\alpha_{\kappa,a} y_2 + \beta_{\kappa,a}} \right) \right] + \left\{ \begin{array}{l} m_1 \leftrightarrow m_2 \\ m_4 \leftrightarrow m_6 \end{array} \right\}, \quad (216) \\
\alpha_{\kappa,a} &= P^2 x_1 y_2 + m_4^2 - m_5^2, \quad \beta_{\kappa,a} = -P^2 x_1^2 y_2^2 + x_1 y_2 (m_6^2 - m_4^2) + m_5^2, \quad \gamma_\kappa = \frac{y_2}{x_2 (1 - x_2)}. \quad (217)
\end{aligned}$$

There are special configurations where the result can be further simplified integrating in one additional variable. This step becomes necessary to achieve numerical stability in all cases where special relations between masses move some zeros of the denominator to the border of the integration domain, as in Eq.(216) when  $m_3 = 0$ ,  $m_1 = m_4$  and  $m_2 = m_6$ ; in this case we can factorize  $x_2^2$  from  $\mathcal{B}_{\kappa,i}$  and carry on the integration in  $x_2$ ,

$$\int_0^1 \frac{dx_2}{x_2} \left[ \ln \left( 1 + \frac{Ax_2}{1-x_2} \right) - \ln \left( 1 + \frac{Bx_2}{1-x_2} \right) \right] = -\text{Li}_2(1-A) + \text{Li}_2(1-B). \quad (218)$$

$V^H$  family. For evaluating diagrams of the  $V^H$  family without collinear singularities, we rely on the methods developed in Ref. [3] where the requirement is that two external squared momenta vanish, as in the process  $H \rightarrow \gamma\gamma$ ; this condition allows for a double integration by parts in parametric space. However, the method described in Ref. [3] needs special care when applied in the region above threshold (a case not covered in Ref. [3]). Following the same parametrization procedure described in section 6.3.2, we set  $p_1^2 = p_2^2 = 0$  and obtain for diagrams up to rank two

$$\begin{aligned}
V^H|_{p_1^2=p_2^2=0} &= - \int dC_5(x, y, \{z\}) x y (1-x) (1-y) Y_H^{-2}, \\
V^H[q_i^\mu]_{p_1^2=p_2^2=0} &= - \int dC_5(x, y, \{z\}) x y (1-x) (1-y) Y_H^{-2} p_{H,i}^\mu, \quad p_{H,i}^\mu = \sum_{h=1}^2 a_{H,i}^h p_h^\mu, \\
V^H[q_i^\mu q_j^\nu]_{p_1^2=p_2^2=0} &= - \int dC_5(x, y, \{z\}) \frac{1-y}{Y_H} \left[ x y (1-x) Y_H^{-1} p_{H,i}^\mu p_{H,j}^\nu + \frac{1}{2} a_{H,ij}^0 \delta^{\mu\nu} \right], \quad (219)
\end{aligned}$$

where  $Y_H$  is given by

$$\begin{aligned}
Y_H &= xy(1-x)(1-y)\chi_{H,0} + y(1-x)\chi_{H,1} + xy\chi_{H,2} + x(1-x)(1-y)\chi_{H,3}, \quad \chi_{H,0} = (1-z_2-z_3)(1-z_1-z_2)P^2, \\
\chi_{H,1} &= m_1^2(1-z_1) + m_2^2 z_1, \quad \chi_{H,2} = P^2 z_2(1-z_2) + m_3^2(1-z_2) + m_4^2 z_2, \quad \chi_{H,3} = m_5^2(1-z_3) + m_6^2 z_3, \quad (220)
\end{aligned}$$

and the coefficients of the tensor structures read as

$$a_{H,1}^1 = -x(1-y)(1-z_2-z_3), \quad a_{H,1}^2 = 1-z_1-x(1-y)(1-z_2-z_1), \quad a_{H,2}^1 = z_3+y(1-z_2-z_3),$$

$$a_{H,2}^2 = y(1-z_1-z_2), \quad a_{H,11}^0 = x[1-x(1-y)], \quad a_{H,12}^0 = xy, \quad a_{H,22}^0 = y. \quad (221)$$

Focusing on the configurations which appear for the  $H \rightarrow \gamma\gamma$  decay, we set  $m_2 = m_1$ ,  $m_4 = m_3$ ,  $m_6 = m_5$  and use the symmetries of the result; vector integrals can be simply written in terms of the scalar one,

$$V_s^H[q_1^\mu] = \frac{1}{2} V_s^H p_2^\mu, \quad V_s^H[q_2^\mu] = \frac{1}{2} V_s^H p_1^\mu, \quad (222)$$

where the subscript  $s$  denotes the configuration  $p_1^2 = p_2^2 = 0$ ,  $m_2 = m_1$ ,  $m_4 = m_3$ ,  $m_6 = m_5$ . Furthermore, the expression for  $Y_H$  shows a simple dependence on  $z_1$  and  $z_3$ ,

$$\begin{aligned} Y_H &= \alpha_H [z_1 z_3 - (1-z_2)(z_1+z_3) + (1-z_2)^2] + \beta_H, & \alpha_H &= xy(1-x)(1-y)P^2, \\ \beta_H &= y(1-x)m_1^2 + xy\chi_{H,2} + x(1-x)(1-y)m_5^2, & \chi_{H,2} &= P^2 z_2(1-z_2) + m_3^2. \end{aligned} \quad (223)$$

This structure corresponds to the collinear case  $V_{sc}^H$  discussed in section 6.2.3; integrating by parts in  $z_1$  and  $z_3$  according to Eq.(154) and Eq.(155), we obtain ( $n, k \neq 0$ )

$$\begin{aligned} \int_0^1 dz_1 dz_3 \frac{z_1^n z_3^k}{Y_H^2} &= \frac{nk}{\alpha_H \beta_H} \int_0^1 dz_1 dz_3 z_1^{n-1} z_3^{k-1} \left[ \ln \frac{\alpha_H(1-z_2-z_3)(1-z_1-z_2) + \beta_H}{-\alpha_H z_2(1-z_1-z_2) + \beta_H} + \ln \frac{\alpha_H z_2^2 + \beta_H}{-\alpha_H z_2(1-z_3-z_2) + \beta_H} \right], \\ \int_0^1 dz_1 dz_3 \frac{z_1^n}{Y_H^2} &= \frac{n}{\alpha_H \beta_H} \int_0^1 dz_1 z_1^{n-1} \left[ \ln \frac{\alpha_H(1-z_2)(1-z_1-z_2) + \beta_H}{-\alpha_H z_2(1-z_1-z_2) + \beta_H} + \ln \frac{\alpha_H z_2^2 + \beta_H}{-\alpha_H z_2(1-z_2) + \beta_H} \right], \\ \int_0^1 dz_1 dz_3 \frac{z_3^k}{Y_H^2} &= \frac{k}{\alpha_H \beta_H} \int_0^1 dz_3 z_3^{k-1} \left[ \ln \frac{\alpha_H(1-z_2)(1-z_3-z_2) + \beta_H}{-\alpha_H z_2(1-z_3-z_2) + \beta_H} + \ln \frac{\alpha_H z_2^2 + \beta_H}{-\alpha_H z_2(1-z_2) + \beta_H} \right], \\ \int_0^1 dz_1 dz_3 \frac{1}{Y_H^2} &= \frac{1}{\alpha_H \beta_H} \left[ \ln \frac{\alpha_H(1-z_2)^2 + \beta_H}{-\alpha_H z_2(1-z_2) + \beta_H} + \ln \frac{\alpha_H z_2^2 + \beta_H}{-\alpha_H z_2(1-z_2) + \beta_H} \right], \\ \int_0^1 dz_3 \frac{1}{Y_H} &= -\frac{1}{\alpha_H(1-z_1-z_2)} \ln \left( 1 - \frac{\alpha_H(1-z_1-z_2)}{\alpha_H(1-z_2)(1-z_1-z_2) + \beta_H} \right), \end{aligned} \quad (224)$$

where in the last equation, which is related to the tensor form factors proportional to  $\delta^{\mu\nu}$ , we can carry on numerical integration. For the other four expressions in Eq.(224) we have to pay attention to the zeros of  $\beta_H$  (the factor  $\alpha_H^{-1}$  cancels with the numerator in Eq.(219)). It can be easily proved that the real part of the expression contained in the squared bracket vanishes in the limit  $\beta_H \rightarrow 0$ ; however, an imaginary part can in general survive. Below threshold, for  $s = -P^2 < 4m_3^2$ ,  $\beta_H$  does not change sign in the integration region; therefore, for the real part of the diagram below threshold (as done in [3]) it is enough to take the real part of the integrand and then integrate numerically. For  $H \rightarrow \gamma\gamma$ , we are interested also in the behavior above threshold, where we have to take into account the imaginary part of the squared bracket. Following the approach of section 6.2.3, we make explicit the  $i0$  prescription for masses and perform the following symbolic decomposition:

$$\frac{1}{\beta_H} \ln \frac{\mathcal{Q}_1 + \beta_H}{\mathcal{Q}_2 + \beta_H} = \frac{1}{\beta_H} \ln \frac{\mathcal{Q}_1 + \beta_H - i0}{\mathcal{Q}_2 + \beta_H - i0} = \frac{1}{\beta_H} \left[ \ln \left( 1 + \frac{\beta_H}{\mathcal{Q}_1 - i0} \right) - \ln \left( 1 + \frac{\beta_H}{\mathcal{Q}_2 - i0} \right) + \ln \frac{\mathcal{Q}_1 - i0}{\mathcal{Q}_2 - i0} \right]. \quad (225)$$

The first two terms are regular when  $\beta_H \rightarrow 0$ ; for the last term of Eq.(225) we notice that  $\beta_H$  is linearly dependent on  $y$  and in the argument of the logarithm a factor  $y$  can be simplified between  $\mathcal{Q}_1$  and  $\mathcal{Q}_2$ . Therefore, we can integrate by parts in  $y$  getting

$$\begin{aligned} V_s^H &= \frac{1}{P^2} \int_0^1 dx dy dz_2 \left\{ \frac{2}{\beta_H} \left[ \ln \left( 1 - \frac{\beta_H}{\beta_1} \right) - \ln \left( 1 - \frac{\beta_H}{\beta_2} \right) \right] + i\pi \operatorname{sign}(P^2) \frac{2}{\beta_H} \ln \left( 1 + \frac{\bar{\beta}_H}{\beta_0} \right) \right\}, \\ V_s^H[q_i^\mu q_j^\nu] &= \frac{1}{P^2} \int dC_5(x, y, \{z\}) \left\{ \delta^{\mu\nu} \frac{a_{H,ij}^0(1-y)}{2\alpha_H(1-z_1-z_2)} \ln \left( 1 + \frac{\alpha_H(1-z_1-z_2)}{\beta_3} \right) \right. \\ &\quad \left. + \sum_{h,k=1}^2 p_h^\mu p_k^\nu \left[ \sum_{n=1}^4 \frac{\alpha_{H,ij}^{n,hk}}{\beta_H} \ln \left( 1 - \frac{\beta_H}{\beta_n} \right) - i\pi \operatorname{sign}(P^2) \frac{1}{\beta_H} \sum_{l=1}^2 \Theta_{H,ij}^{l,hk} \ln \left( 1 + \frac{u_l \bar{\beta}_H}{\beta_0} \right) \right] \right\}, \end{aligned} \quad (226)$$

with  $u_1 = 1$  and  $u_2 = y$ . Here we have introduced short-hand notations for the  $\beta$  factors,

$$\begin{aligned} \beta_H &= \bar{\beta}_H y + \beta_0, & \bar{\beta}_H &= (1-x)m_1^2 + x\chi_{H,2} - x(1-x)m_5^2, & \beta_0 &= x(1-x)m_5^2, & \beta_n &= \beta_H + \alpha_H \sigma_n, \\ \sigma_1 &= (1-z_2)^2, & \sigma_2 &= -z_2(1-z_2), & \sigma_3 &= (1-z_2)(1-z_1-z_2), & \sigma_4 &= (1-z_3-z_2)(1-z_1-z_2), \end{aligned} \quad (227)$$

for the  $\Theta$ -functions and for the  $\alpha$ ,  $\beta$ ,  $\gamma$  and  $\delta$  coefficients

$$\Theta_{H,ij}^{lhk} = \beta_{H,ij}^{lhk} + \gamma_{H,ij}^{lhk} \Theta(z_1+z_2-1) + \delta_{H,ij}^{lhk} \Theta(z_1+z_2-1)\Theta(z_3+z_2-1), \quad l = 1, 2, \quad (228)$$

$$\begin{aligned} \alpha_{H,11}^{1,11} &= 2x^2(1-y)^2(1-z_2)^2, & \alpha_{H,11}^{2,11} &= -\frac{x^2}{2}(1-y)^2(4z_2^2-6z_2+3), \\ \alpha_{H,11}^{3,11} &= -4x^2(1-y)^2(1-z_1-z_2), & \alpha_{H,11}^{4,11} &= 0, \\ \alpha_{H,11}^{1,12} &= \alpha_{H,11}^{1,21} = -x(1-y)(1-z_2)[1-2x(1-y)(1-z_2)], & \alpha_{H,11}^{2,12} &= \alpha_{H,11}^{2,21} = -\frac{x}{2}(1-y)[1+x(1-y)(4z_2^2-6z_2+1)], \\ \alpha_{H,11}^{3,12} &= \alpha_{H,11}^{3,21} = x(1-y)\{1+2(1-z_2)[1-2x(1-y)]\}, & \alpha_{H,11}^{4,12} &= \alpha_{H,11}^{4,21} = -x(1-y)[1-x(1-y)], \\ \alpha_{H,11}^{1,22} &= 1-2x(1-y)(1-z_2)[1-x(1-y)(1-z_2)], & \alpha_{H,11}^{2,22} &= -[1-x(1-y) + \frac{x^2}{2}(1-y)^2(4z_2^2-6z_2+3)], \\ \alpha_{H,11}^{3,22} &= -2[1-x(1-y)][1-2z_1-2x(1-y)(1-z_1-z_2)], & \alpha_{H,11}^{4,22} &= 0, \end{aligned} \quad (229)$$

$$\begin{aligned} \beta_{H,11}^{1,11} &= 0, & \beta_{H,11}^{2,11} &= 2x^2(1-y)(1-z_2)(1-2z_2), \\ \gamma_{H,11}^{1,11} &= 0, & \gamma_{H,11}^{2,11} &= 2x^2(1-y)(5-4z_1-4z_2), \\ \delta_{H,11}^{1,11} &= \delta_{H,11}^{2,11} = \beta_{H,12}^{1,11} = \beta_{H,21}^{1,11} = 0, & \beta_{H,12}^{2,11} &= \beta_{H,21}^{2,11} = \frac{x}{2}[1+2x(1-y)(4z_2^2-6z_2+1)], \\ \gamma_{H,12}^{1,11} &= \gamma_{H,21}^{1,11} = 0, & \gamma_{H,12}^{2,11} &= \gamma_{H,21}^{2,11} = -x(1-2z_2)[1-4x(1-y)], \\ \delta_{H,12}^{1,11} &= \delta_{H,21}^{1,11} = 0, & \delta_{H,12}^{2,11} &= \delta_{H,21}^{2,11} = -2x[1-2x(1-y)], \\ \beta_{H,22}^{1,11} &= \frac{1}{2}, & \beta_{H,22}^{2,11} &= x[1-2xz_2(1-y)(3-2z_2)], \\ \gamma_{H,22}^{1,11} &= 3-4z_1, & \gamma_{H,22}^{2,11} &= -2x[5-4z_1-2z_2-x(1-y)(7-4z_1-4z_2)], \\ \delta_{H,22}^{1,11} &= 0, & \delta_{H,22}^{2,11} &= 0. \end{aligned} \quad (230)$$

Note that we have presented here only the coefficients of  $V_s^H[q_1^\mu q_1^\nu]$ , the surviving configuration after the reduction  $\otimes$  symmetrization procedure. Other tensor structures can be obtained with the help of the same procedure.

## 8 Numerical results

In this section we discuss the numerical results for the two-loop corrections to the decay widths of the processes  $H \rightarrow gg$  and  $H \rightarrow \gamma\gamma$ , given by

$$\Gamma(H \rightarrow gg) = \frac{\alpha_s^2(\mu_R^2)G_F M_W^2}{4\sqrt{2}\pi^3 M_H} \left| A_{\text{phys}}^{gg} \right|^2 \quad \text{and} \quad \Gamma(H \rightarrow \gamma\gamma) = \frac{\alpha^2 G_F M_W^2}{32\sqrt{2}\pi^3 M_H} \left| A_{\text{phys}}^{\gamma\gamma} \right|^2, \quad (231)$$

with  $A_{\text{phys}}^{gg} \frac{\alpha_s(\mu_R^2)}{2\pi} \left( \sqrt{2} G_F M_W^2 \right)^{1/2} = \mathcal{A}$  from Eq.(69) and  $A_{\text{phys}}^{\gamma\gamma} \frac{\alpha}{2\pi} \left( \sqrt{2} G_F M_W^2 \right)^{1/2} = \mathcal{A}$  from Eq.(65).

One important production mechanism of the Standard Model Higgs boson at the LHC is the gluon-fusion channel,  $pp \rightarrow gg + X \rightarrow H + X$ . Its partonic cross section  $\sigma$ , to LO in QCD, can be related to  $A_{\text{phys}}^{gg}$  via

$$\sigma(gg \rightarrow H) = \frac{\alpha_s^2(\mu_R^2)G_F M_W^2}{32\sqrt{2}\pi M_H^4} \left| A_{\text{phys}}^{gg} \right|^2. \quad (232)$$

The relative correction  $\delta$ , induced by the higher order corrections, is given by  $\Gamma = \Gamma_0(1+\delta)$  ( $\sigma = \sigma_0(1+\delta)$ ), where  $\Gamma_0$  ( $\sigma_0$ ) is the lowest order quantity. For the decay  $H \rightarrow \gamma\gamma$  we split the relative correction in  $\delta =$

$\delta_{\text{EW}} + \delta_{\text{QCD}}$ , to distinguish the contributions arising from electroweak and QCD corrections. For the process  $H \rightarrow gg(gg \rightarrow H)$  we consider only two-loop electroweak corrections; interplay between electroweak and QCD corrections has been discussed in Ref. [88] where an estimate of the remaining theoretical uncertainty is also presented.

As discussed in section 5.1 and section 5.2, threshold singularities appear in both reactions if we restrict the calculation to the RM scheme (see section 5.3). For the case  $H \rightarrow \gamma\gamma$  we consider a phenomenologically relevant Higgs-mass range from 100 GeV to 170 GeV, which contains the  $WW$  threshold. For the gluon-gluon case we consider a Higgs-mass range from 100 GeV to 500 GeV. Here we cross not only the  $WW$  threshold, but also the  $ZZ$  and  $\bar{t}t$  thresholds. The  $WW$  and  $ZZ$  thresholds have a different behavior as compared to the  $\bar{t}t$  threshold. Indeed, the amplitude around the  $\bar{t}t$  threshold contains a potentially dangerous two-point function, as explained in section 5, but in contrast to the  $WW$  and  $ZZ$  cases this singular function (for  $M_H^2 = 4 M_t^2$ ) is here protected by a multiplicative factor  $\beta^2 = 1 - 4M_t^2/s$ . In order to cure these singularities we have introduced complex masses [60] as described in section 5.3. We stress the fact that at the single  $W$  and  $Z$  thresholds no special enhancement occurs.

All light-fermion masses have been set to zero in the collinear-free amplitude and we have defined the  $W$ - and  $Z$ -boson *experimental* complex poles by

$$s_j = \mu_j (\mu_j - i \gamma_j), \quad \mu_j^2 = M_j^2 - \Gamma_j^2, \quad \gamma_j = \Gamma_j (1 - \Gamma_j^2/(2 M_j^2)), \quad (233)$$

with  $j = \{W, Z\}$ . As input parameters for the numerical evaluation we have used the following values [86,87]:

$$\begin{aligned} M_W &= 80.398 \text{ GeV}, & M_Z &= 91.1876 \text{ GeV}, & M_t &= 170.9 \text{ GeV}, & \Gamma_W &= 2.093 \text{ GeV}, \\ G_F &= 1.16637 \times 10^{-5} \text{ GeV}^{-2}, & \alpha(0) &= 1/137.0359911, & \alpha_s(M_Z) &= 0.118, & \Gamma_Z &= 2.4952 \text{ GeV}. \end{aligned}$$

For  $\Gamma(H \rightarrow gg)$  and  $\sigma(gg \rightarrow H)$  the behavior of  $\delta_{\text{EW}}$  as a function of  $M_H$  is given in Fig. 21. For the gluon-gluon case, treated in the CM scheme, we observe a smooth behavior in the full range of  $M_H$  where all cusps present in the MCM scheme have disappeared; we may conclude that results in the CM scheme nicely interpolate those of the RM scheme around thresholds. Therefore, all pathological aspects associated to the crossing of thresholds have disappeared. It is also worth mentioning that the CM scheme greatly improves stability in the numerical evaluation of all master integrals, especially those in the  $V^H$  family.

In the shown Higgs-mass range the percentage correction varies between about +6% and -4%.

It is important to consider this result in more details: around the  $WW$  threshold we find a maximum for the total electroweak percentage correction, and only a light shoulder of the curve around the  $ZZ$  threshold. Both characteristics are less suppressed if one considers only light fermions with real masses, shown in Fig. 23. Let us define light-fermion correction as those coming from the first and second generation of light (massless) quarks and the one from bottom quarks only; each of these three classes of diagrams constitutes a gauge-invariant subset.

It is worth noting that below the  $WW$  threshold the contributions from top quarks are small but they become significant above the  $ZZ$  threshold and even more important around the  $\bar{t}t$  threshold, where the curve exhibits a minimum, which is absent for light fermions, see Fig. 23. In this region the top-quark contribution leads to a sizable effect of about -4%.

The results for  $\Gamma(H \rightarrow gg)$  have been used to derive NLO electroweak corrections to Higgs production at hadron colliders in Ref. [88].

The numerical result for the percentage correction to the partial width  $\Gamma(H \rightarrow \gamma\gamma)$  has been presented in Ref.[38] in the minimal complex-mass (MCM) setup and is shown in Fig. 22, as well as the extension to the full complex-mass (CM) scheme. The QCD corrections (dotted curve) as well as the CM electroweak corrections (solid-line) are shown separately. If it is true that below the  $WW$  threshold  $\delta_{\text{QCD}}$  and  $\delta_{\text{EW}}$  almost compensate and lead to a small total correction (dash-dot line), the new results tell us that, above the  $WW$  threshold, both contributions are positive and lead to a sizable overall effect of approximately 4%. In the considered Higgs-boson mass range the total correction varies between  $-1\% < \delta_{\text{tot}} < 4\%$ .

To summarize, the electroweak correction around the  $WW$  threshold shown in Fig. 22 (dash-line) has been produced by minimally modifying the two-loop amplitude through the usage of a complex  $M_W$  mass. We have extended our calculation in order to treat the whole amplitude completely with complex  $W$  and  $Z$

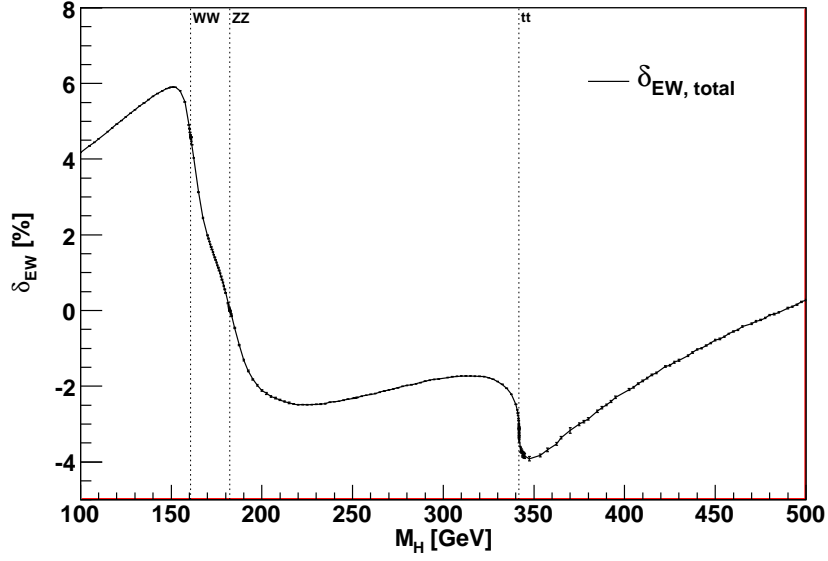


Figure 21: The two-loop electroweak percentage corrections for the decay width  $\Gamma(H \rightarrow gg)$  and the total partonic cross section  $\sigma(gg \rightarrow H)$ . The solid line denotes the total electroweak correction, including also top quarks (first + second + third generation). The vertical dash-lines indicate the location of electroweak thresholds.

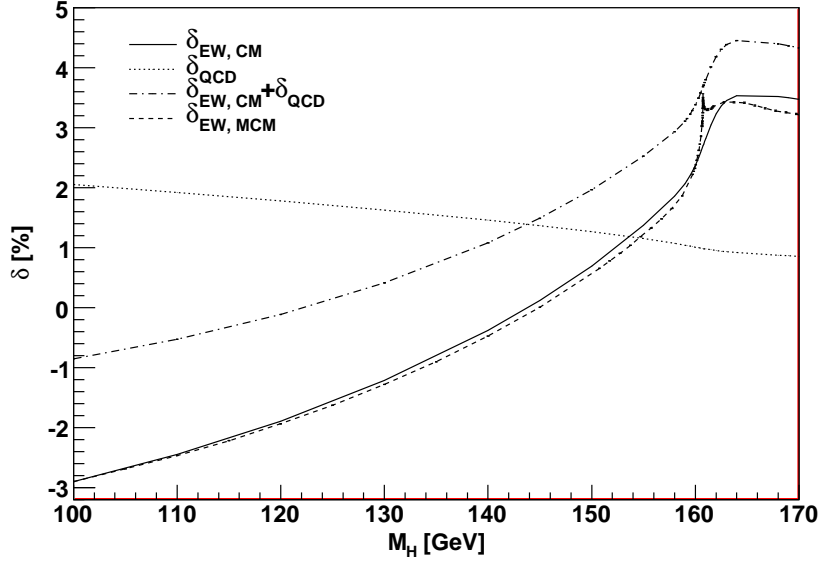


Figure 22: The two-loop electroweak and QCD percentage corrections for the  $H \rightarrow \gamma\gamma$  decay.

masses. This allows us to study the remaining cusp and the influence of the complex mass on the electroweak correction, which is shown through the solid line.

We have compared our numerical results in the region below the  $WW$  threshold with those of Ref. [28].

Eqs.(8) and (11) of Ref. [28] contain typos<sup>3</sup>; once we correct, very good agreement between our calculations, up to 130 – 140 GeV, is found. To be more precise, we split the total contribution into light fermions and top (namely diagrams with at least one top line); for the light-fermion contribution the agreement is always very good because the result of Ref. [27] is exact, whereas, for the top part, the comparison gives a check of how good is the expansion of Ref. [28]. We confirm what is expected, for light Higgs-boson masses (say, around 115 GeV) the agreement between our results is again very good and starts deteriorating for heavier values (say, starting from 140 GeV). In Fig. 23 we have summarized our findings for  $\delta_{EW}$  in gluon-gluon

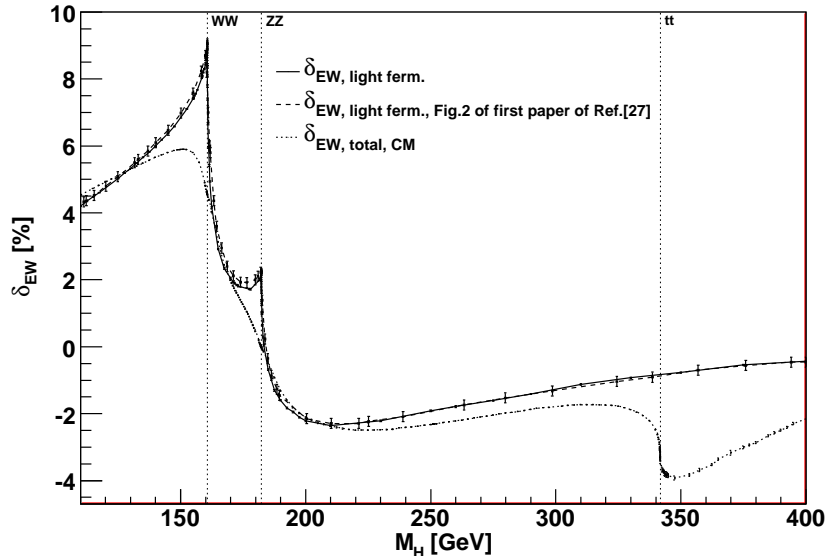


Figure 23: The two-loop electroweak percentage corrections for  $H \rightarrow gg$  showing a comparison: total in CM scheme, light fermions only in RM scheme, light fermions only obtained from Ref. [27] (see main text for the error bars).

fusion; here we also include the light-fermion part of the corrections compared with the ones of Ref. [27]. The result of Ref. [27] is known completely in terms of harmonic poly-logarithms. For simplicity we used the tool EasyNData [89] to read out the result from Fig. 2 of the first paper of Ref. [27], which is shown in Fig. 23 as a dash-line. The error bars originate from our estimation of how good we can read out the data from the plot. Once again, the relevant news are the behavior above  $WW$  threshold induced by top quarks and the around-threshold behavior in the CM scheme.

Differences become even more striking when we consider the total corrections in a narrower range in the Higgs-boson mass, as done in Fig. 24. Here we concentrate our attention around the region containing both  $WW$  and  $ZZ$  thresholds and compare our final result (CM scheme) with the one obtained from Tab. 2 of Ref. [28].

The very good agreement when we use the MCM scheme and the subsequent extension to CM scheme make us confident of the goodness of the result.

## 9 Conclusions

In this paper we have provided all technical details for a stand-alone numerical calculation of the full two-loop corrections to the decay widths  $H \rightarrow \gamma\gamma$  and  $H \rightarrow gg$ , where  $H$  stands for the Standard Model Higgs boson. The techniques introduced in this context, however, have a much wider range of application,

<sup>3</sup>Thanks to G. Degrossi and F. Maltoni for prompt confirmation.

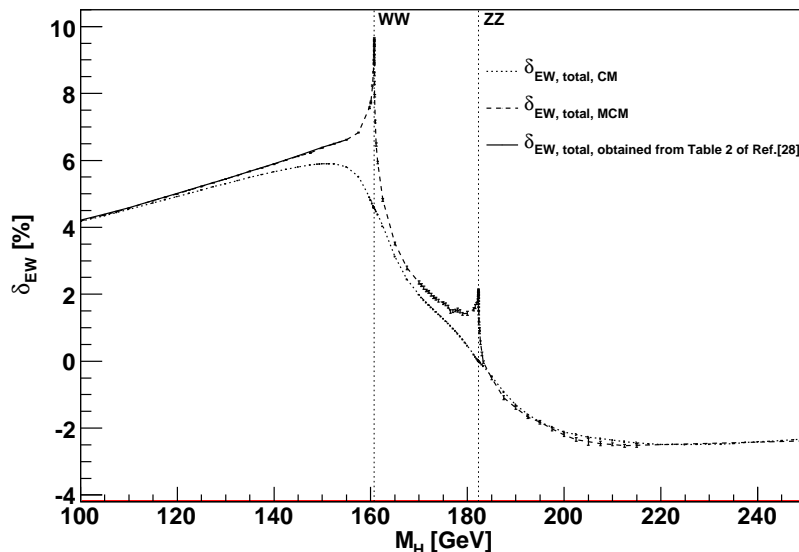


Figure 24: An analogous plot to Fig. 23 for a narrower range of the Higgs-boson mass. Here we compare our results in the CM and MCM schemes with the results (below 155 GeV) of Ref. [28]

i.e. they are general enough to be used for all kinematical configurations of  $1 \rightarrow 2$  processes at the two-loop level.

The generation of diagrams for any given process has always been performed with the FORM [39] program *GraphShot* [40] which performs simplifications and symbolic manipulations of the loop integrals, like performing traces, removing reducible scalar products and symmetrizing the integrals.

The amplitudes contain both QCD and electroweak contributions and our strategy has been to present complete calculations where all enhanced terms are extracted analytically and their cancellation shown, whenever it occurs; the remainder of the amplitude is a multi-dimensional integral in parametric space with an integrand which, after suitable algebraic manipulations, is transformed into a smooth function therefore avoiding well-known problems of numerical instabilities, even in those regions of parametric space which are notoriously plagued by normal threshold singularities; the latter are always cured by the introduction of complex masses, solving at the same time a conceptual problem, internal unstable particles, and a practical one, avoiding numerical instabilities associated with the behavior around singularities lying on the real axis of the external Mandelstam invariant.

The strategy for the rest of the calculations consists in regularizing the collinear singularities and in extracting the singular pieces from all singular terms. After checking – analytically – that singular parts cancel in the total (if it applies), one can safely take rid of the regularization parameter and include all collinear-free remainders into the total amplitude.

As far as numerical results are concerned we can safely state that the methods developed in this paper produce extremely accurate predictions for any value of the Higgs-boson mass, including the full dependence on the  $W$ -,  $Z$ - and Higgs-boson masses and on the top-quark mass. A consistent and gauge-invariant treatment of unstable particles allows to produce precise results around the physical thresholds: both a minimal and a complete version of this scheme are studied. It is found that the use of the complex mass scheme smoothens the threshold singularities and that a complete implementation of this scheme is needed in order to get the NLO electroweak corrections under control.

When applied to the gluon fusion channel,  $pp \rightarrow gg + X \rightarrow H + X$ , our results show that the electroweak scaling factor which should multiply the QCD-corrected cross-section is between  $-4\%$  and  $+6\%$  in the range

$100 \text{ GeV} < M_H < 500 \text{ GeV}$ , without incongruent effects around the physical electroweak thresholds. Finally we observe that around the  $t\bar{t}$  threshold the top-quark contribution to  $H \rightarrow gg$  leads to a sizable effect of about  $-4\%$ .

## Acknowledgments

We gratefully acknowledge important discussions with Giuseppe Degrossi, Ansgar Denner, Stefan Dittmaier, Robert Harlander, Philipp Kant, Massimiliano Grazzini, Fabio Maltoni, Michael Spira and Peter Zerwas.

The authors thank the Galileo Galilei Institute for Theoretical Physics for the hospitality and the INFN for partial support during the completion of this work.

This work has been supported by MIUR under contract 2001023713\_006, by the European Community's Marie Curie Research Training Network *Tools and Precision Calculations for Physics Discoveries at Colliders* under contract MRTN-CT-2006-035505, by the U.S. Department of Energy under contract No. DE-AC02-98CH10886 and by the Deutsche Forschungsgemeinschaft through Sonderforschungsbereich/Transregio 9 *Computergestützte Theoretische Teilchenphysik*. Feynman diagrams have been drawn with the packages AXODRAW [90] and JAXODRAW [91].

## A Self-energies, vertices and tadpoles

In this section we collect our conventions for the diagrams involved in the paper.

$$\begin{aligned}
 [f(q)] \xrightarrow{P} \text{Diagram B} &= \frac{\mu^\epsilon}{i\pi^2} \int d^n q \frac{f(q)}{[1][2]}, \quad \text{with} \quad \begin{cases} [1] = q^2 + m_1^2 \\ [2] = (q+P)^2 + m_2^2 \end{cases} \\
 [f(q)] \xrightarrow{-P} \text{Diagram C} &= \frac{\mu^\epsilon}{i\pi^2} \int d^n q \frac{f(q)}{[1][2][3]}, \quad \text{with} \quad \begin{cases} [1] = q^2 + m_1^2 \\ [2] = (q+p_1)^2 + m_2^2 \\ [3] = (q+P)^2 + m_3^2 \end{cases}
 \end{aligned}$$

Figure 25: The one-loop self-energy and vertex.  $f$  is a generic polynomial in the loop momentum  $q$ . The dimension of the space-time is  $n = 4 - \epsilon$  and  $\mu$  is the renormalization scale.

$$\begin{aligned}
 [f(q_1, q_2)] \xrightarrow{P} \text{Diagram S}^A &= \frac{\mu^{2\epsilon}}{\pi^4} \int d^n q_1 d^n q_2 \frac{f(q_1, q_2)}{[1][2][3]}, \quad \text{with} \quad \begin{cases} [1] = q_1^2 + m_1^2 \\ [2] = (q_1 - q_2 + P)^2 + m_2^2 \\ [3] = q_2^2 + m_3^2 \end{cases} \\
 [f(q_1, q_2)] \xrightarrow{P} \text{Diagram S}^C &= \frac{\mu^{2\epsilon}}{\pi^4} \int d^n q_1 d^n q_2 \frac{f(q_1, q_2)}{[1][2][3][4]}, \quad \text{with} \quad \begin{cases} [1] = q_1^2 + m_1^2 \\ [2] = (q_1 - q_2)^2 + m_2^2 \\ [3] = q_2^2 + m_3^2 \\ [4] = (q_2 + P)^2 + m_4^2 \end{cases} \\
 [f(q_1, q_2)] \xrightarrow{P} \text{Diagram S}^E &= \frac{\mu^{2\epsilon}}{\pi^4} \int d^n q_1 d^n q_2 \frac{f(q_1, q_2)}{[1][2][3][4][5]}, \quad \text{with} \quad \begin{cases} [1] = q_1^2 + m_1^2 \\ [2] = (q_1 - q_2)^2 + m_2^2 \\ [3] = q_2^2 + m_3^2 \\ [4] = (q_2 + P)^2 + m_4^2 \\ [5] = q_2^2 + m_5^2 \end{cases} \\
 [f(q_1, q_2)] \xrightarrow{P} \text{Diagram S}^D &= \frac{\mu^{2\epsilon}}{\pi^4} \int d^n q_1 d^n q_2 \frac{f(q_1, q_2)}{[1][2][3][4][5]}, \quad \text{with} \quad \begin{cases} [1] = q_1^2 + m_1^2 \\ [2] = (q_1 + P)^2 + m_2^2 \\ [3] = (q_1 - q_2)^2 + m_3^2 \\ [4] = q_2^2 + m_4^2 \\ [5] = (q_2 + P)^2 + m_5^2 \end{cases}
 \end{aligned}$$

Figure 26: The irreducible two-loop self-energies diagrams.  $f$  is a generic polynomial in the loop momenta  $q_1$  and  $q_2$ . The dimension of the space-time is  $n = 4 - \epsilon$  and  $\mu$  is the renormalization scale.

Figure 27 shows six irreducible two-loop vertex diagrams, each associated with a specific integral representation. The diagrams are labeled  $V^E$ ,  $V^I$ ,  $V^M$ ,  $V^G$ ,  $V^K$ , and  $V^H$ . Each diagram has an incoming line with momentum  $-P$  and two outgoing lines with momenta  $p_1$  and  $p_2$ . The diagrams are connected to an integral expression for  $[f(q_1, q_2)]$  in  $n$  dimensions, with a renormalization scale  $\mu$ .

The integral representations are as follows:

- $V^E$ :  $[f(q_1, q_2)] = \frac{\mu^{2\epsilon}}{\pi^4} \int d^n q_1 d^n q_2 \frac{f(q_1, q_2)}{[1][2][3][4]}$ , with  $\begin{cases} [1] = q_1^2 + m_1^2 \\ [2] = (q_1 - q_2)^2 + m_2^2 \\ [3] = (q_2 + p_2)^2 + m_3^2 \\ [4] = (q_2 + P)^2 + m_4^2 \end{cases}$
- $V^I$ :  $[f(q_1, q_2)] = \frac{\mu^{2\epsilon}}{\pi^4} \int d^n q_1 d^n q_2 \frac{f(q_1, q_2)}{[1][2][3][4][5]}$ , with  $\begin{cases} [1] = q_1^2 + m_1^2 \\ [2] = (q_1 - q_2)^2 + m_2^2 \\ [3] = q_2^2 + m_3^2 \\ [4] = (q_2 + p_1)^2 + m_4^2 \\ [5] = (q_2 + P)^2 + m_5^2 \end{cases}$
- $V^M$ :  $[f(q_1, q_2)] = \frac{\mu^{2\epsilon}}{\pi^4} \int d^n q_1 d^n q_2 \frac{f(q_1, q_2)}{[1][2][3][4][5]}$ , with  $\begin{cases} [1] = q_1^2 + m_1^2 \\ [2] = (q_1 - q_2)^2 + m_2^2 \\ [3] = q_2^2 + m_3^2 \\ [4] = (q_2 + p_1)^2 + m_4^2 \\ [5] = (q_2 + P)^2 + m_5^2 \\ [6] = q_2^2 + m_6^2 \end{cases}$
- $V^G$ :  $[f(q_1, q_2)] = \frac{\mu^{2\epsilon}}{\pi^4} \int d^n q_1 d^n q_2 \frac{f(q_1, q_2)}{[1][2][3][4][5]}$ , with  $\begin{cases} [1] = q_1^2 + m_1^2 \\ [2] = (q_1 + p_1)^2 + m_2^2 \\ [3] = (q_1 - q_2)^2 + m_3^2 \\ [4] = (q_2 + p_1)^2 + m_4^2 \\ [5] = (q_2 + P)^2 + m_5^2 \end{cases}$
- $V^K$ :  $[f(q_1, q_2)] = \frac{\mu^{2\epsilon}}{\pi^4} \int d^n q_1 d^n q_2 \frac{f(q_1, q_2)}{[1][2][3][4][5][6]}$ , with  $\begin{cases} [1] = q_1^2 + m_1^2 \\ [2] = (q_1 + P)^2 + m_2^2 \\ [3] = (q_1 - q_2)^2 + m_3^2 \\ [4] = q_2^2 + m_4^2 \\ [5] = (q_2 + p_1)^2 + m_5^2 \\ [6] = (q_2 + P)^2 + m_6^2 \end{cases}$
- $V^H$ :  $[f(q_1, q_2)] = \frac{\mu^{2\epsilon}}{\pi^4} \int d^n q_1 d^n q_2 \frac{f(q_1, q_2)}{[1][2][3][4][5][6]}$ , with  $\begin{cases} [1] = q_1^2 + m_1^2 \\ [2] = (q_1 - p_2)^2 + m_2^2 \\ [3] = (q_1 - q_2 + p_1)^2 + m_3^2 \\ [4] = (q_1 - q_2 - p_2)^2 + m_4^2 \\ [5] = q_2^2 + m_5^2 \\ [6] = (q_2 - p_1)^2 + m_6^2 \end{cases}$

Figure 27: The irreducible two-loop vertex diagrams.  $f$  is a generic polynomial in the loop momenta  $q_1$  and  $q_2$ . The dimension of the space-time is  $n = 4 - \epsilon$  and  $\mu$  is the renormalization scale.

## B Properties of projectors

In this appendix we briefly summarize a general approach based on the work of Ref. [52]. Amplitudes for two-loop  $1 \rightarrow 2$  processes are decomposed into form factors which have to be extracted with proper projection operators. Let us consider tensor, one-loop,  $N$ -point functions in  $n$  dimensions ( $N \leq 5, n = 4 - \epsilon$ )

$$S_n^{\mu \dots \nu} = \frac{\mu^\epsilon}{i \pi^2} \int d^n q \frac{q^\mu \dots q^\nu}{\prod_{i=0, N-1} (i)}, \quad (i) = (q + p_1 + \dots + p_i)^2 + m_i^2, \quad (234)$$

$$\begin{aligned}
A \quad \textcircled{1} &= \frac{\mu^\epsilon}{i\pi^2} \int d^n q_1 \frac{1}{[1]}, \quad \text{with} \quad [1] = q_1^2 + m_1^2 \\
T^A \quad \textcircled{1 \mid 2 \mid 3} &= \frac{\mu^{2\epsilon}}{\pi^4} \int d^n q_1 d^n q_2 \frac{1}{[1][2][3]}, \quad \text{with} \quad \begin{cases} [1] = q_1^2 + m_1^2 \\ [2] = (q_1 - q_2)^2 + m_2^2 \\ [3] = q_2^2 + m_3^2 \end{cases}
\end{aligned}$$

Figure 28: The irreducible one- and two-loop vacuum diagrams. The dimension of the space-time is  $n = 4 - \epsilon$  and  $\mu$  is the renormalization scale.

where  $p_0 = 0$ . We select  $N - 1$  independent vectors,  $r_i$ ,  $i = 1, \dots, N - 1$  and introduce the following notations:

$$G_{ij}^N = G_{N;ij} = 2 r_i \cdot r_j, \quad \mathcal{G}^N = \det G^N. \quad (235)$$

For definiteness we will choose  $r_i = p_i$ . Next we introduce

$$D_{N;\mu\nu} = \frac{1}{n - N + 1} \left[ \delta_{\mu\nu} - 2 r_\mu^t G_N^{-1} r_\nu \right], \quad R_N^\mu = 2 G_N^{-1} r^\mu. \quad (236)$$

They satisfy the following properties:

$$\delta_{\mu\nu} D_N^{\mu\nu} = 1, \quad D_N^{\mu\alpha} D_{N;\alpha}^\nu = \frac{1}{n - N + 1} D_N^{\mu\nu}, \quad (237)$$

$$D_{N;\mu\nu} R_i^{N;\nu} = D_{N;\mu\nu} r_i^\nu = 0, \quad R_i^N \cdot r_j = \delta_{ij}, \quad R_i^N \cdot R_j^N = 2 G_{N;ij}^{-1}. \quad (238)$$

Let us consider now the action of these projectors on tensor integrals: we consider first

$$S_{nN}^{\mu\nu} = \frac{\mu^\epsilon}{i\pi^2} \int d^n q \frac{q^\mu q^\nu}{\prod_{i=0,N} (i)} = \frac{\mu^\epsilon}{i\pi^2} \Gamma(N) \int d^n q \int dS_{N-1} \frac{q^\mu q^\nu}{(q \cdot q + 2 P \cdot q + M^2)^N}, \quad (239)$$

$$P^\mu = \sum_{i=1}^{N-1} x_i p_i^\mu, \quad M^2 = \sum_{i=0}^{N-1} (x_i - x_{i+1}) \left[ (p_1 + \dots + p_i)^2 + m_i^2 \right], \quad (240)$$

with  $x_0 = 1$  and  $x_N = 0$ . Introducing  $\chi(\{x\}) = M^2 - P \cdot P$ , we obtain

$$S_{nN}^{\mu\nu} = \left( \frac{\mu^2}{\pi} \right)^{\epsilon/2} \int dS_{N-1} \chi^{2-N-\epsilon/2} \left[ \Gamma \left( N - 2 + \frac{\epsilon}{2} \right) P^\mu P^\nu + \frac{1}{2} \Gamma \left( N - 3 + \frac{\epsilon}{2} \right) \chi \delta^{\mu\nu} \right]. \quad (241)$$

When the integral is projected with  $D$  we have

$$P D_N P = \sum_{i,j=1}^{N-1} x_i x_j p_i D_N p_j = 0, \quad D_{N;\mu\nu} S_{nN}^{\mu\nu} = \frac{1}{2} S_{n+2N}. \quad (242)$$

For scalar diagrams we define the fundamental parametric representation,

$$\begin{aligned}
S_{nN} &= \left( \frac{\mu^2}{\pi} \right)^{2-n/2} \Gamma \left( N - \frac{n}{2} \right) \int dS_{N-1} \chi^{n/2-N}, \\
\chi &= x^t H_{N-1} x + 2 K_{N-1}^t x + L_{N-1} = (x - X)^t H_{N-1} (x - X) + B_N.
\end{aligned} \quad (243)$$

Furthermore, we define new scalar objects,

$$S_{nN}(i, \dots, j) = \left( \frac{\mu^2}{\pi} \right)^{2-n/2} \Gamma \left( N - \frac{n}{2} \right) \int dS_{N-1} x_i \dots x_j \chi^{n/2-N}. \quad (244)$$

$$S_{nl}(i, \dots, j) = \left(\frac{\mu^2}{\pi}\right)^{2-n/2} \Gamma\left(l - \frac{n}{2}\right) (l)_n(i, \dots, j), \quad (245)$$

where (2) = B, (3) = C etc. We obtain

$$R_{i\mu}^N R_{j\nu}^N S_{nN}^{\mu\nu} = 2 G_{N;ij}^{-1} S_{nN}(0) + \frac{1}{2} S_{n+2N}(i, j). \quad (246)$$

Next we consider integrals with three momenta in the numerator

$$S_{nN}^{\mu\nu\alpha} = - \left(\frac{\mu^2}{\pi}\right)^{2-n/2} \int dS_{N-1} \chi^{n/2-N} \left[ \Gamma\left(N - \frac{n}{2}\right) P^\mu P^\nu P^\alpha + \frac{1}{2} \Gamma\left(N - 1 - \frac{n}{2}\right) \chi \delta^{\{\mu\nu} P^{\alpha\}} \right], \quad (247)$$

where fully symmetrized tensors have been introduced. There are two kind of projections,

$$\begin{aligned} D_{\mu\nu}^N R_{i\alpha}^N S_{nN}^{\mu\nu\alpha} &= -\frac{1}{2} S_{n+2N}(i), \\ R_{i\mu}^N R_{j\nu}^N R_{k\alpha}^N S_{nN}^{\mu\nu\alpha} &= -S_{nN}(ijk) - G_{N;ij}^{-1} S_{n+2N}(k) - G_{N;ik}^{-1} S_{n+2N}(j) - G_{N;jk}^{-1} S_{n+2N}(i). \end{aligned} \quad (248)$$

With four momenta in the numerator we have

$$\begin{aligned} S_{nN}^{\mu\nu\alpha\beta} &= \left(\frac{\mu^2}{\pi}\right)^{2-n/2} \int dS_{N-1} \chi^{n/2-N} \left[ \Gamma\left(N - \frac{n}{2}\right) P^\mu P^\nu P^\alpha P^\beta \right. \\ &\quad \left. + \frac{1}{2} \Gamma\left(N - 1 - \frac{n}{2}\right) \chi \delta^{\{\mu\nu} P^\beta P^{\alpha\}} + \frac{1}{4} \Gamma\left(N - 2 - \frac{n}{2}\right) \chi^2 + \delta^{\{\mu\nu} \delta^{\beta\alpha\}} \right], \end{aligned} \quad (249)$$

where fully symmetrized tensors have been introduced. Projections to be considered are:

$$D_{\mu\nu}^N D_{\alpha\beta}^N S_{nN}^{\mu\nu\alpha\beta} = \frac{1}{4} \frac{n - N + 3}{n - N + 1} S_{n+4N}(0), \quad (250)$$

$$D_{\mu\nu}^N R_{i\alpha}^N R_{j\beta}^N S_{nN}^{\mu\nu\alpha\beta} = \frac{1}{2} S_{n+2N}(ij), \quad R_{i\mu}^N R_{j\nu}^N R_{k\alpha}^N R_{l\beta}^N S_{nN}^{\mu\nu\alpha\beta} = S_{nN}(ijkl). \quad (251)$$

## C Non-abelian soft and collinear diagrams in $H \rightarrow gg$

In this appendix we present a short summary of our procedure for extracting soft/collinear divergent parts of the two-loop diagrams that contribute to the process  $H \rightarrow gg$ . Mass-singular, virtual, configurations appear when a) a massless, internal, line is connected to two on-shell, external lines (*soft*); b) a massless, external, line is connected to two massless, internal lines (*collinear*). Furthermore, we have a soft singularity whenever we attach an extra massless line to an on-shell external line; if the latter is also massless an additional collinear divergence arises. These QCD-like configurations have been extensively discussed in the literature, e.g. see Ref. [8], and in this section we briefly illustrate our approach to the problem.

It is worth noting that in the QCD sector of the corrections to  $H \rightarrow gg$  we select the regulator of collinear divergences to be the space-time dimension and not the masses of the light quarks. On the contrary we select the latter in all situations where collinear singularities cancel in the total. In the following we adopt the convention that a letter  $i$  inside a one-loop diagram denotes the scalar product  $q \cdot p_i$ , where  $q$  is the corresponding loop momentum.

In the soft/collinear decomposition of a two-loop diagram we could highlight the nature of the singularity by introducing factors  $F_i^{IR} = F_i^2$  and write a soft/collinear decomposition for an arbitrary two-loop vertex,

$$V_{\text{lab}}^I = \sum_{i=0,2} V_{\text{lab};i}^I F_{-i}^{IR}(M_H^2), \quad (252)$$

where the superscript  $I$  denotes the family whereas the subscript  $lab$  denotes the rank of the tensor (0 for scalar, etc.) as given in Ref. [49]. For those integrals where also ultraviolet divergences are present we need to extend the decomposition of Eq.(252) to include higher orders of  $\epsilon$  poles by introducing

$$F_{-3}^2(x) = -\frac{1}{\epsilon^3} + \frac{\Delta_{UV}(x)}{\epsilon^2} - \frac{1}{2} \frac{\Delta_{UV}^2(x)}{\epsilon} + \frac{1}{3} \Delta_{UV}^3(x). \quad (253)$$

Alternatively, we can factorize UV and IR/collinear divergences. Suppose that we are considering a two-loop diagram with a single UV pole; remembering that each loop can contribute at most one soft and collinear  $1/\epsilon^2$  term the highest possible pole in our integral is  $1/\epsilon^5$ . Consider the case where the highest pole is  $1/\epsilon^3$ , then we first give the UV decomposition and further decompose the coefficients with new IR factors:

$$V_{lab}^I = \sum_{i=0,3} V_{lab;i}^I F_{-i}^2(M_H^2) = \sum_{i=0,1} V_{lab;i}^{I;UV} F_{-i}^2(M_H^2), \quad (254)$$

$$V_{lab;1}^{I;UV} = V_{lab;3}^I \overline{F}_{-2}^{2;IR}(M_H^2), \quad V_{lab;0}^{I;UV} = \sum_{i=0,2} V_{lab;i}^I F_{-i}^{2;IR}(M_H^2), \quad (255)$$

$$F_i^{2;IR}(x) = F_i^{IR}(x), \quad \overline{F}_{-2}^{2;IR}(x) = -\frac{1}{\epsilon^2} + \frac{1}{6} \Delta_{UV}^2(x). \quad (256)$$

In the following we give a sample of our results; the full list can be found in [92].

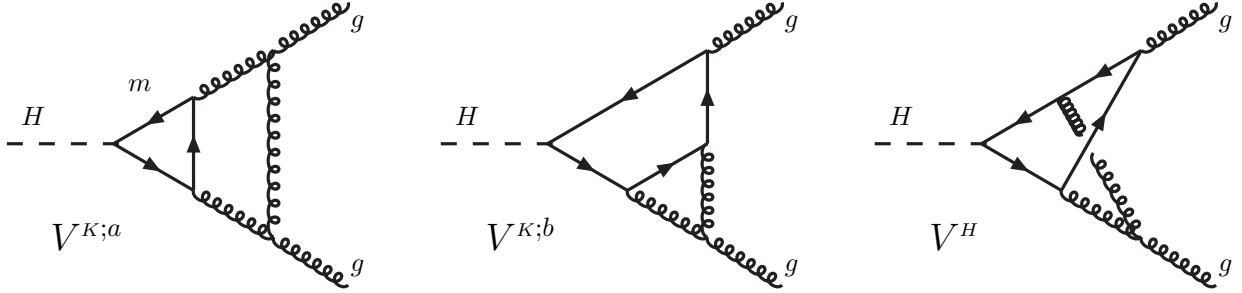


Figure 29: The  $V^{K;a}$ ,  $V^{K;b}$  and  $V^H$  non-abelian soft/collinear configurations. Solid lines stand for a common mass  $m$ .

For the  $V^{K;a}$  configuration we introduce a quadratic form,  $\chi(x) = x(x-1) + m^2/M_H^2$ , where  $m$  is the mass in the triangle of Fig. 29, and obtain

$$V_{-2}^{K;a} = 4 \int_0^1 dx \frac{x}{\chi},$$

$$V_{-1}^{K;a} = 2 \int_0^1 \frac{dx}{\chi} \left\{ \int_0^x dy \ln(\chi - y(x-y)) - \frac{1}{1-x} \ln\left(1 - \frac{x(1-x)}{\chi}\right) + x \left[ \ln(\chi - x(1-x)) - 3 \ln \chi + i\pi \right] \right\}. \quad (257)$$

For the  $V^{K;b}$  configuration, we introduce a new quadratic form,  $\xi(x, y) = \chi(x) + y^2 m^2/M_H^2$ , and derive the following result:

$$V_{-2}^{K;b} = 0, \quad V_{-1}^{K;b} = \int_0^1 dx \int_0^x dy \frac{\ln(1-y)}{\xi(x, y)}. \quad (258)$$

Integrating over  $y$  we obtain

$$V_{-1}^{K;b} = \frac{M_H}{2m} \int_0^1 dx (-\chi)^{-1/2} \left[ \text{Li}_2\left(\frac{1}{y_+}\right) - \text{Li}_2\left(\frac{1}{y_-}\right) - \text{Li}_2\left(\frac{1-x}{y_+}\right) + \text{Li}_2\left(\frac{1-x}{y_-}\right) \right], \quad (259)$$

with  $y_{\pm} = 1 \pm M_H / (m \sqrt{-\chi})$ .

Finally, for the non-planar  $V^H$  configuration of Fig. 29, we obtain the following result:

$$V_{-2}^H = 0, \quad V_{-1}^H = 4 \int_0^1 \frac{dx}{x} \ln^2 \left( 1 - \frac{M_H^2}{m^2} x(1-x) \right), \quad (260)$$

and carry on the  $x$  integration,

$$V_{-1}^H = 8 \left\{ S_{1,2} \left( \frac{1}{x_-} \right) + S_{1,2} \left( \frac{1}{x_+} \right) + S_{1,2}(x_-) + S_{1,2}(x_+) + \ln \frac{x_-}{x_+} \left[ \text{Li}_2 \left( \frac{x_- - x_+}{x_-} \right) - \text{Li}_2 \left( \frac{x_- - x_+}{x_-(1-x_+)} \right) \right] - S_{1,2} \left( \frac{x_- - x_+}{x_-} \right) + S_{1,2} \left( \frac{x_- - x_+}{x_-(1-x_+)} \right) - S_{1,2} \left( \frac{x_+ - x_-}{x_+ - 1} \right) \right\}, \quad (261)$$

with  $x_{\pm} = 1/2 \pm 1/2 \sqrt{1 - 4m^2/M_H^2}$ . Here  $\text{Li}_2(z)$  and  $S_{1,2}(z)$  are Nielsen poly-logarithms.

## D Loop integrals with complex masses and momenta

Consider the logarithm of a complex number  $z = z_R + i z_I$ . Let  $\tilde{z} = z_R - i 0$ , we define

$$\ln_{(2)}(z; \tilde{z}) = \ln z - 2i\pi\theta(-z_R), \quad (262)$$

which satisfies

$$\lim_{z_I \rightarrow 0} \ln_{(2)}(z; \tilde{z}) = \ln(\tilde{z}). \quad (263)$$

When computing the amplitude in the CM scheme we will encounter, after reduction, one-loop two-point functions where both masses and the external invariant are complex. Let

$$\chi(x) = s_P x^2 + (M_2^2 - M_1^2 - s_P) x + M_1^2, \quad (264)$$

$$s_P = M^2 - i\Gamma M, \quad M_i^2 = m_i^2 - i\gamma_i m_i. \quad (265)$$

The correct definition of the  $B_0$  sfunction is as follows:

$$B_0 = \frac{1}{\epsilon} - \int_0^1 dx \ln_{(2)}(\chi; \tilde{\chi}), \quad \tilde{\chi} = \chi \Big|_{\Gamma, \gamma_i=0} - i 0, \quad (266)$$

with the only restriction that  $\chi(x)$  does not cross the negative real axis for  $x \in [0, 1]$  (in which case the definition itself of a two-point function becomes dubious). The best way of understanding the second Riemann sheet is to consider complex  $p^2$  and zero masses; here  $\chi = p^2 x(1-x)$ , therefore  $\text{Re } \chi(x) < 0$  but  $\text{Im } \chi(x) > 0$  which is the opposite of the  $-i 0$  prescription. Thus  $\ln$  gives the wrong answer and  $\ln_{(2)}$  the correct one based on the fact that we require a continuous limit  $\text{widths} \rightarrow 0$ . Therefore, to compute  $B_0$  one should start with the definition of the corresponding function with masses and  $p^2$  real and continue to complex masses and  $p^2$  on the correct Riemann sheet, i.e. with  $\ln_{(2)}$  instead of  $\ln$ . Note that in this function  $y \pm i 0$  is always treated as  $y \pm i$ . Of course, one could use directly the logarithm of a complex number to compute  $\ln x$ .

When only the internal masses are complex there is no problem at all; indeed we find

$$\text{Im } \chi = -\gamma_1 m_1(1-x) - \gamma_2 m_2 x < 0, \quad \text{Im } \tilde{\chi} = -0 < 0. \quad (267)$$

This fact is also true for arbitrary two-loop diagrams as long as only internal masses are continued into the complex plane. There are special cases of complex  $p^2$ , complex masses. In the actual calculation we have at most two scales: consider this situation where we are free to set  $p^2 = -M_2^2$  and obtain

$$\chi(x) = M_2^2 x^2 + M_1^2(1-x), \quad (268)$$

which means that  $\text{Re } \chi(x) > 0$  for  $x \in [0, 1]$  and, therefore, we can use *standard* results, i.e.  $\ln_{(2)} \rightarrow \ln$ . Furthermore, when  $M_1 = 0$  we obtain

$$\chi(x) = p^2(1-x) + M_2^2. \quad (269)$$

If  $p^2 = -M^2 + i\Gamma M$  then  $\text{Re } \chi(x) < 0$  requires  $M > m_2$  which is never satisfied in our case ( $M_W < M_t, M_H$ ). Also here  $\ln_{(2)} \rightarrow \ln$ . Therefore, as far as the calculation reported in this paper is concerned, the only relevant case is complex  $p^2$  and zero internal masses.

## References

- [1] M. Butenschön, F. Fugel and B.A. Kniehl, Phys. Rev. Lett. **98** (2007) 071602, hep-ph/0612184; Nucl. Phys. B **772** (2007) 25, hep-ph/0702215.
- [2] M. Awramik, M. Czakon, A. Freitas and G. Weiglein, Phys. Rev. Lett. **93** (2004) 201805, hep-ph/0407317; W. Hollik, U. Meier and S. Uccirati, Nucl. Phys. B **731** (2005) 213, hep-ph/0507158.
- [3] W. Hollik, U. Meier and S. Uccirati, Phys. Lett. B **632** (2006) 680, hep-ph/0509302.
- [4] M. Awramik, M. Czakon and A. Freitas, Phys. Lett. B **642** (2006) 563, hep-ph/0605339; JHEP **0611** (2006) 048, hep-ph/0608099; W. Hollik, U. Meier and S. Uccirati, Nucl. Phys. B **765** (2007) 154, hep-ph/0610312.
- [5] A. Djouadi, M. Spira and P.M. Zerwas, Phys. Lett. B **264** (1991) 440.
- [6] S. Dawson, Nucl. Phys. B **359** (1991) 283.
- [7] D. Graudenz, M. Spira and P.M. Zerwas, Phys. Rev. Lett. **70** (1993) 1372.
- [8] M. Spira, A. Djouadi, D. Graudenz and P.M. Zerwas, Nucl. Phys. B **453** (1995) 17, hep-ph/9504378.
- [9] R. Harlander and P. Kant, JHEP **0512** (2005) 015, hep-ph/0509189.
- [10] C. Anastasiou, S. Beerli, S. Bucherer, A. Daleo and Z. Kunszt, JHEP **0701** (2007) 082, hep-ph/0611236.
- [11] U. Aglietti, R. Bonciani, G. Degrossi and A. Vicini, JHEP **0701** (2007) 021, hep-ph/0611266.
- [12] M. Mühlleitner and M. Spira, Nucl. Phys. B **790** (2008) 1, hep-ph/0612254.
- [13] R.V. Harlander, Phys. Lett. B **492** (2000) 74, hep-ph/0007289.
- [14] S. Catani, D. de Florian and M. Grazzini, JHEP **0105** (2001) 025, hep-ph/0102227; R.V. Harlander and W.B. Kilgore, Phys. Rev. D **64** (2001) 013015, hep-ph/0102241.
- [15] R.V. Harlander and W.B. Kilgore, Phys. Rev. Lett. **88** (2002) 201801, hep-ph/0201206; C. Anastasiou and K. Melnikov, Nucl. Phys. B **646** (2002) 220, hep-ph/0207004; V. Ravindran, J. Smith and W.L. van Neerven, Nucl. Phys. B **665** (2003) 325, hep-ph/0302135; Nucl. Phys. Proc. Suppl. **135** (2004) 35, hep-ph/0405263.
- [16] S. Catani, D. de Florian, M. Grazzini and P. Nason, JHEP **0307** (2003) 028, hep-ph/0306211.
- [17] S.O. Moch and A. Vogt, Phys. Lett. B **631** (2005) 48, hep-ph/0508265.
- [18] V. Ahrens, T. Becher, M. Neubert and L.L. Yang, arXiv:0808.3008 [hep-ph].
- [19] S. Catani, D. de Florian and M. Grazzini, JHEP **0201** (2002) 015, hep-ph/0111164.
- [20] S. Marzani, R.D. Ball, V. Del Duca, S. Forte and A. Vicini, Nucl. Phys. B **800** (2008) 127, arXiv:0801.2544 [hep-ph].
- [21] C. Anastasiou, K. Melnikov and F. Petriello, Phys. Rev. Lett. **93** (2004) 262002, hep-ph/0409088; Nucl. Phys. B **724** (2005) 197, hep-ph/0501130.
- [22] S. Catani and M. Grazzini, Phys. Rev. Lett. **98** (2007) 222002, hep-ph/0703012; PoS *RADCOR2007* (2007) 046, arXiv:0802.1410 [hep-ph].
- [23] C. Anastasiou, G. Dissertori and F. Stockli, JHEP **0709** (2007) 018, arXiv:0707.2373 [hep-ph].

- [24] M. Schreck and M. Steinhauser, Phys. Lett. B **655** (2007) 148, arXiv:0708.0916 [hep-ph];  
P.A. Baikov and K.G. Chetyrkin, Phys. Rev. Lett. **97** (2006) 061803, hep-ph/0604194.
- [25] A. Djouadi and P. Gambino, Phys. Rev. Lett. **73** (1994) 2528, hep-ph/9406432.
- [26] A. Djouadi, P. Gambino and B. A. Kniehl, Nucl. Phys. B **523**, 17 (1998), hep-ph/9712330.
- [27] U. Aglietti, R. Bonciani, G. Degrassi and A. Vicini, Phys. Lett. B **595** (2004) 432, hep-ph/0404071;  
Phys. Lett. B **600** (2004) 57, hep-ph/0407162.
- [28] G. Degrassi and F. Maltoni, Phys. Lett. B **600** (2004) 255, hep-ph/0407249.
- [29] U. Aglietti, R. Bonciani, G. Degrassi and A. Vicini, contribution to the workshop *TeV<sub>4</sub>LHC*,  
Brookhaven, USA, 2005, hep-ph/0610033.
- [30] K. Cranmer, B. Mellado, W. Quayle and S.L. Wu, ATL-PHYS-2003-036, hep-ph/0401088;  
M. Pieri, S. Bhattacharya, I. Fisk, J. Letts, V. Litvin and J.G. Branson, CERN-CMS-NOTE-2006-112;  
L. Carminati [for the ATLAS Collaboration], Acta Phys. Polon. B **38** (2007) 747.
- [31] K. Mönig and A. Rosca, DESY-06-065, arXiv:0705.1259 [hep-ph].
- [32] H. Zheng and D. Wu, Phys. Rev. D **42** (1990) 3760;  
A. Djouadi, M. Spira, J.J. van der Bij and P.M. Zerwas, Phys. Lett. B **257** (1991) 187;  
S. Dawson and R.P. Kauffman, Phys. Rev. D **47** (1993) 1264.
- [33] M. Steinhauser, contribution to the *Ringberg workshop on the Higgs puzzle*, Ringberg, Germany, 1996,  
hep-ph/9612395.
- [34] K. Melnikov and O.I. Yakovlev, Phys. Lett. B **312** (1993) 179, hep-ph/9302281;  
A. Djouadi, M. Spira and P.M. Zerwas, Phys. Lett. B **311** (1993) 255, hep-ph/9305335;  
M. Inoue, R. Najima, T. Oka and J. Saito, Mod. Phys. Lett. A **9** (1994) 1189;  
J. Fleischer, O.V. Tarasov and V.O. Tarasov, Phys. Lett. B **584** (2004) 294, hep-ph/0401090.
- [35] Y. Liao and X. Li, Phys. Lett. B **396** (1997) 225, hep-ph/9605310;  
F. Fugel, B.A. Kniehl and M. Steinhauser, Nucl. Phys. B **702** (2004) 333, hep-ph/0405232.
- [36] J.G. Korner, K. Melnikov and O.I. Yakovlev, Phys. Rev. D **53** (1996) 3737, hep-ph/9508334.
- [37] G. Degrassi and F. Maltoni, Nucl. Phys. B **724** (2005) 183, hep-ph/0504137.
- [38] G. Passarino, C. Sturm and S. Uccirati, Phys. Lett. B **655** (2007) 298, arXiv:0707.1401 [hep-ph].
- [39] J.A.M. Vermaseren, *New features of FORM*, math-ph/0010025.
- [40] S. Actis, A. Ferroglia, G. Passarino, M. Passera, C. Sturm, and S. Uccirati, *GraphShot*, a FORM pack-  
age for automatic generation and manipulation of one- and two-loop feynman diagrams, unpublished.
- [41] F. V. Tkachov, Phys. Lett. B **100** (1981) 65;  
K.G. Chetyrkin and F.V. Tkachov, Nucl. Phys. B **192** (1981) 159;  
F.V. Tkachov, *New methods for evaluation of multi-loop Feynman diagrams*, PhD thesis, INR, Moscow,  
Russia, 1984.
- [42] S. Actis, A. Ferroglia, M. Passera and G. Passarino, Nucl. Phys. B **777** (2007) 1, hep-ph/0612122.
- [43] S. Actis and G. Passarino, Nucl. Phys. B **777** (2007) 35, hep-ph/0612123.
- [44] S. Actis and G. Passarino, Nucl. Phys. B **777** (2007) 100, hep-ph/0612124.
- [45] G. Passarino, Nucl. Phys. B **619** (2001) 257, hep-ph/0108252.

- [46] G. Passarino and S. Uccirati, Nucl. Phys. B **629** (2002) 97, hep-ph/0112004.
- [47] A. Ferroglia, M. Passera, G. Passarino and S. Uccirati, Nucl. Phys. B **680** (2004) 199, hep-ph/0311186.
- [48] G. Passarino and S. Uccirati, Nucl. Phys. B **747** (2006) 113, hep-ph/0603121.
- [49] S. Actis, A. Ferroglia, G. Passarino, M. Passera and S. Uccirati, Nucl. Phys. B **703** (2004) 3, hep-ph/0402132.
- [50] G. 't Hooft and M.J.G. Veltman, Nucl. Phys. B **44** (1972) 189.
- [51] G. Passarino and M.J.G. Veltman, Nucl. Phys. B **160** (1979) 151.
- [52] T. Binoth, Nucl. Phys. Proc. Suppl. **116** (2003) 387, hep-ph/0211125.
- [53] F. Jegerlehner, Eur. Phys. J. C **18** (2001) 673, hep-th/0005255.
- [54] R.G. Stuart, Phys. Lett. B **262** (1991) 113.
- [55] P. Gambino and P.A. Grassi, Phys. Rev. D **62** (2000) 076002, hep-ph/9907254.
- [56] H. Lehmann, K. Symanzik and W. Zimmermann, Nuovo Cim. **1** (1955) 205.
- [57] I. Bialynicki-Birula, Phys. Rev. D **2** (1970) 2877.
- [58] G. 't Hooft and M.J.G. Veltman, Nucl. Phys. B **50** (1972) 318.
- [59] A. Freitas, W. Hollik, W. Walter and G. Weiglein, Nucl. Phys. B **632** (2002) 189 [Erratum-ibid. B **666** (2003) 305], hep-ph/0202131.
- [60] A. Denner, S. Dittmaier, M. Roth and L.H. Wieders, Nucl. Phys. B **724** (2005) 247, hep-ph/0505042;  
A. Denner and S. Dittmaier, Nucl. Phys. Proc. Suppl. **160** (2006) 22, hep-ph/0605312;  
A. Denner, S. Dittmaier, M. Roth and D. Wackeroth, Nucl. Phys. B **560** (1999) 33, hep-ph/9904472.
- [61] A. Denner and T. Hahn, Nucl. Phys. B **525** (1998) 27, hep-ph/9711302.
- [62] M.J.G. Veltman, Physica **29** (1963) 186.
- [63] J.C. Ward, Phys. Rev. **78** (1950) 182;  
A.A. Slavnov, Theor. Math. Phys. **10** (1972) 99 [Teor. Mat. Fiz. **10** (1972) 153];  
J.C. Taylor, Nucl. Phys. B **33** (1971) 436.
- [64] M.J.G. Veltman, *Diagrammatica: The Path to Feynman rules*, Cambridge University Press, Cambridge, 1994.
- [65] D.Y. Bardin and G. Passarino, *The Standard Model in the Making: Precision Study of the Electroweak Interactions*, Clarendon Press, Oxford, 1999.
- [66] G. Passarino, Nucl. Phys. B **361** (1991) 351.
- [67] G. Degrossi and A. Vicini, Phys. Rev. D **69** (2004) 073007, hep-ph/0307122.
- [68] M. Green and M.J.G. Veltman, Nucl. Phys. B **169** (1980) 137 [Erratum-ibid. B **175** (1980) 547].
- [69] G. Passarino and R. Pittau, Phys. Lett. B **228** (1989) 89.
- [70] G. Weiglein, R. Scharf and M. Bohm, Nucl. Phys. B **416** (1994) 606, hep-ph/9310358.
- [71] M. Caffo, H. Czyz, S. Laporta and E. Remiddi, Nuovo Cim. A **111** (1998) 365, hep-th/9805118.
- [72] NAG Fortran Library, Mark 19. *The Numerical Algorithms Group Ltd*, Oxford UK, 1999.

- [73] L.D. Landau, Nucl. Phys. **13** (1959) 181.
- [74] A. Ferroglia, M. Passera, G. Passarino and S. Uccirati, Nucl. Phys. B **650** (2003) 162, hep-ph/0209219.
- [75] M.Y. Kalmykov and A. Sheplyakov, Comput. Phys. Commun. **172** (2005) 45, hep-ph/0411100.
- [76] K. Melnikov, M. Spira and O. I. Yakovlev, Z. Phys. C **64** (1994) 401, hep-ph/9405301.
- [77] B. A. Kniehl, C. P. Palisoc and A. Sirlin, Phys. Rev. D **66** (2002) 057902, hep-ph/0205304.
- [78] S. Actis, G. Passarino, C. Sturm and S. Uccirati, arXiv:0809.1302 [hep-ph].
- [79] A. Denner and S. Pozzorini, Eur. Phys. J. C **18** (2001) 461, hep-ph/0010201; Eur. Phys. J. C **21** (2001) 63, hep-ph/0104127;  
A. Denner, M. Melles and S. Pozzorini, Nucl. Phys. B **662** (2003) 299, hep-ph/0301241.
- [80] A. Denner, B. Jantzen and S. Pozzorini, Nucl. Phys. B **761** (2007) 1, hep-ph/0608326; arXiv:0801.2647 [hep-ph]; arXiv:0809.0800 [hep-ph].
- [81] S. Laporta and E. Remiddi, Phys. Lett. B **379** (1996) 283, hep-ph/9602417;  
S. Laporta, Int. J. Mod. Phys. A **15** (2000) 5087, hep-ph/0102033.
- [82] O.V. Tarasov, Nucl. Instrum. Meth. A **534** (2004) 293, hep-ph/0403253;  
A.V. Smirnov and V.A. Smirnov, contribution to the *11th International Workshop on Advanced Physics Research (ACAT 2007)*, Amsterdam, The Netherlands, 2007, arXiv:0707.3993 [hep-ph].
- [83] S. Gorla and G. Passarino, arXiv:0807.0698 [hep-ph].
- [84] F. V. Tkachov, Nucl. Instrum. Meth. A **389** (1997) 309, hep-ph/9609429 ;  
L.N. Bertstein, Functional Analysis and its Applications, **6** (1972) 66;  
M. Sato, Nagoya Mat. J. **120** (1990) 1.
- [85] T. Binoth and G. Heinrich, Nucl. Phys. B **585** (2000) 741, hep-ph/0004013.
- [86] C. Amsler *et al.* [Particle Data Group], Phys. Lett. B **667** (2008) 1.
- [87] [CDF Collaboration and D0 Collaboration], arXiv:hep-ex/0703034.
- [88] S. Actis, G. Passarino, C. Sturm and S. Uccirati, arXiv:0809.1301 [hep-ph].
- [89] P. Uwer, *EasyNData: A Simple tool to extract numerical values from published plots*, arXiv:0710.2896 [physics.comp-ph].
- [90] J.A.M. Vermaseren, Comput. Phys. Commun. **83** (1994) 45.
- [91] D. Binosi and L. Theussl, Comput. Phys. Commun. **161** (2004) 76, hep-ph/0309015.
- [92] <http://personalpages.to.infn.it/~giampier/add/LongNAB.ps>